eman ta zabal zazu

Universidad del País Vasco

Euskal Herriko Unibertsitatea

Lactide-based thermoplastic elastomers: topography-mediated approaches to alleviate neuroinflammation

Carlos Bello Álvarez

PhD Thesis

2023

Thesis supervisors: Dr. Aitor Larrañaga Espartero, Dr. Ester Zuza Hernández

Doctorate program: Engineering of Materials and Sustainable Processes

Group in Science and Engineering of Polymeric Biomaterials (ZIBIO Group)

Department of Mining-Metallurgy Engineering and Material Science

Bilbao School of Engineering

University of the Basque Country (UPV/EHU)

And Polymat

Agradecimientos

En primer lugar, agradecer al Departamento de Ingeniería Minera y Metalúrgica y Ciencia de los Materiales y a Polymat por hacer posible la realización de esta tesis, y a la Universidad del País Vasco/Euskal Herriko Unibertsitatea (UPV/EHU) por la beca predoctoral de investigación. A Jose-Ramon Sarasua, por haberme permitido formar parte del grupo ZIBIO en el que me pude sentir uno más. A mi tutora Ester Zuza, por haber estado siempre ahí para enseñarme y apoyarme y a mi codirector Aitor Larrañaga Espartero, quién me ha ayudado desde el Máster y me ha sabido llevar y guiar tanto en los momentos buenos como en los malos. Muchas gracias también al resto del grupo, especialmente a Ainhoa Lejardi, Xabier Larrañaga, Jone Muñoz y Emilio Meaurio por estar siempre disponibles para mí. También darle las gracias a Iker Bustinza, por ayudarme y enseñarme a cacharrear con los equipos. No me puedo olvidar tampoco de las últimas incorporaciones del laboratorio: Maria Angela, Moha, Richard, Sara, Upashi, Irene, Asier y todos los que pasaron por él, gracias también por estar ahí en el día a día. Agradecer a Blanca Atxa, Jone Muñoz, Laura Sebastián y Agustín Etxeberria por toda la ayuda en el Capítulo 3 y de nuevo a Agustín Etxeberria y a Yurena Polo la ayuda en el Capítulo 5. También me gustaría agradecer a los técnicos de los Servicios Generales de Investigación de la UPV/EHU (SGIker) por su apoyo con el uso de técnicas de microscopía (Alejandro Díez y Ricardo Andrade). Y cómo no, a Oroitz Sánchez, Iulia Caraseva, Yurena Polo y Ulyana Semenenko ya que no solo fueron compañeras de trabajo, sino que también llegaron a convertirse en personas muy importantes. Gracias a mis padres, mi hermana y mi familia por siempre apoyarme y dármelo todo. Y gracias a mis amigos por ser los que siempre han estado ahí.

Abstract

The use of biomaterials in the human body for different therapeutic and diagnostic purposes is a very common practice nowadays. Among the available materials, polymers show huge potential thanks to their ability to be manufactured specifically for different needs. Among the polymers used in biomedical applications, polylactide (PLA) is one of the most used due to its well-known biocompatibility and bioresorbability, in addition of being approved by the FDA for its use in the human body. Despite all the advantages associated to PLA, its use is restricted in certain applications because of its inherent brittleness and stiffness; this makes PLA unsuitable for the regeneration of soft tissues (e.g., nervous tissue). One of the most used strategies to solve this problem relies on its copolymerization with a comonomer that provides flexibility to the final material. Via the precise control over the synthesis conditions (i.e., comonomer ratio, catalyst, temperature and reaction time), it is possible to adapt the properties of the final copolymer to the requirements of the specific biomedical application. The appropriate mechanical properties, cytocompatibility and surface topography will be decisive for a correct interaction between the cells and the material. Thus, the material should ideally mimic the extracellular matrix in which the cells reside to achieve the viability of the implanted device, thus avoiding an inflammatory process after its implantation that could promote the formation of a scar tissue around the implant. In the present thesis, different polymeric systems based on PLA were synthesized and characterized. Subsequently, they were processed in different ways with the aim of studying their interaction with representative cells of the nervous system. Firstly (Chapter 3), the synthesis of poly(L-lactide-co-ε-caprolactone) (PLCL) has been explored, obtaining different mechanical behaviours depending on the composition and chain microstructure. Furthermore, through different thermal treatments, a variety of surface topographies and roughness have been obtained. The most representative ones have been selected to study the interaction between the seeded cells (fibroblasts) and the different surfaces. Next (Chapter 4), ethylene brassylate has been studied as an alternative of caprolactone in copolymerization with lactide. In this way, the copolymers poly(L-lactide-co-ethylene brassylate) (PLEB) and poly(D,L-lactide-co-ethylene brassylate) (PDLEB) have been synthesized. Additionally, through a sonication process, carbon nanotubes have been incorporated into the polymer matrix. Again, the copolymers obtained have been characterized and the viability and interaction of astrocytes with them have been studied, also exploring the nanostructuring of the samples and how it affects the cell behaviour. Finally (Chapter 5), a study has been carried out on the inflammatory process of cells (microglia) when faced with a lipopolysaccharide (LPS) stimulus, for which an inflammatory model has been

generated based on cell viability and the measurement of different characteristic markers of this state. Based on this inflammatory model, the interplay between PDLEB copolymers and microglia has been studied.

In summary, in this thesis various copolymers based on lactide have been synthesized, which show mechanical properties compatible with those observed in the nervous tissue. The interaction of these materials with astrocytes and microglia has been subsequently studied, placing particular attention on the effect of surface topography and addition of carbon nanotubes on the cell response. We expect that the present thesis may open the doors to future work related to the neuroinflammatory response of cells in presence of implantable polymeric devices.

Resumen

El uso de biomateriales en el cuerpo humano para diferentes fines terapéuticos y de diagnosis es una práctica muy común hoy en día. Entre los materiales disponibles, los polímeros muestran un gran potencial gracias a su capacidad para ser fabricados de forma específica para las diferentes necesidades. Entre los polímeros empleados en aplicaciones biomédicas, la polilactida (PLA) es de los más usados debido a su más que conocida biocompatibilidad y bioreabsorbilidad, además de estar aprobada por la FDA para su uso en el cuerpo humano. A pesar de todas las ventajas asociadas al PLA, su uso está restringido en determinadas aplicaciones debido a su inherente fragilidad y rigidez; esto hace que el PLA no sea adecuado para la regeneración de tejidos blandos (p.ej., el tejido nervioso). Una de las estrategias más usadas para solventar este problema reside en su copolimerización con un comonómero que aporte flexibilidad al material final. Mediante un preciso control sobre las condiciones de la síntesis (es decir, el ratio de comonómero, catalizador, temperatura y tiempo de reacción), es posible adaptar las propiedades del copolímero final a los requisitos de la aplicación biomédica específica. Las propiedades mecánicas adecuadas, la citocompatibilidad y la topografía superficial serán determinantes para que se dé una correcta interacción entre las células y el material. Así pues, idealmente el material debería imitar la matriz extracelular en la que residen las células para lograr la viabilidad del dispositivo implantado, evitando así un proceso inflamatorio tras su implantación que podría inducir la formación de tejido cicatricial alrededor del implante. En la presente tesis, se sintetizaron y caracterizaron diferentes sistemas poliméricos basados en el PLA. Tras ello, fueron procesados de diferentes formas con el objetivo de estudiar su interacción con células representativas del sistema nervioso. En primer lugar (Capítulo 3), se ha explorado la síntesis de poli(L-lactida-co-ε-caprolactona) (PLCL), obteniendo diferentes comportamientos mecánicos dependiendo de la composición y la microestructura de la cadena. Además, mediante diferentes tratamientos térmicos, se han obtenido una variedad de topografías superficiales y rugosidades. De las cuales, se han seleccionado las más representativas para estudiar la interacción entre las células (fibroblastos) sembradas y las diferentes superficies. Seguidamente (Capítulo 4) se ha estudiado el brasilato de etileno como una alternativa a la caprolactona en la copolimerización con la lactida. De esta manera, se han sintetizado los copolímeros poli(L-lactida-co-brasilato de etileno) (PLEB) y poli(D,L-lactida-co-brasilato de etileno) (PDLEB). Además, mediante un proceso de sonicación, se han incorporado nanotubos de carbono a la matriz polimérica. De nuevo, se han caracterizado los copolímeros obtenidos y se ha estudiado la viabilidad y la interacción de astrocitos con los mismos, explorando también la

nanoestructuración de las muestras y cómo afecta sobre el comportamiento de las células. Finalmente (Capítulo 5), se ha llevado a cabo un estudio sobre el proceso inflamatorio de las células (microglía) ante un estímulo de lipopolisacáridos (LPS), para lo cual se ha generado un modelo inflamatorio en base a la viabilidad celular y la medición de diferentes marcadores característicos de este estado. Sobre la base de este modelo inflamatorio, se ha estudiado la interacción entre los copolímeros de PDLEB y la microglía.

En resumen, en esta tesis se han sintetizado varios copolímeros basados en la lactida que muestran propiedades mecánicas compatibles con las observadas en el tejido nervioso. Posteriormente se ha estudiado la interacción de estos materiales con astrocitos y microglía, poniendo especial atención al efecto de la topografía superficial y a la adición de nanotubos de carbono sobre la respuesta celular. Con todo ello, esperamos que la presente tesis pueda abrir las puertas a futuros trabajos relacionados con la respuesta neuroinflamatoria de las células en presencia de dispositivos poliméricos implantables.

Laburpena

Giza gorputzean helburu terapeutiko eta diagnosi desberdinetarako biomaterialak erabiltzea oso ohikoa da gaur egun. Eskuragarri dauden materialen artean, polimeroek ahalmen handia dute, behar desberdinetarako berariaz fabrikatzeko duten gaitasunari esker. Aplikazio biomedikoetan erabiltzen diren polimeroen artean, polilaktida (PLA) da gehien erabiltzen den horietako bat, biobateragarritasun eta bioxurgagarritasun ezagunak dituelako. Gainera, FDAk onartzen du, giza gorputzean erabiltzeko. PLAri lotutako abantaila guztiak gorabehera, erabilera mugatua du aplikazio jakin batzuetan, berezko hauskortasuna eta zurruntasuna dituelako; horren ondorioz, PLA ez da egokia ehun bigunak birsortzeko (adibidez, nerbio-ehuna). Arazo hori konpontzeko estrategia erabilienetako bat azken materialari malgutasuna ematen dion komonomero batekin kopolimerizatzea da. Sintesiaren baldintzak zehatz-mehatz kontrolatuta (hau da, komonomeroaren erlazioa, katalizatzailea, tenperatura eta erreakzio-denbora), posible da amaierako kopolimeroaren propietateak berariazko aplikazio biomedikoaren eskakizunetara egokitzea. Propietate mekaniko egokiak, zitokonpatibilitatea eta azaleko topografia erabakigarriak izango dira zelulen eta materialaren arteko elkarrekintza egokia gerta dadin. Beraz, idealki, zelulak bizi diren zelulaz kanpoko matrizea antzeratu beharko luke materialak, ezarritako gailuaren bideragarritasuna lortzeko. Horrela, inplantearen inguruan orbain-ehuna sortzea eragin lezakeen hantura-prozesu bat saihestuko litzateke. Tesi honetan, PLAn oinarritutako hainbat sistema polimeriko sintetizatu eta ezaugarritu ziren. Ondoren, hainbat modutan prozesatu zituzten, nerbio-sistemako zelula adierazgarriekin duten elkarreragina aztertzeko. Lehenik eta behin (3. kapitulua), poli(L-laktida-ko-ε-kaprolaktona)ren (PLCL) sintesia aztertu da, katearen konposizioaren eta mikroegituraren arabera portaera mekaniko desberdinak lortuz. Gainera, hainbat tratamendu termikoren bidez, azaleko topografia eta zimurtasun ugari lortu dira. Horietatik adierazgarrienak hautatu dira ereindako zelulen (fibroblastoak) eta gainazalen arteko elkarreragina aztertzeko. Jarraian (4. kapitulua), etileno-brasilatoa aztertu da, kaprolaktonaren alternatiba gisa, laktidarekin kopolimerizatzeko. Horrela, poli(L-laktida-ko-etilen brasilatoa) (PLEB) eta poli(D,L-laktida-ko-etilen brasilatoa) (PDLEB) kopolimeroak sintetizatu dira. Gainera, sonikazio-prozesu baten bidez, karbonozko nanohodiak sartu dira matrize polimerikoan. Berriz ere, lortutako kopolimeroak ezaugarritu dira, eta astrozitoek horiekin duten bideragarritasuna eta elkarrekintza aztertu dira, laginen nanoegituraketa ere aztertuz eta zelulen portaeran nola eragiten duen aztertuz. Azkenik (5. kapitulua), lipopolisakaridoen (LPS) estimulu baten aurrean zelulen hantura-prozesuari (mikroglia) buruzko azterketa bat egin da. Horretarako, hantura-eredu bat sortu da, zelulen

bideragarritasunean eta egoera horretako markatzaile bereizgarrien neurketan oinarrituta. Hantura-eredu hori oinarri hartuta, PDLEB kopolimeroen eta mikrogliaren arteko interakzioa aztertu da.

Laburbilduz, tesi honetan PLAn oinarritutako kopolimero batzuk sintetizatu dira, nerbio-ehunean behatutakoekin bateragarriak diren propietate mekanikoak erakusten dituztenak. Ondoren, material horiek astrozitoekin eta mikrogliarekin duten elkarreragina aztertu da, eta arreta berezia jarri da azaleko topografiaren efektuan eta erantzun zelularrean karbonozko nanohodiak gehitzean. Beraz, espero dugu tesi honek ateak ireki ahal izatea zelulen erantzun neuroinflamatorioarekin zerikusia duten etorkizuneko lanei, gailu polimeriko inplantagarrien arloan.

Publications related to this thesis

- C. Bello-Álvarez, A. Etxeberria, Y. Polo, J.R. Sarasua, E. Zuza, A. Larrañaga, Lactide and Ethylene Brassylate-Based Thermoplastic Elastomers and Their Nanocomposites with Carbon Nanotubes: Synthesis, Mechanical Properties and Interaction with Astrocytes, Polymers. 14 (2022) 4656. https://doi.org/10.3390/polym14214656.

- C. Bello-Álvarez, B. Atxa Ainz, J.M. Ugartemendia, L. Sebastián, A. Etxeberria, J.-R. Sarasua, E. Zuza, A. Larrañaga, Thermoplastic elastomers based on lactide and caprolactone: The influence of chain microstructure on surface topography and subsequent interaction with cells, Polymer Testing. 128 (2023) 108220. https://doi.org/10.1016/j.polymertesting.2023.108220.

Participation in international congresses

- I. Romayor, Y. Polo, S. Martín-Colomo, C. Bello, R. Basanta-Torres, I. Manero-Roig, B. Pardo-Rodriguez, J. Luzuriaga, F. Unda, G. Ibarretxe, J.-R. Sarasua, A. Larrañaga, C. Eguizabal, J.R. Pineda, Nanotopography with bioresorbable polymeric scaffolds to design and guide shape and growth of human pluripotent and embrionic stem cells. IBRO Neuroscience Reports. 15 (2023) S200–S201. https://doi.org/10.1016/j.ibneur.2023.08.311.

Other Publications

- A. Larrañaga, C. Bello-Álvarez, E. Lizundia, Cytotoxicity and Inflammatory Effects of Chitin Nanofibrils Isolated from Fungi, Biomacromolecules. (2023). https://doi.org/10.1021/acs.biomac.3c00710.

Table of content

CHAPTER 1

Hypothesis and Aims

CHAPTER 1. Hypothesis and Aims

HYPOTHESIS

The topographical aspects and mechanical properties of lactide based copolymers can be adjusted by a precise control over the synthesis conditions (i.e., comonomer feed ratio, catalyst/initiator, reaction time and temperature), the incorporation of nanofillers into the copolymer matrix and by thermal treatments, which modulates the cell behaviour and the neuroinflammatory process.

AIMS

The main aim of this thesis is the fabrication of polymeric scaffolds with the capacity of attenuating the inflammatory response of cells implicated in the neuroinflammatory response after the device implantation. To achieve this general aim, three specific objectives were stablished:

1. Synthesis of poly(lactide-co-ε-caprolactone) (PLCL) copolymer films with mechanical properties compatible with the neural tissue showing a wide variety of surface topographies.
2. Synthesis of poly(lactide-co-ethylene brassylate) (PLEB) copolymers reinforced with carbon nanotubes (CNT) with mechanical properties that match with nervous system.
3. Fabrication of nanopatterned and smooth polymeric scaffolds and their role on the neuroinflammation process.

To achieve these principal objectives, the following sub-objectives should be considered:

1. **Synthesis of poly(lactide-co-ε-caprolactone) (PLCL) copolymer films with mechanical properties compatible with the neural tissue showing a wide variety of surface topographies (Chapter 3).**
    - 1.1. Synthesis of PLCL copolymers with different compositions and chain microstructures.
        - 1.1.1. Synthesis of PLCL copolymers controlling the comonomer mass feed ratio and the catalyst/initiator.

1.1.2. Analysis of the different copolymer compositions, their mechanical properties and the resulting chain microstructures.

1.2. Obtention of different surface topographies.

1.2.1. Isothermal treatments to control crystallinity degree and crystal morphology.

1.2.2. Characterization of the different topographies obtained.

1.3. Interaction between cells and different surface topographies.

1.3.1. Analysis of the cell adhesion to the different surfaces.

1.3.2. Evaluation of the impact of surface topography on cell morphology.

2. Synthesis of poly(lactide-co-ethylene brassylate) (PLEB) copolymers reinforced with carbon nanotubes (CNT) with mechanical properties that match with nervous system (Chapter 4).

2.1. Synthesis of LA-EB copolymers, CNT addition and film fabrication.

2.1.1. Synthesis of poly(D,L-lactide-co-ethylene brassylate) (PDLEB) and poly(L-lactide-co-ethylene brassylate) (PLEB) copolymers and characterization.

2.1.2. Incorporation of CNT.

2.1.3. Film fabrication by compression moulding.

2.2. Analysis of mechanical properties and surface properties.

2.2.1. Analysis of mechanical properties at room and body temperature.

2.2.2. Studying of contact angle by sessile drop method.

2.3. Cytotoxicity analysis and cell morphology.

2.3.1. Cell viability of astrocytes on copolymer samples.

2.3.2. Cell morphology of astrocytes by immunostaining.

3. Fabrication of nanopatterned and smooth polymeric scaffolds and their role on the neuroinflammation process (Chapter 5).

3.1. Fabrication of nanopatterned poly(D,L-lactide-co-ethylene brassylate) (PDLEB) scaffolds and their examination.

3.1.1. Fabrication of nanostructured scaffolds by nanolithography.

3.1.2. Examination of nanostructured scaffolds by scanning electron microscopy.

3.2. Establishment of an inflammatory model.

3.2.1. Cell viability assay of microglia stimulated with lipopolysaccharides (LPS).

3.2.2. Measurements of nitrites and TNF-α secreted by Griess and ELISA assays, respectively.

3.2.3. Measurements of ROS and Iba-1 expression.

3.3. Study of the interaction between poly(D,L-lactide-co-ethylene brassylate) (PDLEB) scaffolds with cells.

3.3.1. Secretion of nitrites and TNF-α by microglia seeded on smooth poly(D,L-lactide-co-ethylene brassylate) (PDLEB) scaffolds with different CNT concentrations.

3.3.2. Secretion of nitrites and TNF-α by microglia seeded on and nanopatterned poly(D,L-lactide-co-ethylene brassylate) (PDLEB) scaffolds with different CNT concentrations.

3.3.3. Cell viability assay of microglia seeded on smooth and nanopatterned poly(D,L-lactide-co-ethylene brassylate) (PDLEB) scaffolds with different CNT concentrations.

CHAPTER 2

Introduction

CHAPTER 2. Introduction

Abstract

Although biomaterials have been used throughout human history, it was not until 2009 when a complete definition was stablished. By studying and developing new biomaterials, we are now able to fabricate scaffolds for tissue engineering applications to repair, regenerate or replace injured tissues in the human body. Ideally, these scaffolds should replicate the physical, chemical, mechanical and morphological properties of the extracellular matrix where cells reside. For this purpose, polymers are a good alternative to elaborate these scaffolds due to the possibility to finely tune their final properties. Among the polymers, one of the most used is the polylactide (PLA) which owns well-reported biocompatible and bioresorbable properties and is widely used for drug delivery systems, implants and cellular scaffolds. In spite of these properties, the use of PLA for the replacement and regeneration of soft tissues in the human body is restricted due to its inherent stiffness and brittleness. To modulate this behaviour, the copolymerization with macro(lactones) as ε-caprolactone or ethylene brassylate, is one of the most explored strategies to provide flexibility to the polymeric chain. Also, the thermoplastic nature of these LA-based copolymers allows the addition of (nano)fillers in the polymer matrix as carbon nanotubes to enhance copolymers properties (i.e., roughness and mechanical properties). Being the tissue of the central nervous system the target of this thesis work, the mechanical properties of this soft tissue should be considered to avoid the mechanical mismatch with the material. Also, the interaction of the surface topography of copolymers with astrocytes and microglia, which have a main role in the immune response of nervous system, should be studied. These strategies could modulate the inflammatory response to a foreign body that could lead in cellular death and the encapsulation of the biomaterial by the glial scar.

2.1. Biomaterials in tissue engineering

Although the concept of biomaterials is relatively recent, different materials have interfaced with the human body (e.g., implants, prostheses, etc.) throughout history. For example, the Romans, Egyptians and Etruscans already used gold in the field of dentistry more than 2000 years ago (Figure 2.1.) [1]. Glass eyes [2] or wooden teeth [3] have also been frequently used in the past. Through the development and use of synthetic plastics at the beginning of the 20th century, these materials were used to develop novel implants.

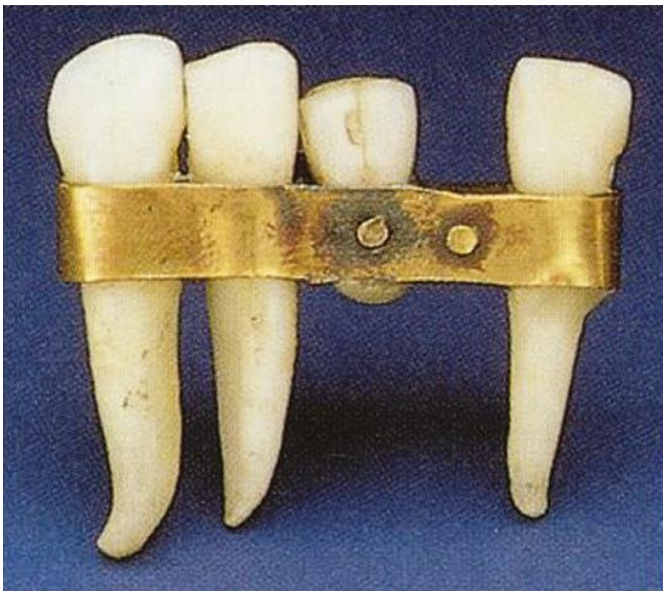

Figure 2.1. Etruscan multi-material dental bridgework composed of carved dog or calf teeth joined by gold plates [4].

As an example, poly(methyl methacrylate) (PMMA) was first considered in the field of dentistry in 1937 [5]. Also, after the World War II, it was observed that fragments of PMMA from war machinery were embedded in soldiers' eyes without causing major problems, suggesting that some materials would cause only a mild reaction to a foreign body [3]. Later, research was also carried out with different tissues commonly used for vascular replacements [6].

Despite the term "biomaterial" was still not coined, their study was already underway. But it was not until 1975, when the Society for Biomaterials was stablished due to the growing success the biomaterials were experiencing. Nevertheless, it was not until 1999 when the definition for biomaterials was given in The Williams Dictionary of Biomaterials [7]. According to this dictionary, a biomaterial was considered as a "material intended to interface with biological systems to evaluate, treat, augment or replace any tissue, organ or function of the body" [7]. Later, in 2009, the definition was expanded determining that "A biomaterial is a substance that

has been engineered to take a form which, alone or as part of a complex system, is used to direct through the control of the interactions with components of living systems, the course of any therapeutic or diagnostic procedure, in human or veterinary medicine" [8]. Gradually, a new scientific discipline focused on the exploration and use of these biomaterials was developed until reaching the present day.

Accordingly, material science and the knowledge about biomaterials are part of the wide variety of disciplines that are included within biomedical engineering. Biomedical engineering is defined as the application of the engineering and design to medicine and biology, in order to advance in diagnosis, monitoring and therapy, besides the management and development of medical equipment [9]. Among all the disciplines covered by biomedical engineering (e.g., biosensor, medical imaging, prosthetic devices, biomechanics, rehabilitation, etc.), tissue engineering is what concerns us in the framework of the present thesis. In the context of tissue engineering, scaffolds represent one of the approaches followed to repair, regenerate or replace injured tissues in the human body, improving and supporting conventional therapies (e.g., autografts, allografts, xenografts) [10]. These scaffolds should resemble the physical, chemical, mechanical and morphological properties of the extracellular matrix (ECM) where cells reside (Figure 2.2.) [11,12].

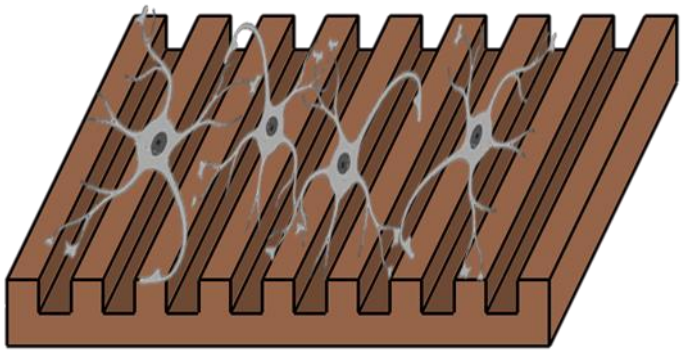

Figure 2.2. Schematic representation of astrocytes seeded on a polymeric scaffold which provides a subtract similar to the extracellular matrix.

For this purpose, different materials are used depending of the specific applications, including titanium and aluminium oxide for dental implants [13]; titanium alloys, stainless steel and poly(tetrafluoroethylene) (PTFE) for hip replacement prostheses [14]; poly(vinyl alcohol) (PVA), chitosan and bioactive glass for bone regeneration [15], etc.

2.2. Polylactide and its copolymers as biomaterials

Among the most used materials, probably polymers are the most versatile biomaterials for the fabrication of scaffolds, allowing to be processed with adequate control of their properties (i.e., pore size, morphology, surface topography, mechanical properties, etc.) which will be essential for cell seeding, migration, growth and tissue formation [16]. One of the most used polymers in this field is polylactide (PLA). PLA is an aliphatic polyester with well-reported biocompatible and bioresorbable properties, used in different biomedical applications as drug delivery systems, implants and cellular scaffolds for tissue engineering applications [17]. PLA became as a great alternative to replace petroleum-based polymers, being part of the solution to the global problem of "plastic" waste [18], since it is a derivate of lactic acid (LA), which is produced from renewable resources as corn, straw or wheat [19]. Among the different methods of synthesizing PLA, ring-opening polymerization (ROP) is the most commonly used approach to obtain polymers with high molecular weight [20]. On this way, it is possible to change the properties of PLA via the control of polymerization parameters as temperature, isomer composition, catalyst and reaction time [21]. Also, due to the chirality of the LA molecule, there are two different forms of lactic acid (enantiomers): L-lactic acid (L-LA) and D-lactic acid (D-LA) (Figure 2.3.) [22].

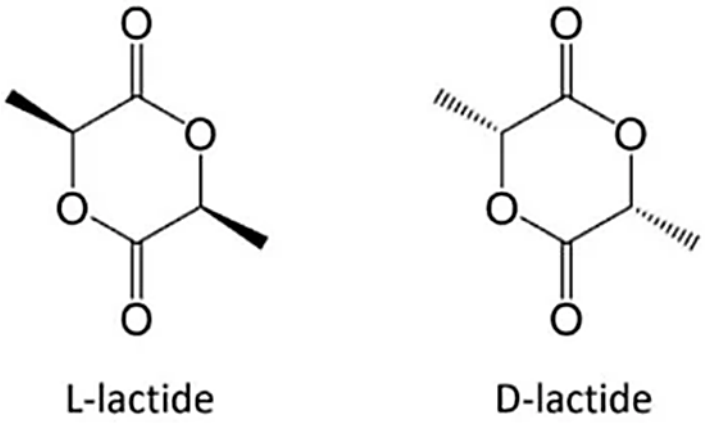

Figure 2.3. Schematic representation of enantiomeric forms of lactic acid [23].

As a result, three different forms of PLA could be produced: poly(L-lactide) (PLLA), poly(D-lactide) (PDLA) and poly(D,L-lactide) (PDLLA) [24]. Controlling the ratio and distribution of L-LA and D-LA in the polymer chains, properties of PLA would be different. L-LA would produce PLLA (semicrystalline), while the racemic mixture of DL-LA would produce PDLLA (amorphous) [25]. As a thermoplastic, the glass transition temperature (T_g) of PLA is around 60 °C for both [25] and the melting temperature (T_m) for PLLA ranges from 150 to 200 °C depending on several factors as molecular weight or crystallinity [26]. Regarding mechanical properties, the Young's modulus

(E) of PDLLA is between 1 - 3.5 GPa and 2.7 - 4.1 GPa for PLLA and the elongation at break (ε) around 10% for both PDLLA and PLLA [27].

These properties restrict the use of PLA for the replacement and regeneration of several tissues in the human body. For example, nerve tissue demands materials with an elastomeric and soft behaviour showing a Young's modulus between 0.5 and 16 MPa and an ultimate strain of 61 - 81% [28-30]. Among all the strategies to modulate the inherent stiffness and brittleness of PLA, copolymerization with (macro)lactones has been widely explored to provide flexibility to the polymeric chain and the resulting polymeric devices [31]. One of these macro(lactones) is the ε-caprolactone (ε-CL), used to synthesize poly(ε-caprolactone) (PCL), which is a thermoplastic semicrystalline polymer with T_g = -60 °C and T_m = 60 °C [32]. The copolymerization of ε-CL with L-LA results in poly(L-lactide-co-ε-caprolactone) (PLCL), whit properties that will depend of the comonomer ratio and the catalyst/initiator used, among other parameters, being common commercially available compositions between 70:30 (L-LA:ε-CL) and 85:15 (L-LA: ε-CL) [33]. Due to the semicrystalline nature of these copolymers, it is possible to apply thermal treatments, modulating this crystallinity in order to create different crystal morphologies that may affect the surface roughness [34]. Other macro(lactone) proposed herein is the ethylene brassylate that is traditionally used as a fragrance ingredient in cosmetic industry [35]. It is extracted from castor oil, allowing us to avoid dependence on fossil feedstock [36], representing a more economical and greener alternative to ε-caprolactone.

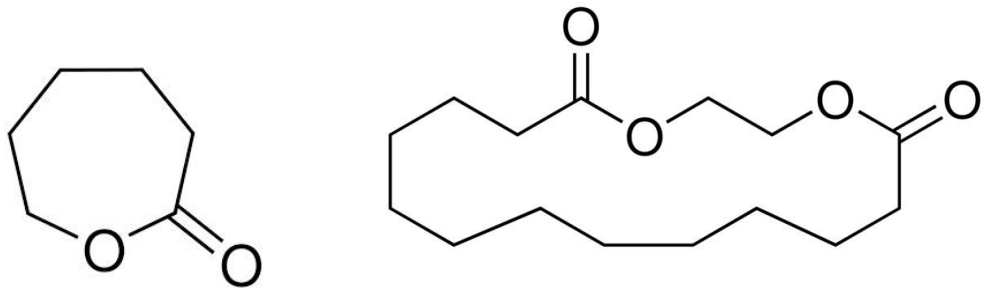

Figure 2.4. Schematic representation of monomers of ε-caprolactone [37] and ethylene brassylate [38].

With thermal properties similar to PCL with T_g = -30 °C and T_m = 70 °C, poly(ethylene brassylate) acquires high molecular weights (up to 247,000 $g \cdot mol^{-1}$) when it is synthesized using triphenyl bismuth (Ph_3Bi) as catalyst [39]. The copolymerization with LA results in poly(D,L-lactide-co-ethylene brassylate) (PDLEB) or poly(L-lactide-co-ethylene brassylate) (PLEB) with adjustable mechanical properties that can match those of the nervous system. Accordingly, lactide-ethylene

brassylate copolymers could represent an interesting alternative to the more widely explored PLCL copolymers [40].

Also, thanks to the thermoplastic nature of PLA and LA-based copolymers synthesized here, it is possible to add (nano)fillers in the polymeric matrix during its processing. Hence, carbon nanotubes (CNTs) were studied in this thesis as a strategy to enhance PLA properties. Being allotropic forms of carbon, CNTs are cylinders-shaped constituted by layers of graphene ideally with carbon atoms distributed in hexagonal lattice. Depending on the number of graphene layers, there exist single-walled carbon nanotubes (SWCNTs) and multi-walled carbon nanotubes (MWCNTs). MWCNTs were first observed in 1991 by Iijima [41], formed by concentric layers of graphene with diameters that could be from 5 to 100 nm [42]. In 1993, single-walled carbon nanotubes (SWCNTs) were first synthesized [43,44], being a unique layer of graphene rolled with a diameter that could vary from 0.8 to 2 nm [42]. The lengths of CNTs range from less than 100 nm to even few centimetres [45]. Both for its mechanical properties (Young's modulus of 1 TPa [46] and tensile strength of 100 GPa [42]) and its electrical properties (metal or semiconductor depending on the orientation of the graphene lattice [42]) turned the CNTs as good candidates as reinforcement fillers in several polymeric matrices. Additionally, these CNTs can impart electrical conductivity to the resulting polymeric devices, every time a critical concentration of CNTs dispersed in the polymer matrix is achieved, called percolation [47]. Also, the addition of CNTs in the polymer matrix could grant of nanoroughness to the composite surface [48]. Considering all these properties, CNTs are a good strategy for their use in the biomedical field due to their good compatibility shown and the ability to promote the adhesion and proliferation of various cell lines [49], particularly for the regeneration of the nervous system [50].

2.3. Nervous tissue: function and cellular structure

With all this in mind, and being the tissue of the nervous system the target of this thesis work, some points should be taken into account. Nervous system is responsible of all the body's functions and it can be divided in two parts (Figure 2.5.): central nervous system (CNS) conformed by all nervous tissue enclosed by bones (spinal cord and brain), and peripheral nervous system (PNS) formed by the rest of nerves and ganglia [51].

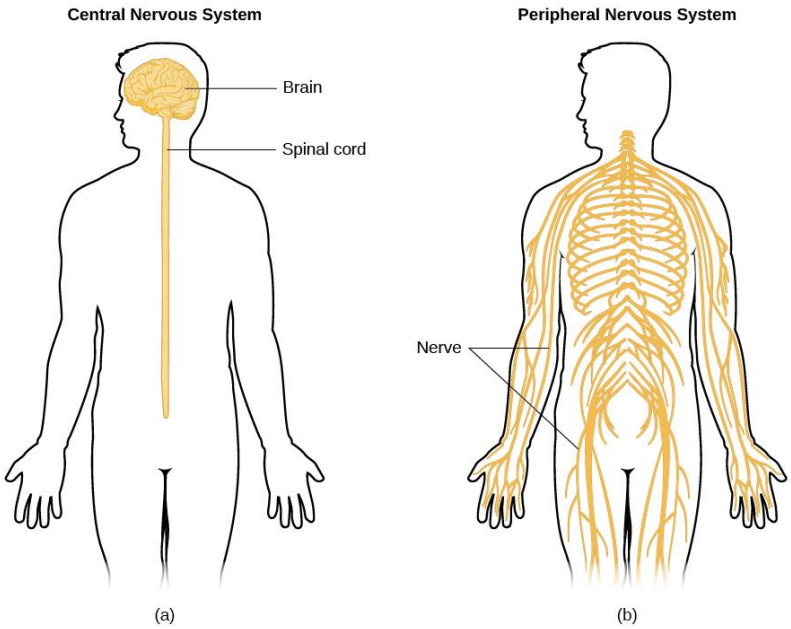

Figure 2.5. Schematic representation of central nervous system (CNS) **a)** and peripheral nervous system (PNS) **b)** [52].

At cellular level, the nervous system consists on specialized cells with different functions. The most recognized are the neurons, which are responsible of transmitting and receiving signals in form of electrochemical impulses and neurotransmitters. Neurons form large networks that generate a perception of the environment and determine the behaviour of the organism [53]. In a second level are the glial cells (in CNS mainly oligodendrocytes, astrocytes, ependymal cells and microglia, and in PNS: Schwann cells and the satellite glial cells) that own auxiliary functions in the nervous system [54]. All these systems (i.e., neural cells, extra cellular matrix, fluids, blood vessels, etc.) are compromised when a disorder or an injury takes place due to the limited capacity of self-healing of CNS [55]. Different reasons could be the initiator of the disease that leads to neuron death by a cationic imbalance of sodium (Na^+), potassium (K^+) and calcium (Ca^{2+}) increasing the concentration of free radicals inside cells and the consequent degradation of them. This Ca^{2+} imbalance produces the release of reactive oxygen species and nitrites and consequently the neuronal death [56]. In addition, a disorder in the blood-brain barrier could take place becoming permeable to cells from immunological system and causing the secretion of inflammatory molecules as the tumour necrosis factor (TNF-α) and the interleukin-1β (IL-1β) [57]. This would activate the microglia and the astrocytes complicating the situation increasing the cellular death [58,59]. Consequently, from the injured area, a cascade of inflammatory signals is initiated, with detrimental consequences in surrounding cells and tissues [60], leading to an immune response for which microglia and astrocytes will isolate the damaged area and will

form the glial scar [61]. This immune response is mainly mediated by the microglia and astrocytes.

Astrocytes are star-shaped glial cells that represent the most abundant cells in the brain [59]. These cells participate in several functions as: maintenance and repair of blood-brain barrier, supply of nutrients to the nervous tissue, maintain the extracellular ion balance, regulation of cerebral blood flow, support for neural function, regulation of synapses and a role in the repair and scarring process of the brain and spinal cord before injuries [62-64]. On the other hand, microglia, which represents approximately the 12% cells in the mammalian brain [58], are the macrophages that reside in CNS. They are responsible of: monitor the environment, clean the extracellular space, the maintenance of the brain homeostasis [55]. As mentioned before, in response to any external danger, microglia become activated releasing cytokines to communicate with surrounding cells and change their functioning [54]. Also, if they detect any malfunction in neurons, microglia will lead to the cell death by stimulating the production of nitric oxide and the secretion of inflammatory signals (as reactive oxygen species) and cytotoxic factors [58,65]. These events could lead to damage of the surrounding tissue and the destruction of healthy neurons, if the inflammation becomes chronic [66]. On this way, a persistent inflammation state is related with neurodegenerative diseases (i.e., Parkinson, Alzheimer, multiple sclerosis, etc.) [53,67,68]. These processes limit the use of biomaterials for the regeneration, therapy and diagnosis of the nervous system.

On the same way, after the implantation of a biomaterial, a cascade of neuroinflammation processes is initiated and a chronic foreign body response is produced, leading to the encapsulation of the biomaterial by the glial scar [69]. This automatically supresses the function of the biomaterial, resulting in its failure and requiring its replacement. In the worst-case scenario, the chronic neuroinflammation could induce neuronal death around the implanted material. One of the more representative examples of biomaterial interfacing with the nervous system are neuroelectrodes, commonly used to treat and monitor central nervous system disorders. Most of them fail after being implanted due to the formation of a glial scar around the implant that suppresses its function (Figure 2.6.) [66].

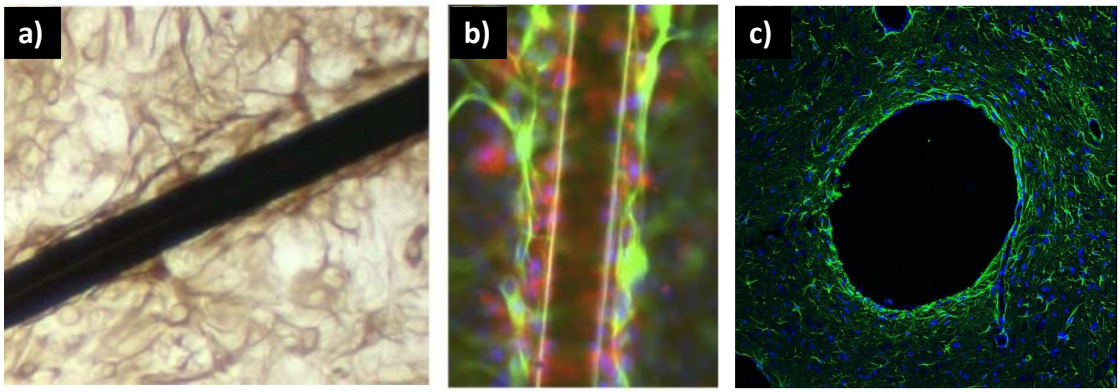

Figure 2.6. a) Detail of the astrocyte glial scarring response to microwires placed in culture. **b)** The fluorescent labelling with DAPI staining nuclei blue, GFAP staining green, and OX-42 staining microglia red, shows the glial scarring and a layer of microglia (red) around the microwire and astrocytes (green) outside of the microglial layer [66]. **c)** Fluorescent image of a Pt/Ir electrode implanted for 8 weeks in the rat subthalamic nucleus shows stained in green for GFAP and blue for DAPI [70].

One of the main reasons behind the failure of the implanted biomaterial can be ascribed to the mechanical mismatch between the neuroelectrode and the nervous tissue. The mechanical mismatch can be reduced by using soft and elastomeric copolymers with adequate mechanical properties that can match the mechanical properties of the nervous tissue [71]. Another property that could influences the glial scar formation is the surface topography and roughness of the neuroelectrode. Considering that the implanted devices should mimic the ECM, topographical cues at the micro- and nanoscale will determine the foreign body response and can even suppress this response and improve the integration of the biomaterial in the host tissue [72]. For all this reasons, the present thesis aims to synthesize different LA-based thermoplastic copolymers with mechanical properties matching those of neural tissue. Then several strategies to achieve different surface topographies were explored, including thermal treatments in order to get different crystal structures, incorporation of CNTs on the copolymer matrix or the nanolithography. Finally, we performed a study on the behaviour of different cell lines seeded on the several varieties of scaffolds formulated.

2.4. References

[1] V. Migonney, History of Biomaterials, in: Biomaterials, John Wiley & Sons, Ltd, 2014: pp. 1–10. https://doi.org/10.1002/9781119043553.ch1.

[2] F. Gan, H. Cheng, Y. Hu, B. Ma, D. Gu, Study on the most early glass eye-beads in China unearthed from Xu Jialing Tomb in Xichuan of Henan Province, China, Sci. China Ser. E-Technol. Sci. 52 (2009) 922–927. https://doi.org/10.1007/s11431-008-0341-0.

[3] B.D. Ratner, Biomaterials Science: An Interdisciplinary Endeavor, in: B.D. Ratner, A.S. Hoffman, F.J. Schoen, J.E. Lemons (Eds.), Biomaterials Science, Academic Press, San Diego, 1996: pp. 1–8. https://doi.org/10.1016/B978-0-08-050014-0.50005-5.

[4] H.F. Hildebrand, Biomaterials – a history of 7000 years, BioNanoMaterials. 14 (2013) 119–133. https://doi.org/10.1515/bnm-2013-0014.

[5] M.S. Zafar, Prosthodontic Applications of Polymethyl Methacrylate (PMMA): An Update, Polymers. 12 (2020) 2299. https://doi.org/10.3390/polym12102299.

[6] R. Guidoin, M. King, P. Blais, M. Marois, C. Gosselin, P. Roy, R. Courbier, M. David, H. Noel, A biological and structural evaluation of retrieved Dacron arterial prostheses, NBS Special Report. 601 (1981) 29–129.

[7] D.F. Williams, The Williams Dictionary of Biomaterials, 1st ed., Liverpool University Press, 1999. https://doi.org/10.5949/UPO9781846314438.

[8] D.F. Williams, On the nature of biomaterials, Biomaterials. 30 (2009) 5897–5909. https://doi.org/10.1016/j.biomaterials.2009.07.027.

[9] J.D. Enderle, J.D. Bronzino, S.M. Blanchard, eds., Introduction to biomedical engineering, 2nd ed, Elsevier Academic Press, Amsterdam ; Boston, 2005.

[10] F.J. O'Brien, Biomaterials & scaffolds for tissue engineering, Materials Today. 14 (2011) 88–95. https://doi.org/10.1016/S1369-7021(11)70058-X.

[11] B.P. Chan, K.W. Leong, Scaffolding in tissue engineering: general approaches and tissue-specific considerations, Eur Spine J. 17 (2008) 467–479. https://doi.org/10.1007/s00586-008-0745-3.

[12] H. Ye, K. Zhang, D. Kai, Z. Li, X.J. Loh, Polyester elastomers for soft tissue engineering, Chem. Soc. Rev. 47 (2018) 4545–4580. https://doi.org/10.1039/C8CS00161H.

[13] H. Ananth, V. Kundapur, H.S. Mohammed, M. Anand, G.S. Amarnath, S. Mankar, A Review on Biomaterials in Dental Implantology, Int J Biomed Sci. 11 (2015) 113–120.

[14] M. Merola, S. Affatato, Materials for Hip Prostheses: A Review of Wear and Loading Considerations, Materials. 12 (2019) 495. https://doi.org/10.3390/ma12030495.

[15] O. Sánchez-Aguinagalde, A. Lejardi, E. Meaurio, R. Hernández, C. Mijangos, J.-R. Sarasua, Novel Hydrogels of Chitosan and Poly(vinyl alcohol) Reinforced with Inorganic Particles of Bioactive Glass, Polymers. 13 (2021) 691. https://doi.org/10.3390/polym13050691.

[16] V. Perez-Puyana, M. Jiménez-Rosado, A. Romero, A. Guerrero, Polymer-Based Scaffolds for Soft-Tissue Engineering, Polymers. 12 (2020) 1566. https://doi.org/10.3390/polym12071566.

[17] B.D. Ulery, L.S. Nair, C.T. Laurencin, Biomedical applications of biodegradable polymers, J. Polym. Sci. B Polym. Phys. 49 (2011) 832–864. https://doi.org/10.1002/polb.22259.

[18] N.-A.A.B. Taib, M.R. Rahman, D. Huda, K.K. Kuok, S. Hamdan, M.K.B. Bakri, M.R.M.B. Julaihi, A. Khan, A review on poly lactic acid (PLA) as a biodegradable polymer, Polym. Bull. 80 (2023) 1179–1213. https://doi.org/10.1007/s00289-022-04160-y.

[19] M.G. Adsul, A.J. Varma, D.V. Gokhale, Lactic acid production from waste sugarcane bagasse derived cellulose, Green Chem. 9 (2007) 58–62. https://doi.org/10.1039/B605839F.

[20] S.-B. Park, E. Lih, K.-S. Park, Y.K. Joung, D.K. Han, Biopolymer-based functional composites for medical applications, Progress in Polymer Science. 68 (2017) 77–105. https://doi.org/10.1016/j.progpolymsci.2016.12.003.

[21] C. Gonçalves, I.C. Gonçalves, F.D. Magalhães, A.M. Pinto, Poly(lactic acid) Composites Containing Carbon-Based Nanomaterials: A Review, Polymers. 9 (2017) 269. https://doi.org/10.3390/polym9070269.

[22] S.M. Ameen, G. Caruso, Lactic Acid in the Food Industry, Springer International Publishing, Cham, 2017. https://doi.org/10.1007/978-3-319-58146-0.

[23] E. Capuana, F. Lopresti, M. Ceraulo, V. La Carrubba, Poly-l-Lactic Acid (PLLA)-Based Biomaterials for Regenerative Medicine: A Review on Processing and Applications, Polymers. 14 (2022) 1153. https://doi.org/10.3390/polym14061153.

[24] A. Larrañaga, E. Lizundia, A review on the thermomechanical properties and biodegradation behaviour of polyesters, European Polymer Journal. 121 (2019) 109296. https://doi.org/10.1016/j.eurpolymj.2019.109296.

[25] Y. Pan, M. Farmahini-Farahani, P. O'Hearn, H. Xiao, H. Ocampo, An overview of bio-based polymers for packaging materials, JBB. 1 (2016) 106–113. https://doi.org/10.21967/jbb.v1i3.49.

[26] J. Shao, S. Xiang, X. Bian, J. Sun, G. Li, X. Chen, Remarkable Melting Behavior of PLA Stereocomplex in Linear PLLA/PDLA Blends, Ind. Eng. Chem. Res. 54 (2015) 2246–2253. https://doi.org/10.1021/ie504484b.

[27] K. Van De Velde, P. Kiekens, Ein Jahrhundert Bahnelektroindustrie, Eb-Elektr. Bahnen. 99 (2001) 483.

[28] G.H. Borschel, K.F. Kia, W.M. Kuzon, R.G. Dennis, Mechanical properties of acellular peripheral nerve, J Surg Res. 114 (2003) 133–139. https://doi.org/10.1016/s0022-4804(03)00255-5.

[29] A.J. Ryan, W.A. Lackington, A.J. Hibbitts, A. Matheson, T. Alekseeva, A. Stejskalova, P. Roche, F.J. O'Brien, A Physicochemically Optimized and Neuroconductive Biphasic Nerve Guidance Conduit for Peripheral Nerve Repair, Adv Healthc Mater. 6 (2017). https://doi.org/10.1002/adhm.201700954.

[30] C.E. Dumont, W. Born, Stimulation of neurite outgrowth in a human nerve scaffold designed for peripheral nerve reconstruction, J Biomed Mater Res B Appl Biomater. 73 (2005) 194–202. https://doi.org/10.1002/jbm.b.30202.

[31] J. Fernández, M. Montero, A. Etxeberria, J.R. Sarasua, Ethylene brassylate: Searching for new comonomers that enhance the ductility and biodegradability of polylactides, Polymer Degradation and Stability. 137 (2017) 23–34. https://doi.org/10.1016/j.polymdegradstab.2017.01.001.

[32] G. Jimenez, N. Ogata, H. Kawai, T. Ogihara, Structure and thermal/mechanical properties of poly (ϵ-caprolactone)-clay blend, Journal of Applied Polymer Science. 64 (1997) 2211–2220. https://doi.org/10.1002/(SICI)1097-4628(19970613)64:11<2211::AID-APP17>3.0.CO;2-6.

[33] J. Fernández, E. Meaurio, A. Chaos, A. Etxeberria, A. Alonso-Varona, J.R. Sarasua, Synthesis and characterization of poly (l-lactide/ε-caprolactone) statistical copolymers with well resolved chain microstructures, Polymer. 54 (2013) 2621–2631. https://doi.org/10.1016/j.polymer.2013.03.009.

[34] C. Bello-Álvarez, B. Atxa Ainz, J.M. Ugartemendia, L. Sebastián, A. Etxeberria, J.-R. Sarasua, E. Zuza, A. Larrañaga, Thermoplastic elastomers based on lactide and caprolactone: The

influence of chain microstructure on surface topography and subsequent interaction with cells, Polymer Testing. 128 (2023) 108220. https://doi.org/10.1016/j.polymertesting.2023.108220.

[35] D. McGinty, C.S. Letizia, A.M. Api, Fragrance material review on ethylene brassylate, Food and Chemical Toxicology. 49 (2011) S174–S182. https://doi.org/10.1016/j.fct.2011.07.023.

[36] A. Pascual, H. Sardon, A. Veloso, F. Ruipérez, D. Mecerreyes, Organocatalyzed Synthesis of Aliphatic Polyesters from Ethylene Brassylate: A Cheap and Renewable Macrolactone, ACS Macro Lett. 3 (2014) 849–853. https://doi.org/10.1021/mz500401u.

[37] ε-Caprolactone 97% | 502-44-3, (n.d.). http://www.sigmaaldrich.com/ (accessed November 15, 2023).

[38] Ethylene brassylate ≥95%, FG | 105-95-3, (n.d.). http://www.sigmaaldrich.com/ (accessed November 15, 2023).

[39] J. Fernández, H. Amestoy, H. Sardon, M. Aguirre, A.L. Varga, J.-R. Sarasua, Effect of molecular weight on the physical properties of poly(ethylene brassylate) homopolymers, Journal of the Mechanical Behavior of Biomedical Materials. 64 (2016) 209–219. https://doi.org/10.1016/j.jmbbm.2016.07.031.

[40] J. Song, B. Sun, S. Liu, W. Chen, Y. Zhang, C. Wang, X. Mo, J. Che, Y. Ouyang, W. Yuan, C. Fan, Polymerizing Pyrrole Coated Poly (l-lactic acid-co-ε-caprolactone) (PLCL) Conductive Nanofibrous Conduit Combined with Electric Stimulation for Long-Range Peripheral Nerve Regeneration, Frontiers in Molecular Neuroscience. 9 (2016). https://doi.org/10.3389/fnmol.2016.00117.

[41] S. Iijima, Helical microtubules of graphitic carbon, Nature. 354 (1991) 56–58. https://doi.org/10.1038/354056a0.

[42] M.F.L. De Volder, S.H. Tawfick, R.H. Baughman, A.J. Hart, Carbon Nanotubes: Present and Future Commercial Applications, Science. 339 (2013) 535–539. https://doi.org/10.1126/science.1222453.

[43] D.S. Bethune, C.H. Kiang, M.S. de Vries, G. Gorman, R. Savoy, J. Vazquez, R. Beyers, Cobalt-catalysed growth of carbon nanotubes with single-atomic-layer walls, Nature. 363 (1993) 605–607. https://doi.org/10.1038/363605a0.

[44] S. Iijima, T. Ichihashi, Single-shell carbon nanotubes of 1-nm diameter, Nature. 363 (1993) 603–605. https://doi.org/10.1038/363603a0.

[45] H. Dai, Carbon nanotubes: opportunities and challenges, Surface Science. 500 (2002) 218–241. https://doi.org/10.1016/S0039-6028(01)01558-8.

[46] N. Yao, V. Lordi, Young's modulus of single-walled carbon nanotubes, Journal of Applied Physics. 84 (1998) 1939–1943. https://doi.org/10.1063/1.368323.

[47] E. Lizundia, J.R. Sarasua, F. D'Angelo, A. Orlacchio, S. Martino, J.M. Kenny, I. Armentano, Biocompatible Poly(L-lactide)/MWCNT Nanocomposites: Morphological Characterization, Electrical Properties, and Stem Cell Interaction, Macromolecular Bioscience. 12 (2012) 870–881. https://doi.org/10.1002/mabi.201200008.

[48] A. Fraczek-Szczypta, Carbon nanomaterials for nerve tissue stimulation and regeneration, Materials Science and Engineering: C. 34 (2014) 35–49. https://doi.org/10.1016/j.msec.2013.09.038.

[49] B.S. Harrison, A. Atala, Carbon nanotube applications for tissue engineering, Biomaterials. 28 (2007) 344–353. https://doi.org/10.1016/j.biomaterials.2006.07.044.

[50] G.-Z. Jin, M. Kim, U.S. Shin, H.-W. Kim, Effect of carbon nanotube coating of aligned nanofibrous polymer scaffolds on the neurite outgrowth of PC-12 cells, Cell Biology International. 35 (2011) 741–745. https://doi.org/10.1042/CBI20100705.

[51] B. Niemczyk, P. Sajkiewicz, D. Kolbuk, Injectable hydrogels as novel materials for central nervous system regeneration, J. Neural Eng. 15 (2018) 051002. https://doi.org/10.1088/1741-2552/aacbab.

[52] Parts of the Nervous System | Introduction to Psychology, (n.d.). https://courses.lumenlearning.com/atd-herkimer-intropsych/chapter/parts-of-the-nervous-system/ (accessed November 20, 2023.

[53] J.B. Hutchins, S.W. Barger, Why neurons die: Cell death in the nervous system, The Anatomical Record. 253 (1998) 79–90. https://doi.org/10.1002/(SICI)1097-0185(199806)253:3<79::AID-AR4>3.0.CO;2-9.

[54] F. He, Y.E. Sun, Glial cells more than support cells?, The International Journal of Biochemistry & Cell Biology. 39 (2007) 661–665. https://doi.org/10.1016/j.biocel.2006.10.022.

[55] S. Sulhan, K.A. Lyon, L.A. Shapiro, J.H. Huang, Neuroinflammation and blood–brain barrier disruption following traumatic brain injury: Pathophysiology and potential therapeutic targets, Journal of Neuroscience Research. 98 (2020) 19–28. https://doi.org/10.1002/jnr.24331.

[56] M. Fricker, A.M. Tolkovsky, V. Borutaite, M. Coleman, G.C. Brown, Neuronal Cell Death, Physiological Reviews. 98 (2018) 813–880. https://doi.org/10.1152/physrev.00011.2017.

[57] S. Meeuwsen, C. Persoon-Deen, M. Bsibsi, R. Ravid, J.M.V. Noort, Cytokine, chemokine and growth factor gene profiling of cultured human astrocytes after exposure to proinflammatory stimuli, Glia. 43 (2003) 243–253. https://doi.org/10.1002/glia.10259.

[58] N.A. Devanney, A.N. Stewart, J.C. Gensel, Microglia and macrophage metabolism in CNS injury and disease: The role of immunometabolism in neurodegeneration and neurotrauma, Experimental Neurology. 329 (2020) 113310. https://doi.org/10.1016/j.expneurol.2020.113310.

[59] G. Yu, Y. Zhang, B. Ning, Reactive Astrocytes in Central Nervous System Injury: Subgroup and Potential Therapy, Frontiers in Cellular Neuroscience. 15 (2021). https://www.frontiersin.org/articles/10.3389/fncel.2021.792764 (accessed October 30, 2023).

[60] C.X. Wang, A. Shuaib, Involvement of inflammatory cytokines in central nervous system injury, Progress in Neurobiology. 67 (2002) 161–172. https://doi.org/10.1016/S0301-0082(02)00010-2.

[61] T. Saxena, J.G. Lyon, S.B. Pai, D. Pare, J. Amero, L. Karumbaiah, S.L. Carroll, E. Gaupp, R.V. Bellamkonda, Engineering Controlled Peritumoral Inflammation to Constrain Brain Tumor Growth, Adv Healthc Mater. 8 (2019) e1801076. https://doi.org/10.1002/adhm.201801076.

[62] K.H. Lee, M. Cha, B.H. Lee, Crosstalk between Neuron and Glial Cells in Oxidative Injury and Neuroprotection, International Journal of Molecular Sciences. 22 (2021) 13315. https://doi.org/10.3390/ijms222413315.

[63] N.J. Abbott, L. Rönnbäck, E. Hansson, Astrocyte–endothelial interactions at the blood–brain barrier, Nat Rev Neurosci. 7 (2006) 41–53. https://doi.org/10.1038/nrn1824.

[64] A. Volterra, J. Meldolesi, Astrocytes, from brain glue to communication elements: the revolution continues, Nat Rev Neurosci. 6 (2005) 626–640. https://doi.org/10.1038/nrn1722.

[65] A. Kelly, N. Farid, K. Krukiewicz, N. Belisle, J. Groarke, E.M. Waters, A. Trotier, F. Laffir, M. Kilcoyne, G.M. O'Connor, M.J. Biggs, Laser-Induced Periodic Surface Structure Enhances Neuroelectrode Charge Transfer Capabilities and Modulates Astrocyte Function, ACS Biomater. Sci. Eng. 6 (2020) 1449–1461. https://doi.org/10.1021/acsbiomaterials.9b01321.

[66] V.S. Polikov, M.L. Block, J.-M. Fellous, J.-S. Hong, W.M. Reichert, In vitro model of glial scarring around neuroelectrodes chronically implanted in the CNS, Biomaterials. 27 (2006) 5368–5376. https://doi.org/10.1016/j.biomaterials.2006.06.018.

[67] S.P. Yun, T.-I. Kam, N. Panicker, S. Kim, Y. Oh, J.-S. Park, S.-H. Kwon, Y.J. Park, S.S. Karuppagounder, H. Park, S. Kim, N. Oh, N.A. Kim, S. Lee, S. Brahmachari, X. Mao, J.H. Lee, M. Kumar, D. An, S.-U. Kang, Y. Lee, K.C. Lee, D.H. Na, D. Kim, S.H. Lee, V.V. Roschke, S.A. Liddelow, Z. Mari, B.A. Barres, V.L. Dawson, S. Lee, T.M. Dawson, H.S. Ko, Block of A1 astrocyte conversion by microglia is neuroprotective in models of Parkinson's disease, Nat Med. 24 (2018) 931–938. https://doi.org/10.1038/s41591-018-0051-5.

[68] S.J. Forrester, D.S. Kikuchi, M.S. Hernandes, Q. Xu, K.K. Griendling, Reactive Oxygen Species in Metabolic and Inflammatory Signaling, Circulation Research. 122 (2018) 877–902. https://doi.org/10.1161/CIRCRESAHA.117.311401.

[69] E.S. Ereifej, C.S. Smith, S.M. Meade, K. Chen, H. Feng, J.R. Capadona, The Neuroinflammatory Response to Nanopatterning Parallel Grooves into the Surface Structure of Intracortical Microelectrodes, Adv. Funct. Mater. 28 (2018) 1704420. https://doi.org/10.1002/adfm.201704420.

[70] A. Trotier, E. Bagnoli, T. Walski, J. Evers, E. Pugliese, M. Lowry, M. Kilcoyne, U. Fitzgerald, M. Biggs, Micromotion derived fluid shear stress mediates peri-electrode gliosis through mechanosensitive ion channels, (2023) 2023.01.13.523766. https://doi.org/10.1101/2023.01.13.523766.

[71] S.P. Lacour, G. Courtine, J. Guck, Materials and technologies for soft implantable neuroprostheses, Nat Rev Mater. 1 (2016) 1–14. https://doi.org/10.1038/natrevmats.2016.63.

[72] J.C. Doloff, O. Veiseh, R. de Mezerville, M. Sforza, T.A. Perry, J. Haupt, M. Jamiel, C. Chambers, A. Nash, S. Aghlara-Fotovat, J.L. Stelzel, S.J. Bauer, S.Y. Neshat, J. Hancock, N.A. Romero, Y.E. Hidalgo, I.M. Leiva, A.M. Munhoz, A. Bayat, B.M. Kinney, H.C. Hodges, R.N. Miranda, M.W. Clemens, R. Langer, The surface topography of silicone breast implants mediates the foreign body response in mice, rabbits and humans, Nat Biomed Eng. 5 (2021) 1115–1130. https://doi.org/10.1038/s41551-021-00739-4.

CHAPTER 3

Thermoplastic elastomers based on lactide and caprolactone: the influence of chain microstructure on surface topography and subsequent interaction with cells

CHAPTER 3. Thermoplastic elastomers based on lactide and caprolactone: the influence of chain microstructure on surface topography and subsequent interaction with cells

Abstract

Surface biophysical properties of biomaterials, including surface topography and roughness, determine the interaction of a biomaterial with the surrounding cells, tissues and organs once implanted in the human body. Herein, the surface topography of thermoplastic copolymers based on lactide and caprolactone showing elastomeric behaviour was modulated by precisely controlling the chain microstructure (i.e., distribution and length of the repetitive units within the polymeric chain). The synthesized copolymers were subjected to different thermal treatments from the melt, leading to polymeric films with various surface textures and roughness values. Copolymers synthesized with triphenyl bismuth as a catalyst, with a more random distribution of the repetitive units, showed limited crystallization capability. Accordingly, only the copolymer with higher amount of L-lactide (i.e., 80 wt.%) subjected to an isothermal treatment from the melt at 70 °C was able to crystallize, and spherulites of around 7 µm were discernible by atomic force microscopy. In contrast, the copolymers synthesized with stannous octoate, which had a more blocky nature, showed axialitic crystalline domains at the submicron- to nanoscale when subjected to an isothermal treatment from the melt at 50 °C, whereas well-defined spherulites of sizes up to 14 µm were obtained at 70 °C. Human fibroblast showed a more elongated morphology when seeded on those samples having higher roughness values and larger spherulites, whereas they had a more spread morphology when seeded on the amorphous, smooth surfaces. As concluded from the present study, by precisely controlling the chain microstructure of the synthesized copolymers, a wide variety of surface topographies can be obtained, which has a clear impact on the way the biomaterial interacts with cells. This opens the possibility to study the influence of surface biophysical properties on more complex cell processes in the future, including inflammatory or foreign body response processes.

3.1. Introduction

Tissue engineering relies on the use of scaffolds to repair, regenerate or replace injured tissues in the human body, thus overcoming the inherent drawbacks of more conventional therapies (e.g., autografts, allografts, xenografts) [1]. Ideally, these scaffolds should mimic the intrinsic physical, chemical, mechanical and morphological properties of the extracellular matrix (ECM) where cells reside [2,3]. The surface topography of the scaffolds is of utmost importance in this context, since it determines the interaction between the cells and the biomaterial, being able to modulate the cell differentiation, adhesion, orientation and morphology [4-7]. Moreover, surface topography also influences the foreign body response and accordingly determines the success of the implanted biomaterial for its intended use. Controlling the surface roughness in silicone breast implants [8] or nanopatterning the surface of intracortical microelectrodes with parallel grooves [9] are clear examples of successful strategies to attenuate the inflammatory response after biomaterial implantation.

Copolymers based on L-lactide (L-LA) and ε-caprolactone (ε-CL) have attracted particular attention for the fabrication of biomaterials that interface with soft tissues in the human body, which are characterized by an elastomeric and soft behaviour [10]. By precisely controlling the copolymer composition, synthesis parameters (e.g., reaction time, temperature and catalyst) and processing conditions [11], poly(L-lactide-co-ε-caprolactone) (PLCL) copolymers presenting a variety of mechanical properties (i.e., ranging from a glassy to an elastomeric behaviour), degradation kinetics, shape-memory behaviour and controlled drug-release profiles can be obtained [11,12]. Several studies around the synthesis, characterization and crystal morphology of PLCL have been accordingly conducted, which show the great potential of this family of copolymers [13–15]. The crystallinity behaviour of the PLCL copolymers is vital for tailoring the surface topography of the scaffolds, as different crystallinity degree and crystal morphologies lead to different surface textures and patterns. Thermal treatments, comonomer ratios and chain microstructure (i.e., distribution of repetitive units and number average sequence lengths of the comonomers) determine the supramolecular arrangements, which lead to different properties and crystal morphologies of the copolymers, ranging from spherulites and axialite-like crystal aggregates to amorphous forms [16–18]. Regarding chain microstructure, PLCLs with shorter average length of L-LA unit sequences show a limited crystallization capability, faster degradation rates and higher strain capability and strain recovery values in comparison with PLCLs with larger average lengths (i.e., blockier character) [19]. Additionally, an increasing ε-CL content results in a reduced crystallization capability of PLCL systems, while increasing the elongation at break and

strain recovery values and leading to copolymers with different mechanical behaviour, ranging from semi-crystalline plastic-like to elastomeric [20].

Chain microstructure can be controlled by adjusting the conditions of the synthesis process, the employed catalysts and the rates of incorporation of the comonomers [19]. In the case of PLCLs, there is a large difference in the reactivity of L-LA and ε-CL units in the ring-opening copolymerization process, which naturally favours the formation of blocky chain microstructures [21,22]. Adjusting the relationship between reactivities, favouring transesterification reactions or controlling the polymerization temperature and reaction time [19] are common strategies to modulate the randomness character of the resulting copolymers. The use of different catalysts/initiators has also been studied as a strategy to tune the chain microstructure of PLCL copolymers [14,15,22,23]. Stannous octoate ($SnOct_2$) is the most commonly used catalyst for ring-opening polymerization due to its good performance, with high conversion and reaction rates and the possibility to obtain (co)polymers with high molecular weights. This catalyst has been reported to lead to blocky PLCLs [14,19]. Bismuth salts (e.g., $BiCl_3$, Bi_2O_3, diphenyl bismuth bromide [24,25]) used in different polymerizations, on the other hand, have been successfully employed to synthesize PLCL systems with more random nature [19]. Triphenyl bismuth (Ph_3Bi), in particular, has been used in the synthesis of other random copolyesters, namely, poly(L-lactide-co-δ-valerolactone) and poly(ethylene brassylate-co-ε-caprolactone) [26,27].

In the present chapter, with the aim of studying the effect of chain microstructures on the surface topography and mechanical properties of the synthesized copolymers, a variety of PLCLs were synthesized by ring-opening polymerization. Controlling the comonomer mass feed ratios and the catalyst/initiator (i.e., $SnOct_2$ or Ph_3Bi), PLCL copolymers showing different compositions and chain microstructures were obtained. These copolymers were subjected to isothermal treatments to control crystallinity degree (determined by means of differential scanning calorimetry) and crystal morphology (assessed by atomic force microscopy). Finally, human pulmonary fibroblasts (i.e., MRC-5 cells) were seeded on PLCLs showing different surface topographies to study the impact of surface topography on cell morphology.

3.2. Materials and methods

3.2.1. Materials

ε-Caprolactone (ε-CL) monomer and Stannous octoate ($SnOct_2$) catalyst were supplied by Merk KGaA (Germany), while L-Lactide (L-LA) monomer was provided by Corbion (The Netherlands). Triphenyl Bismuth (Ph_3Bi) catalyst was obtained from Gelest (USA). Dichloromethane and methanol were supplied by Labbox (Spain). Dulbecco's Modified Eagle Medium (DMEM), Hanks' Balanced Salt Solution (HBSS), Penicillin/Streptomycin (P/S), Foetal Bovine Serum (FBS) and rhodamine-phalloidin (Rd/Ph) were supplied by Fisher Scientific (Spain). Primary antibody Vinculin (ab129002) was supplied by Abcam (UK). Secondary antibody AlexaFluor 488 donkey anti-rabbit IgG and 16% Formaldehyde (PFA) solution were supplied by Thermo Fisher Scientific (USA). Phosphate-buffered saline (PBS), Triton X-100, Tween 20 and Fluoroshield with DAPI were supplied by Sigma Aldrich (Spain). Chloroform was supplied by PanReac (Spain).

3.2.2. Synthesis

Four different PLCL copolymers were synthetized following our previously reported protocol [28]. Briefly, copolymers based on L-LA and ε-CL were synthesized in bulk by one-pot-one-step ring-opening polymerization (ROP) with two different feed mass ratios of 80 wt.% L-LA - 20 wt.% ε-CL and 70 wt.% L-LA - 30 wt.% ε-CL. Predetermined amounts of the comonomers were placed into a round bottom flask and immersed into a controlled temperature oil bath at 140 °C until melting. To ensure an inert atmosphere, a nitrogen stream was initiated under the surface of the melt for 15 min. Subsequently, the catalyst (Ph_3Bi or $SnOct_2$) was added at a 1000:1 comonomers:catalyst molar ratio while stirring. After 24 h of reaction, the resulting product was dissolved in dichloromethane and precipitated in an excess of methanol to remove impurities and those monomers that had not reacted. Finally, the product was dried at room temperature and then dried at 100 °C for 1 h to ensure the complete elimination of remaining solvents.

3.2.3. Differential Scanning Calorimetry (DSC)

The thermal properties of the synthesized copolymers were analysed by Q200-Differential Scanning Calorimeter (TA Instruments). Samples weighing between 5 and 10 mg were encapsulated in hermetic aluminium pans to study the glass transition temperature (T_g), melting temperature (T_m) and melting enthalpy (ΔH_m). Two scans were performed. Both scans were carried out from -40 to 200 °C at 20 °C min^{-1}.

3.2.4. Gel Permeation Chromatography (GPC)

Samples were prepared at a concentration of 10 mg·mL^{-1} using chloroform as solvent. Then, the molecular weight (M_w) and distribution of the synthesized copolymers were determined in a Waters 1515 GPC device equipped with two Styragel columns (10^2 - 10^4 Å).

3.2.5 Nuclear Magnetic Resonance (RMN)

Proton and carbon nuclear magnetic resonance (^{1}H NMR and ^{13}C NMR) spectra were acquired in a Bruker Avance DPX 300 at 300.16 MHz and 75.5 MHz of resonance frequency respectively, using 5 mm O.D. sample tubes, following the previously optimized protocol [11]. Using the tables of structural determination from Prestch et al. [29], the different signals were assigned. By averaging the values of molar contents and the LA-CL dyad relative molar fractions that were obtained by means of ^{1}H and ^{13}C NMR spectroscopy, the copolymer composition data, average sequence lengths, and randomness character were calculated. The number average sequence lengths (l_i), the Bernoullian random number average sequence lengths $(l_i)_{random}$ and the randomness character (R) were obtained using equations (Equations (1)-(4)):

$$l_{\mathrm{LA}} = \frac{(\mathrm{LA}-\mathrm{LA}) + \frac{1}{2}(\mathrm{LA}-\mathrm{CL})}{\frac{1}{2}(\mathrm{LA}-\mathrm{CL})} = \frac{2(\mathrm{LA})}{(\mathrm{LA}-\mathrm{CL})} \qquad (1)$$

$$l_{\mathrm{CL}} = \frac{(\mathrm{CL}-\mathrm{CL}) + \frac{1}{2}(\mathrm{LA}-\mathrm{CL})}{\frac{1}{2}(\mathrm{LA}-\mathrm{CL})} = \frac{2(\mathrm{CL})}{(\mathrm{LA}-\mathrm{CL})} \qquad (2)$$

$$(l_{\mathrm{LA}})_{\mathrm{random}} = \frac{1}{(\mathrm{CL})};\ (l_{\mathrm{CL}})_{\mathrm{random}} = \frac{1}{(\mathrm{LA})} \qquad (3)$$

$$R = \frac{(l_{\mathrm{LA}})_{\mathrm{random}}}{l_{\mathrm{LA}}} = \frac{(l_{\mathrm{CL}})_{\mathrm{random}}}{l_{\mathrm{CL}}} \qquad (4)$$

where (LA) and (CL) are the lactide and caprolactone molar fractions, and (LA-CL), (LA-LA) and (CL-CL) are the LA-CL, LA-LA and CL-CL average dyad relative molar fractions, respectively.

3.2.6. Thermal treatments

The synthesized copolymers were subjected to three different thermal treatments within the Q200-Differential Scanning Calorimeter (TA Instruments): quenching treatment and isothermal crystallization treatments from the melt at 50 °C and 70 °C. Prior to these treatments, the

thermal history of the samples was erased in a first scan by increasing the temperature to 200 °C. Afterwards, the isothermal crystallizations were carried out from the melt, quenching to the specific temperature at a rate of 20 °C·min^{-1} and maintaining at the selected temperature (i.e., 50 or 70 °C) for 24 h. After the isothermal crystallization, the samples were rapidly quenched within the DSC to -40 °C and subjected to a second scan from -40 to 200 °C at a rate of 20 °C·min^{-1}. For the quenching treatments, a similar process was followed, first increasing the temperature to 200 °C, rapidly quenching to -40 °C and performing a second scan up to 200 °C at 20 °C·min^{-1}. The crystallinity degree (χ) of the samples was calculated based on the amount of lactide in the copolymer (determined from NMR analysis) and the enthalpy of fusion of the polylactide crystal (ΔH_m^0 = 106 J·g^{-1}) [30].

3.2.7. Atomic Force Microscopy (AFM)

The surface of the copolymers subjected to different thermal treatments (i.e., quenching and isothermal treatments from the melt at 50 and 70 °C) was analysed using a Nanoscope V Multimode AFM (Bruker). The images were obtained in PeakForce Tapping mode and employing a scanasyst-air silicon tip on nitride lever type tip, with a tip radius of 2 nm, a resonance frequency between 45-95 kHz and spring constant of 0.2-0.8 N·m^{-1}. Polymeric films of 40-70 µm were obtained by solvent casting. Solutions of concentration 5 w/v% (weight/volume ratio) in dichloromethane were poured into petri dishes. Samples were dried under the fume hood for 24 h at room temperature and then were vacuum-dried for another 24 h. Once the films were obtained, they were thermally treated. Firstly, the resulting samples were melted at 200 °C and held at this temperature for 2 min. Then, for isothermal treatments, the samples were cooled from the melt to the selected crystallization temperature (50 or 70 °C) and kept for 24 h. Finally, the films were rapidly cooled to room temperature. For the quenching treatment, the temperature of the films was rapidly lowered from 200 to -20 °C. Finally, the films were placed on glass disks and images of the topography (height image) and peak force error were acquired in different areas and various scan sizes. To obtain a comprehensive view of the morphology of the samples, several locations were scanned for each sample, progressively decreasing the scan size to allow the observation of the smaller structures. Images were then analysed by Nanoscope Analysis software. The size of crystalline formations was measured analysing the cross-sections of the height images. The roughness of the surface topology feature of PLCL films were quantified by the mean roughness (R_a).

3.2.8. Tensile Test

To study the mechanical properties of the resulting materials, the specimens were prepared by compression moulding, as previously described [10]. First, a predetermined amount of copolymer was melted at 180 °C and, subsequently, 250 bar were applied for 45 s. The samples were then rapidly quenched within the compression moulding machine. In this way, films of 250 µm thickness were obtained for mechanical evaluation. The tensile tests were carried out with an Instron 5565 testing machine at a crosshead displacement rate of 10 $mm \cdot min^{-1}$ at room temperature (21 ± 2 °C). All properties were determined as a mean value of at least four determinations, using samples of 100 mm in length and 10 mm wide with an average thickness of 250 µm.

3.2.9. Cell adhesion and immunostaining

MRC-5 cells (ATCC CCL-171) were cultured in DMEM supplemented with 10% FBS and 1% P/S and incubated in a humidified atmosphere (5% CO_2, 95% relative humidity) at 37 °C. Samples of 5x5 mm from the selected systems showing different surfaces textures (PLCL 7030 Sn iso T = 70 °C; PLCL 8020 Bi iso T = 70 °C; PLCL 8020 Sn iso T = 50 °C and PLCL 7030 Sn quenched) were placed in a culture plate, extensively washed with ethanol and subsequently washed with PBS before being air dried inside the biosafety cabinet. Then, samples were placed under ultraviolet light for 15 min to ensure sterilization. For this study, cells were seeded at a density of 2000 cells per sample. After 24 h of incubation, the culture media was aspirated and cells were washed twice with PBS before fixation with 4% PFA for 5 min. Then the PFA solution was removed and samples were washed again twice with PBS. A solution of 0.5% Triton X-100 in PBS was added and kept under slight agitation for 7 min to permeabilize the cell membrane. The solution was removed and the samples were washed again with PBS under slight agitation for 3 min, three times. A solution (1% BSA, 0.1% Tween 20 and 1:100 primary antibody) was prepared and samples were incubated with that solution in a humid chamber overnight at 4 °C. Then, the samples were washed with 0.05% Tween 20 in PBS three times and incubated with a solution containing the secondary antibody (1:200), Rd/Ph (1:100) and 1% BSA in 0.1% Tween 20 in PBS for 2.5 h in the humid chamber at 4 °C. The solution was subsequently aspirated and the samples were washed with a 0.05% Tween 20 in PBS for 7 min twice under agitation. Finally, they were washed with PBS twice for 7 min under agitation and were kept in fresh PBS before observing under fluorescence microscope. Nuclei staining with DAPI was carried out directly on the

samples by adding a drop of mounting medium before observing them under the microscope (Nikon Eclipse Ts2).

3.3 Results and discussion

3.3.1. Characterization of synthesized copolymers

In this work, four different PLCLs showing different comonomer ratios and chain microstructures were synthesized by ring-opening polymerization (Table 3.1.). The M_w achieved with this reaction was slightly higher for those copolymers synthesized with Ph_3Bi (PLCL 8020 Bi: 139,600 g·mol^{-1} and PLCL 7030 Bi: 121,400 g·mol^{-1}) than those with $SnOct_2$ (PLCL 8020 Sn: 101,600 g·mol^{-1}and PLCL 7030 Sn: 112,300 g·mol^{-1}) [31]. As expected from the glass transition temperature values of the homopolymers (i.e., T_g of PLLA around 60 °C and for PCL of -60 °C [32]), a higher T_g was observed in those copolymers with more LA content (PLCL 8020 Bi: 28.2 °C and PLCL 8020 Sn: 27.3 °C) than in those with a lower LA content (PLCL 7030 Bi: 14.0 °C and PLCL 7030 Sn: 18.3 °C). On the other hand, T_m and crystallinity degree (χ) strongly depended on the used catalyst and derived chain microstructure. The use of Ph_3Bi as a catalyst resulted in copolymers with lower T_m and χ (PLCL 8020 Bi: T_m = 105.5 °C; χ = 15.9% and PLCL 7030 Bi T_m = 127.6 °C; χ = 2.0%) in comparison to the copolymers synthesised using $SnOct_2$ (PLCL 8020 Sn: T_m = 144.6 °C; χ = 30.0% and PLCL 7030 Sn T_m = 135.0 °C; χ = 28.6%).

Table 3.1. Characterization of the synthesized copolymers.

	PLCL 8020 Bi	**PLCL 8020 Sn**	**PLCL 7030 Bi**	**PLCL 7030 Sn**
M_w (g·mol^{-1})	139,600	101,600	121,400	112,300
T_g (°C) (2nd scan)	28.2	27.3	14.0	18.3
T_m (°C) (1st scan)	105.5	144.6	127.6	135.0
ΔH_m (J·g^{-1}) (1st scan)	13.3	25.4	1.5	21.0
χ (%)	15.9	30.0	2.0	28.6
I_{LA}	3.65	5.38	2.45	4.31
I_{EB}	1.24	1.70	1.28	2.42
R	1.08	0.77	1.19	0.65
% (weight) LA	78.9	80.0	70.7	69.3
% (weigth) EB	21.1	20.0	29.3	30.7

Regarding the chain microstructure parameters, calculated by averaging the results obtained from ^{1}H and ^{13}C NMR spectroscopy (Figures 3.1. and 3.2.), the use of Ph_3Bi as catalyst favoured the formation of LA-CL dyads and alternating LA-CL-LA triads, shortening the repeat unit length values of LA (l_{LA}) and CL (l_{CL}) and leading to copolymers displaying a random character (R value close to 1). This suggests the presence of alternating monomer sequences (-LA-CL-LA-CL-LA-CL-) in the copolymer chains, explained by the transesterification reactions in the synthesis process, which lead to a shortening of the blocks in the polymer chains [33].

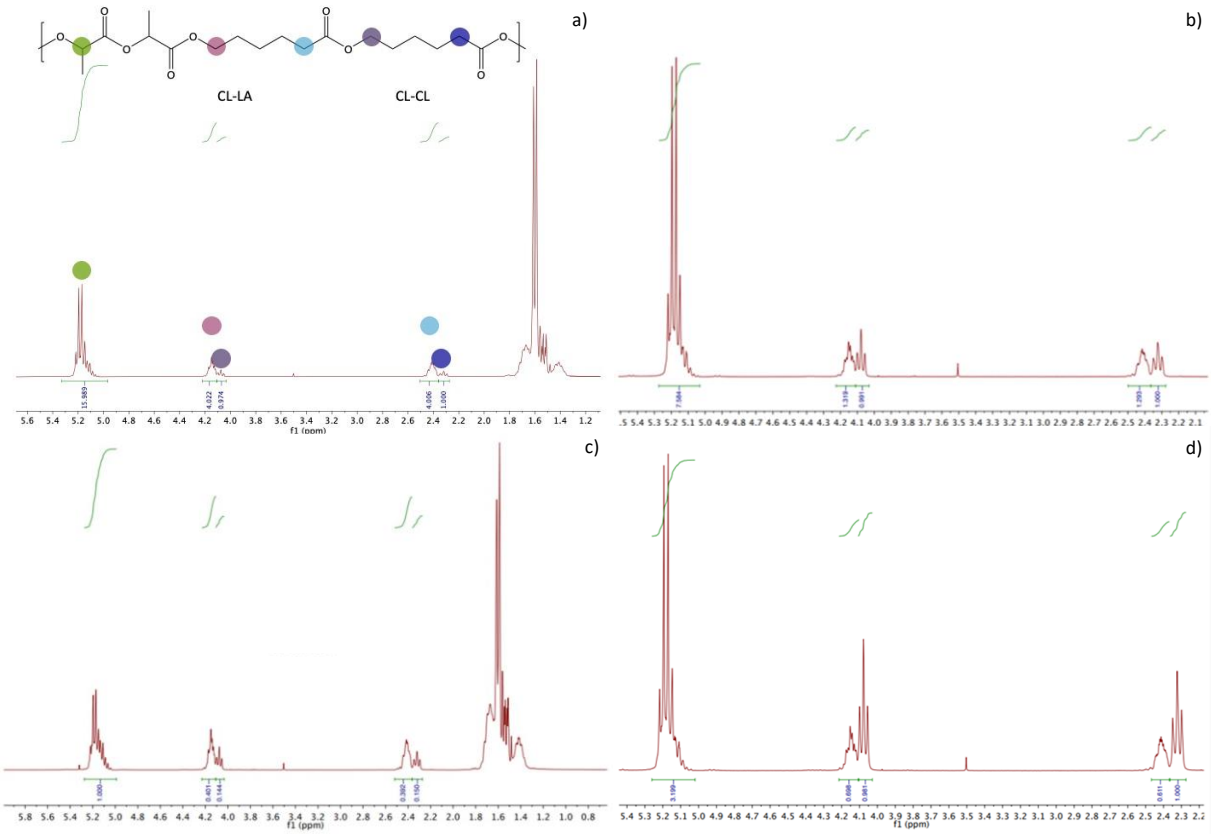

Figure 3.1. a) ^{1}H NMR spectrum of PLCL 8020 Bi and signal association. **b)** ^{1}H NMR spectrum of PLCL 8020 Sn. **c)** ^{1}H NMR spectrum of PLCL 7030 Bi. **d)** ^{1}H NMR spectrum of PLCL 7030 Sn.

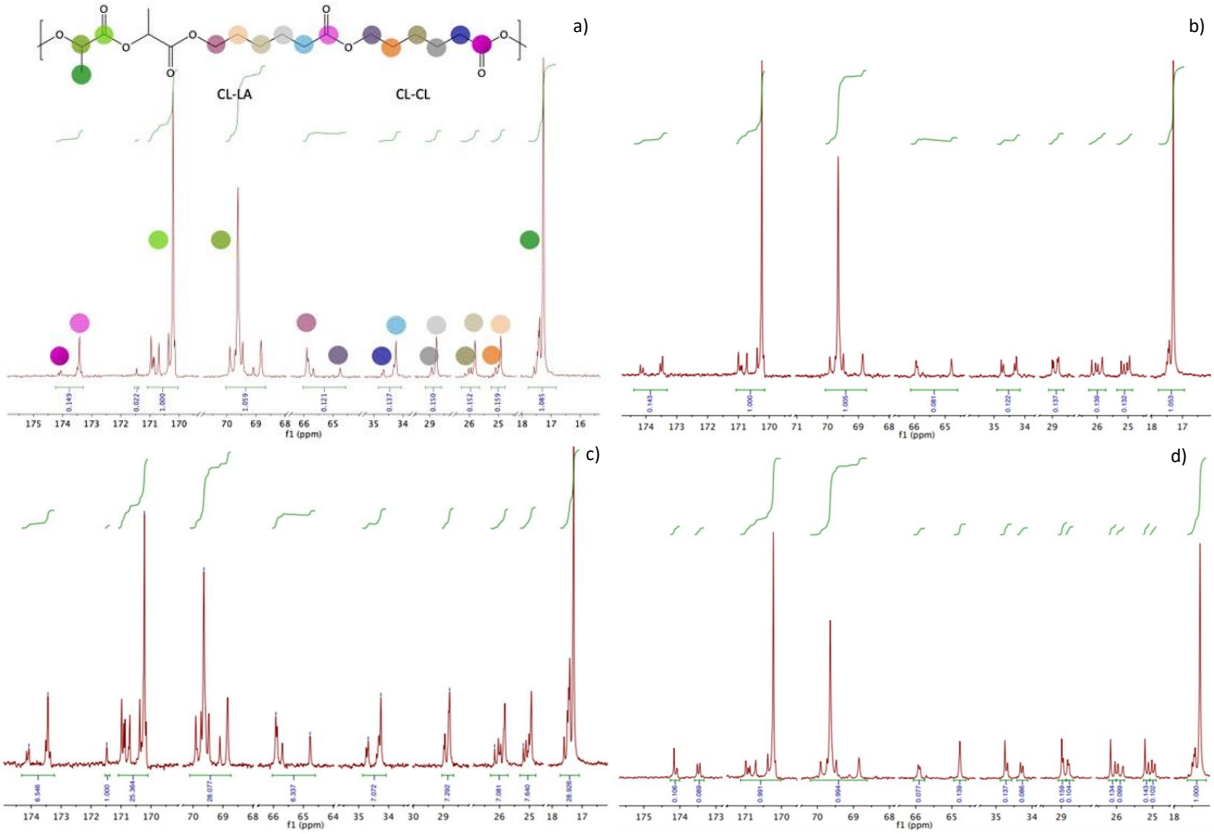

Figure 3.2. a) ^{13}C NMR spectrum of PLCL 8020 Bi. In all the C of caprolactone units the four triads, CL-CL-CL, LA-CL-CL, CL-CL-LA and LL-CL-LL from the left to the right, are observed, except for both ε and β methylene C where only dyads are observed, in CL-LA and CL-CL order for the C of ε methylene C and CL-CL and CL-LA order for the β one. **b)** ^{13}C NMR spectrum of PLCL 8020 Sn. **c)** ^{13}C NMR spectrum of PLCL 7030 Bi. **d)** ^{13}C NMR spectrum of PLCL 7030 Sn.

This effect is especially remarkable in the case of the 70:30 comonomer feed ratio. More ε-CL was available during the synthesis process, allowing the easier formation of these alternating sequences, which also explains the higher *R* value. On the other hand, the systems synthesized using $SnOct_2$ showed a blockier (but still random distribution) tendency with lower values of *R*, and longer repeat unit lengths. Considering the results obtained by NMR and DSC, it can be concluded that a higher *R* and a shorter l_{LA} (copolymers synthesized with Ph_3Bi) limit the capability of crystallization of the lactide units, causing the T_m to be lower and reducing the crystallinity degree greatly, which is evidenced in the first DSC scan (Figure 3.3.).

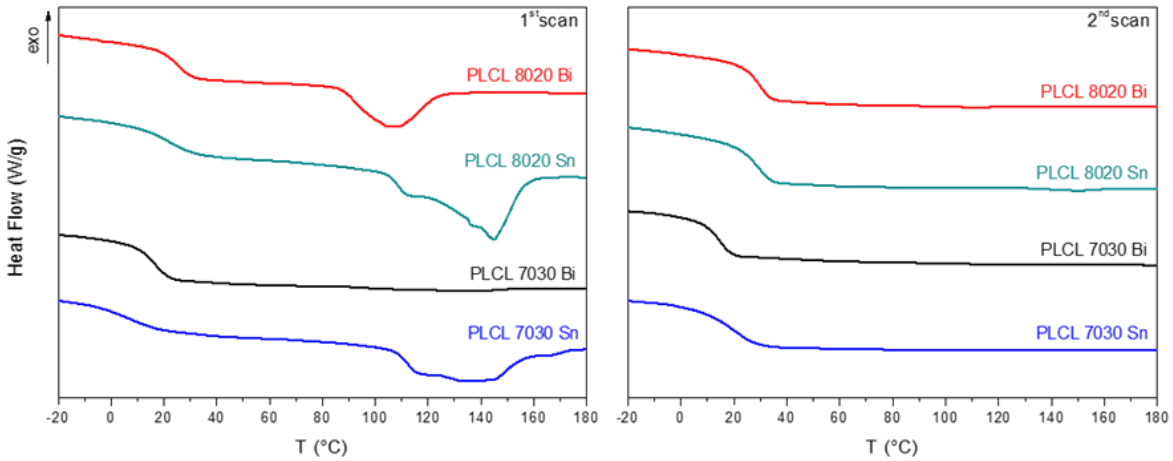

Figure 3.3. DSC thermograms of the synthesized copolymers.

In the case of the PLCL 7030 Bi, the crystallinity degree of the nascent copolymer is negligible. For the copolymers synthesized using $SnOct_2$, a much higher crystallinity degree (χ) was observed, with fractions around 30% in both cases. Both the crystallinity fraction and the T_m were slightly higher in the case of the PLCL 8020 Sn system. This could be explained by both a higher amount of crystallisable L-lactide units and the presence of longer repetitive units. It is worth mentioning that the T_g signals present a larger ΔC_p in the PLCLs with a lower crystallinity degree, as a higher proportion of the copolymer undergoes the glass transition in these cases. In the second scan (Figure 3.3.), all the PLCLs showed a homogeneous amorphous phase except the PLCL 8020 Sn, which showed a minimal melting peak (Figure 3.4.).

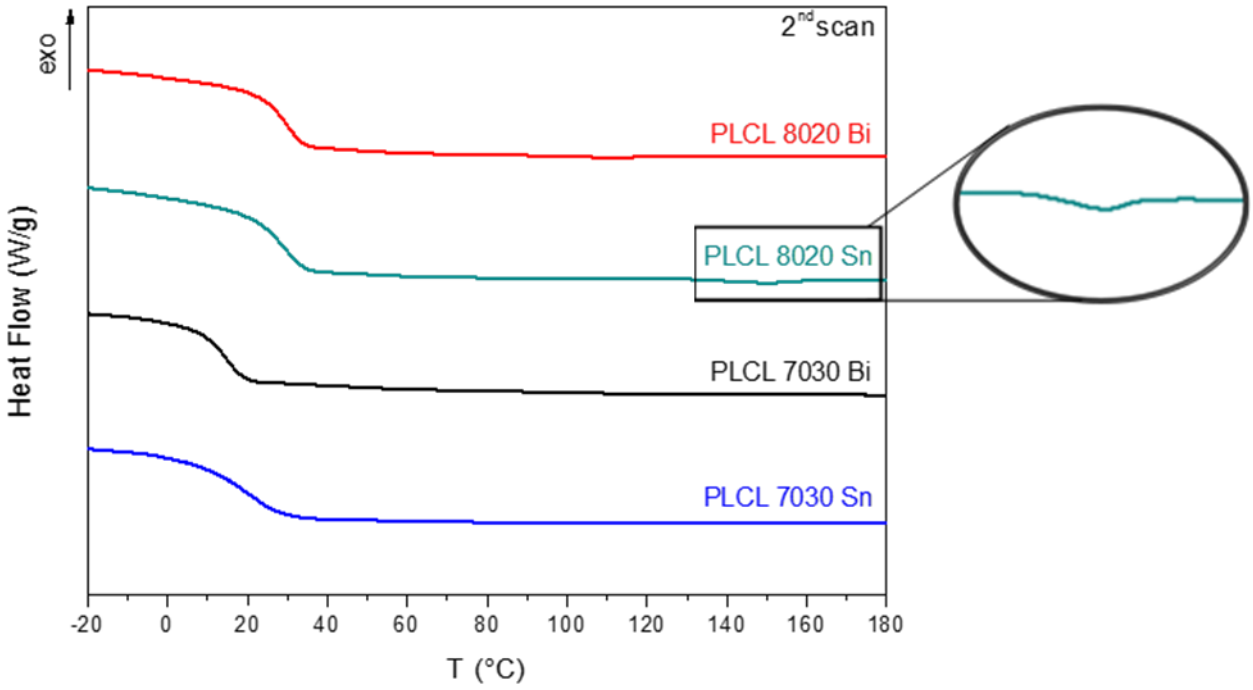

Figure 3.4. Inset of the minimal melting peak observed in PLCL 8020 Sn.

3.3.2. Thermal treatment

The synthesized copolymers were subjected to three thermal treatments (i.e., quenching and isothermal treatments from the melt at either 70 or 50 °C) within the DSC to analyse their crystallization behaviour (Table 3.2. and Figure 3.5.). In general, those copolymers synthesized with Ph_3Bi as catalyst were unable to crystallize under the studied conditions. The exception was the PLCL 8020 Bi copolymer subjected to an isothermal treatment at 70 °C, in which a melting peak centred at 108.6 °C was detected. In contrast, the copolymers synthesized with $SnOct_2$ showed a greater ability to crystallize when they were subjected to isothermal treatments from the melt, showing clearly discernible melting peaks with crystallinity degrees > 20%. However, when these copolymers were rapidly quenched from the melt, they showed a completely amorphous character.

Table 3.2. Thermal properties of quenched and isothermally crystallized poly(L-lactide-co-ε-caprolactone) (PLCL) for 24 h T_c: isothermal crystallization temperature; T_g: glass transition temperature; T_m: melting temperature; ΔH_m: melting enthalpy; χ: crystallinity degree.

	T_c (°C)	T_g 1 (°C)	T_g 2 (°C)	T_m (°C)	ΔH_m (J/g)	χ (%)
PLCL 8020 Bi	quenched	28.2	-	-	-	0.0
	50	31.3	-	-	-	0.0
	70	25.2	-	108.6	16.5	19.8
PLCL 8020 Sn	quenched	27.3	-	-	-	0.0
	50	13.3	69.2	139.4	23.2	27.4
	70	10.6	84.7	138.1	24.0	28.3
PLCL 7030 Bi	quenched	14.0	-	-	-	0.0
	50	16.1	-	-	-	0.0
	70	15.4	-	-	-	0.0
PLCL 7030 Sn	quenched	18.3	-	-	-	0.0
	50	3.4	70.4	139.7	16.7	22.8
	70	2.1	86.2	139.9	15.8	21.5

As expected, the crystallization capability of the copolymers increases with the length of the LA repeat sequences (l_{LA}). Accordingly, the calculated l_{LA} value for the PLCL 7030 Bi (i.e., l_{LA} = 2.45) is not enough to produce crystalline domains under the studied conditions. In contrast, the calculated l_{LA} value for the PLCL 8020 Bi (i.e., l_{LA} = 3.65) is sufficient to form crystalline domains when subjected to an isothermal treatment at 70 °C for 24 h. The copolymers synthesized with $SnOct_2$ as catalyst, thanks to their blockier character and subsequent longer l_{LA} (i.e., l_{LA} > 4), were prone to form crystalline domains after being subjected to isothermal treatments from the melt. Regarding the T_m, for those copolymers synthesized with $SnOct_2$ as catalyst, temperatures around 139 °C were registered. On the other hand, for those copolymers synthesized with Ph_3Bi

as catalyst, the only system capable of crystallizing was PLCL 8020 Bi subjected to an isothermal treatment from the melt at 70 °C, and showed a T_m of 108.6 °C. In any case, the T_m values of these copolymers are significantly lower than the T_m of PLLA homopolymer (T_m = 170 - 183 °C) [28]. These differences could be attributed to the decrease of I_{LA} (Table 3.1.) promoted by the presence of ε-CL repetitive units [16]. Contrarily to the melting peaks commonly observed for pure PLLA, which are relatively well-defined unimodal peaks [34], double endothermic peaks were observed in our synthesized copolymers (Figure 3.5.). This can be explained by a melt-recrystallization phenomenon. Low perfection crystals are melted to recrystallize with higher perfection and melt again at a higher temperature. This could be due to the existence of crystals with different morphologies of lamellae with variable thicknesses or by there being an intermediate constrained phase between the crystalline and the amorphous phases [35].

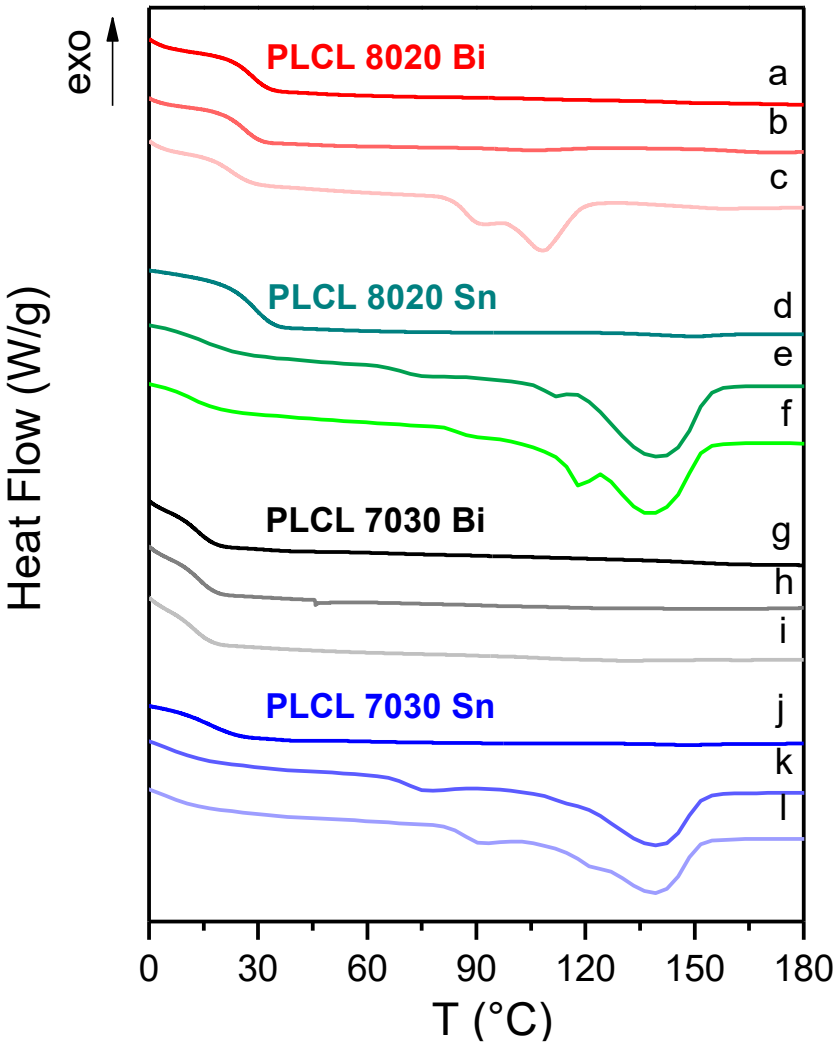

Figure 3.5. Differential scanning calorimetry traces of PLCL quenched (a, d, g and j) and isothermally crystallized at 50 °C (b, e, h and k) and 70 °C (c, f, i and l) for 24 h.

Regarding the variation of the crystallinity degree with the selected isothermal crystallization temperatures, a clear trend was not observed. Those copolymers synthesized with $SnOct_2$ showed very similar crystallinity degree values irrespective of the selected isothermal crystallization temperature (i.e., PLCL 8020 Sn: 27.4 and 28.3% at 50 and 70 °C, respectively; PLCL 7030 Sn: 22.8 and 21.5% at 50 and 70 °C, respectively). For Ph_3Bi systems, PLCL acts as a single-phase amorphous copolymer showing a single hybrid T_g located between the T_g values of the pure homopolymers. However, for those copolymers synthesized with $SnOct_2$, two T_g were registered. The lower T_g is associated to the hybrid amorphous miscible LA-CL phase, composed mostly of ε-CL units and the higher T_g suggests the presence of amorphous LA domains which are phase separated and may be constrained between the crystalline regions [36].

3.3.3. Atomic Force Microscopy (AFM)

The synthesized PLCLs showed distinct topographies depending on the used catalyst (Ph_3Bi or $SnOct_2$) and subsequent heat treatment (quenching, isothermal crystallization at 50 and 70 °C), from very smooth surfaces for amorphous samples to rougher ones for crystallized samples. In line with the DSC observations, those PLCLs synthesized with Ph_3Bi showed amorphous structures, except the PLCL 8020 Bi isothermally treated at 70 °C. The rest of the samples obtained using Ph_3Bi showed a smooth surface (R_a < 2 nm) with no discernible crystalline domains (Figure 3.6.).

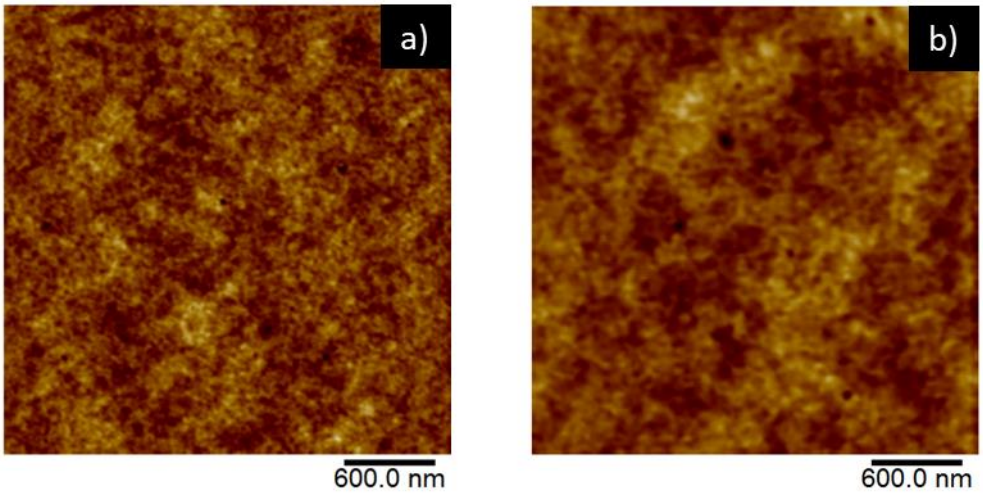

Figure 3.6. Atomic Force Microscopy height images of quenched PLCLs synthesized using Ph_3Bi as catalyst **a)** PLCL 8020 Bi and **b)** PLCL 7030 Bi.

The sample treated at 70 °C presented spherulitic morphology with average size spherulites of 7 µm. Nucleation points (white arrows) around which lamellae branch out and spherulites grow are easily distinguished in Figure 3.7.

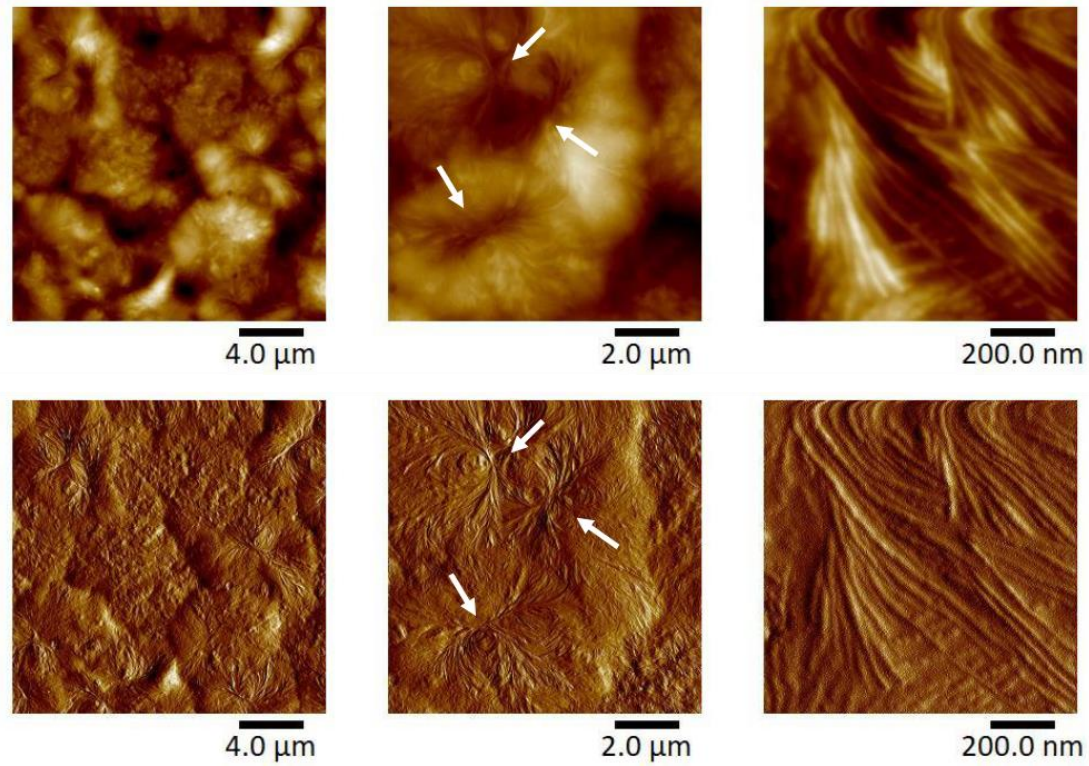

Figure 3.7. Atomic force microscopy height image (above) and peak force error image (below) of PLCL 8020 Bi isothermally crystallized at 70 °C. White arrows highlight nucleation points.

Regarding the PLCLs synthesized with $SnOct_2$, both compositions, 8020 and 7030, presented an amorphous nature after quenching from the melt, similar to those displayed in Figure 3.5.

However, both copolymers showed crystallization capability after isothermal heat treatment at specified temperatures. Interestingly, the final crystal structure varies depending on the degree of undercooling and consequently, a variety of topographic textures were obtained in terms of shape and roughness. This change in surface topology feature of the substrates following the different crystallization strategies could influence not only the mechanical properties, but also the interaction of the biomaterial with the surrounding cells and tissues once implanted. Isothermal treatment at 50 °C resulted in a small axialite-like crystalline structure for both copolymers, PLCL 8020 Sn and PLCL 7030 Sn (Figure 3.8.). The presence of numerous nucleation points at low crystallization temperatures resulted in the early impingement of crystals that cannot further grow resulting in a low roughness lamellar pattern. The average size of these lamellar crystalline structures was calculated to be 285-300 nm and the mean roughness values (R_a) 8.11 nm and 14.3 nm for PLCL 8020 Sn and PLCL 7030 Sn, respectively.

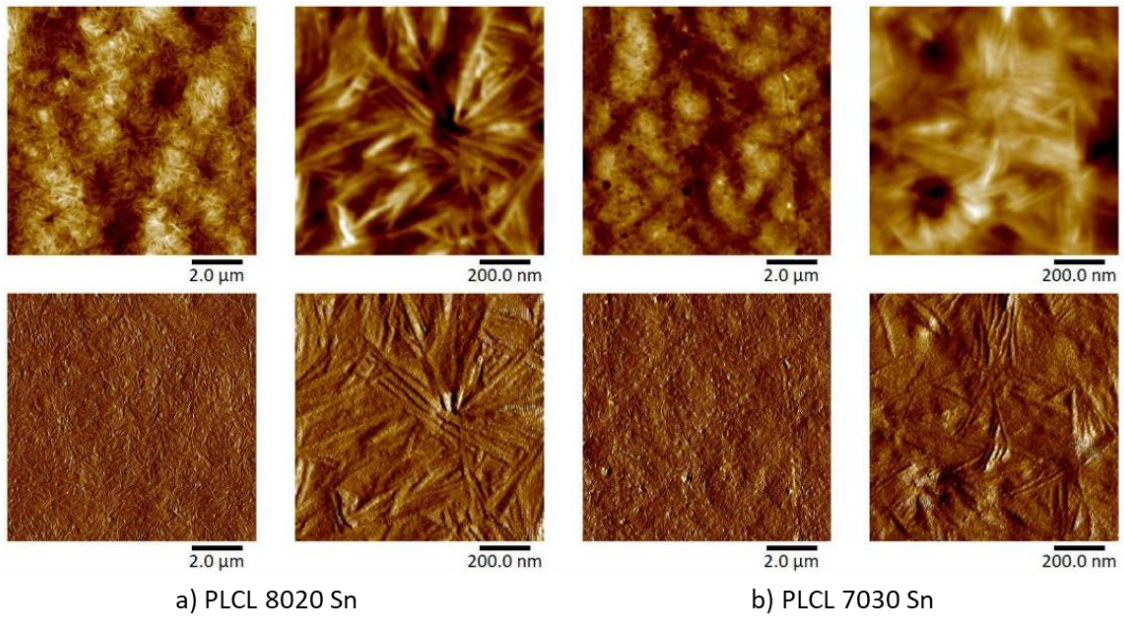

Figure 3.8 Atomic force microscopy height images (above) and peak force error images (below) of **a)** PLCL 8020 Sn and **b)** PLCL 7030 Sn isothermally crystallized at 50 °C.

The isothermal treatment at 70 °C led to clearly defined spherulitic crystalline structures for both copolymers (Figure 3.9.). The observed spherulites showed a typical crystalline structure of the poly(L-lactide) homopolymer where edge-on and flat-on structures, numbered in Figure 3.8. as 1 and 2 respectively, are easily identified in the high magnification AFM images [37]. Although there is a slight difference in the average size of the spherulites for both copolymers, 12 µm for PLCL 8020 Sn and 14 µm for PLCL 7030 Sn, bigger spherulites could be observed for the latter one, measuring up to 18 µm. The fact that PLCL 7030 Sn forms larger crystals even with less lactide content and shorter lactide building blocks (l_{LA} for PLCL 7030 Sn = 4.31 vs. l_{LA} for PLCL 8020

Sn = 5.38), is attributable to two effects: (1) its more multiblock macromolecular chain microstructure (*R* for PLCL 7030 Sn = 0.65 vs. *R* for PLCL 8020 Sn = 0.77), which might help in the crystallization process and (2) the crystallization kinetics. Both copolymers have different glass and melting temperature (see Table 3.1.) and, therefore, the 70 °C crystallization temperature (T_c) involves different levels of undercooling ($\Delta T=T_m-T_c$) for each. Smaller undercooling, as in the case of the PLCL 7030 Sn, implies the formation of less nucleation points, enabling the spherulites to grow bigger before they collide with each other.

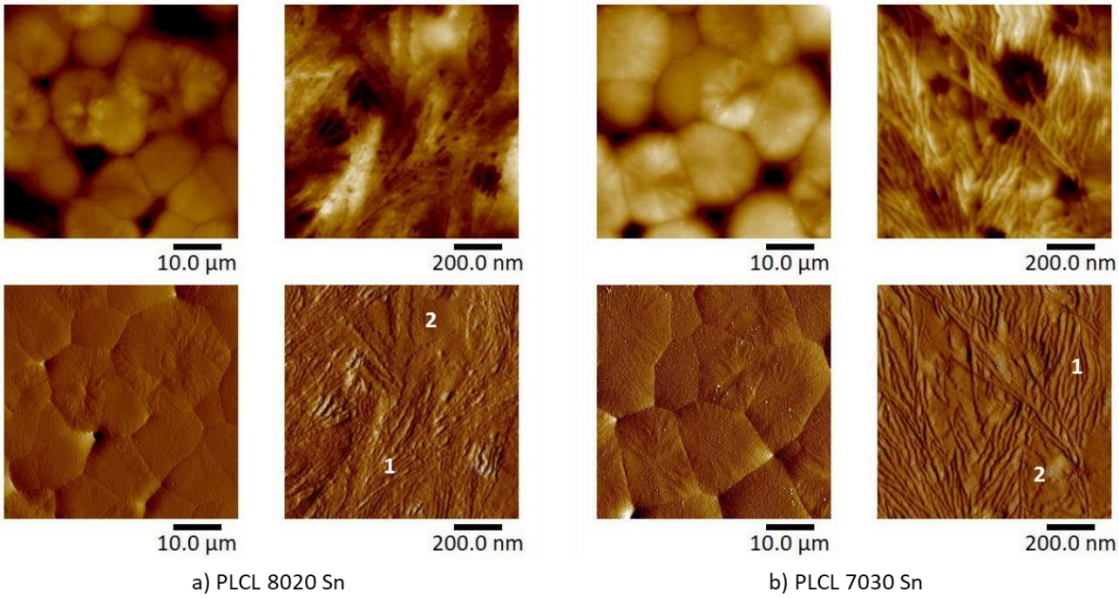

Figure 3.9. Atomic force microscopy height images (above) and peak force error images (below) of **a)** PLCL 8020 Sn and **b)** PLCL 7030 Sn isothermally crystallized at 70 °C. [Number 1 and 2 pointed edge-on and flat-on crystalline structures, respectively].

The values of surface roughness as a function of heat treatment allows us to directly differentiate the effect of crystallization process on PLCLs surface topology feature. Table 3.3. summarizes the morphologies, crystal sizes and mean roughness (R_a) of all the samples. Results revealed a remarkable difference in the roughness of the samples with spherulitic morphologies and those with either amorphous or lamellar morphologies. The presence of spherulitic morphologies, especially the PLCL 8020 Sn and PLCL 7030 Sn systems treated isothermally at 70 °C, have microcavities between the spherulites and characteristic topographies, leading to mean roughness values greater than 110 nm. However, at the same crystallization conditions, the PLCL 8020 Bi samples showed lower mean roughness value, around 39 nm. The crystalline behaviour of these copolymers is very conditioned by their L-lactide average sequence length (l_{LA}) and randomness character (*R*). Shorter l_{LA} and higher randomness character, as in the case of the

PLCL 8020 Bi, involve smaller and less regular/uniform/perfect spherulites as shown in Figure 3.6., resulting in less rough surfaces.

Table 3.3. Morphologies and roughness of quenched and isothermally crystallized PLCL.

	Treatment	Morphology	Size	R_a (nm)
PLCL 8020 Bi	quenching	amorphous	-	0.223
	Iso. 50 °C	amorphous	-	1.76
	Iso. 70 °C	spherulitic	7 µm	39.20
PLCL 8020 Sn	quenching	amorphous	-	0.882
	Iso. 50 °C	lamellar/axialitic	300 x 32 nm/800 nm	8.11
	Iso. 70 °C	spherulitic	12 µm	136
PLCL 7030 Bi	quenching	amorphous	-	0.215
	Iso. 50 °C	amorphous	-	0.302
	Iso. 70 °C	amorphous	-	0.203
PLCL 7030 Sn	quenching	amorphous	-	1.70
	Iso. 50 °C	lamellar	285 nm x 25 nm	14.30
	Iso. 70 °C	spherulitic	14 µm	110

3.3.4. Mechanical properties

The mechanical properties of the synthesized copolymers were determined by tensile test at room temperature (21 ± 2 ºC) (Figure 3.10.), where three well differentiated behaviours are discernible.

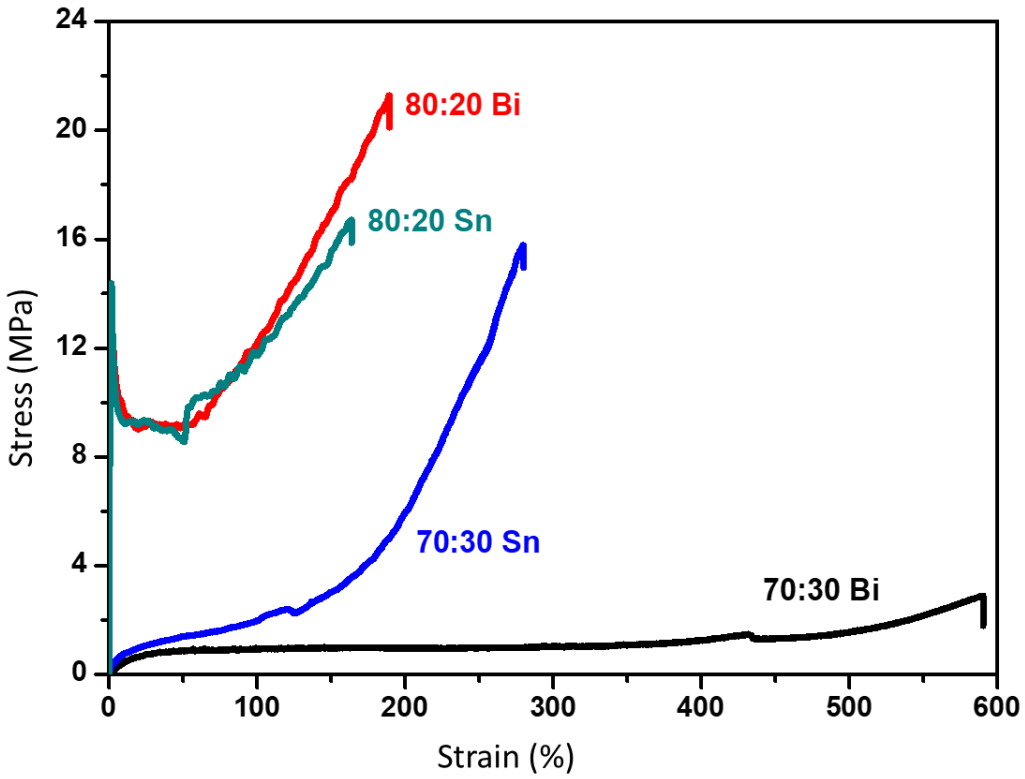

Figure 3.10. Stress-strain curves of the synthesized PLCL copolymers.

Those samples with a lower content in LA (i.e., PLCL 7030 Sn and PLCL 7030 Bi) presented an elastomeric behaviour, characterized by a low stiffness and a high strain recovery capacity after break (Table 3.4.). However, important differences were observed in the mechanical behaviour depending on the selected catalyst (i.e., $SnOct_2$ vs. Ph_3Bi). PLCL 7030 Bi showed a low secant modulus at 2% of 6.5 MPa, a strain recovery of 88.8% and an elongation at break of 589.4%. In contrast, although the PLCL 7030 Sn also showed an elastomeric behaviour, with a low secant modulus at 2% of 18.9 MPa, a strain recovery of 83.5% and an elongation at break of 268.6%, it also presented the strain-hardening phenomena at high deformations, reaching an ultimate tensile strength of 16.5 MPa. On the other hand, the copolymers with higher content in LA (i.e., PLCL 8020 Sn and PLCL 8020 Bi) showed a plastic behaviour, characterized by a well-defined yield point, a lower elongation at break (186.8% for PLCL 8020 Sn and 205.0% for PLCL 8020 Bi) and strain recovery of 32.5% for PLCL 8020 Sn and 41.9% for PLCL 8020 Bi. Also, these copolymers exhibited the strain-hardening phenomena at high deformations, which can be associated to the chain alignment at high deformations.

Table 3.4. Mechanical properties of the synthesized PLCL copolymers.

	Young´s modulus (MPa)	Secant modulus at 2% (MPa)	Ultimate tensile strength (MPa)	Elongation at break (%)	Strain recovery (%)
PLCL 8020 Bi	1795.2 ± 206.2	693.4 ± 63.7	23.1 ± 2.1	205.0 ± 18.8	41.9
PLCL 8020 Sn	2667.3 ± 66.7	714.9 ± 51.4	17.9 ± 1.8	186.8 ± 21.0	32.5
PLCL 7030 Bi	-	6.5 ± 1.8	2.0 ± 0.2	589.4 ± 26.3	88.8
PLCL 7030 Sn	-	18.9 ± 3.1	16.5 ± 0.4	268.6 ± 29.2	83.5

In general terms, it can be concluded that the more random distribution of the repetitive units obtained with the catalyst based on Ph_3Bi, results in softer copolymers with lower stiffness, higher elongation at break and higher strain recovery after break. These behaviours are in line with the results obtained in DSC (Table 3.2.). Copolymers with 80% of LA are tested at a temperature under their T_g (28.2 °C for PLCL 8020 Bi and 27.3 °C for PLCL 8020 Sn), which results in a plastic behaviour. In contrast, copolymers with a 70% in LA are tested above their T_g (14.0 °C for PLCL 7030 Bi and 18.3 °C for PLCL 7030 Sn) and displayed an elastomeric nature.

3.3.5. Interaction of human fibroblasts with various polymeric topographies

The surface topography of a biomaterial is of utmost importance in determining the fate of the surrounding cells, tissues and organs when the biomaterial is implanted in the human body. As demonstrated in the present study, by controlling the chain microstructure of L-lactide and ε-caprolactone based copolymers, a plethora of surface topographies can be developed via several thermal treatments from the melt, which will presumably determine the interaction of cells with the biomaterial. Herein, the interaction of MRC-5 cells (human fibroblasts) with different surface topographies was evaluated as a preliminary in vitro study to gain more insights about the influence of surface topography on cell behaviour. Four PLCL samples displaying different surface topographies were selected for this purpose: i) PLCL 7030 Sn subjected to an isothermal treatment at 70 °C, ii) PLCL 8020 Bi subjected to an isothermal treatment at 70 °C, iii) PLCL 8020 Sn subjected to an isothermal treatment at 50 °C and iv) PLCL 7030 Sn subjected to a rapid quenching from the melt. The selected samples had roughness (R_a) values ranging from 1.7 to 110 nm, crystallinity degrees ranging from 0 to 27.4% and different crystal morphologies (spherulitic, lamellar/axialitic), thus covering a wide range of surface topographies. As observed in the obtained micrographs (Figure 3.11.a-d), cells had a more elongated morphology in the PLCL 7030 Sn sample subjected to an isothermal treatment at 70 °C (Figure 3.11.a). This sample, as previously concluded from the AFM evaluation, had a spherulitic structure with spherulites of ~ 14 µm. In contrast, for the PLCL 7030 Sn sample subjected to a rapid quenching, cells showed a completely different shape, characterized by a more spread morphology. The surface of this sample was smooth and showed the lowest R_a value among the studied samples (R_a of 1.7 nm). These differences observed under the fluorescent microscope were further supported by quantitative values of nuclei area and aspect ratio (Figure 3.11.e and f). Statistically significant differences ($p < 0.05$) were observed in these two parameters between PLCL 7030 Sn sample subjected to an isothermal treatment at 70 °C or rapidly quenched from the melt. Accordingly, the nuclei area increased from 412.2 ± 8.4 μm^2 in the isothermally crystallized copolymer to 571.1 ± 11.3 μm^2 in the rapidly quenched sample. The aspect ratio (length/width) decreased from 1.83 ± 0.03 in the isothermally crystallized copolymer to 1.72 ± 0.02 in the rapidly quenched sample, thus confirming the conclusions drawn from the micrographs. A similar behaviour has been reported in bibliography with human articular chondrocytes [38]. In the reported study, human chondrocytes were seeded on the surface of PLLA with increasing sizes of spherulites. Those cells seeded on the PLLA sample showing largest spherulites (30 - 50 µm) display a more elongated morphology and preferred orientation, similar to the so-called contact guidance observed in nanostructured topographies. The PLCL 8020 Bi subjected to an isothermal

treatment at 70 °C shows an intermediate behaviour between the aforementioned PLCL 7030 Sn samples. In comparison to the PLCL 7030 Sn isothermally crystallized, the PLCL 8020 Bi sample shows lower R_a value (110 vs. 39.2 nm), lower crystallinity degree (21.5 vs. 19.8%) and smaller spherulites (14 vs. 7 µm). Statistically significant differences ($p < 0.05$) were observed in the nuclei area (412.2 ± 8.4 μm^2 for the PLCL 7030 Sn vs. 490.3 ± 9.5 μm^2 for the PLCL8020 Bi) of the cells seeded in these two samples. In the case of nuclei aspect ratio, although not statistically significant, a slight decrease was observed (from 1.83 ± 0.03 for the PLCL 7030 Sn to 1.81 ± 0.03 for the PLCL 8020 Bi), suggesting again that larger spherulites promote a more elongated shape of the seeded cells. Finally, the PLCL 8020 Sn sample subjected to an isothermal treatment at 50 °C was analysed. This sample, contrarily to the previously analysed ones, had a lamellar/axialitic crystal morphology and a R_a value of 8.1 nm. Although no significant differences were observed with respect to the PLCL 8020 Bi sample subjected to an isothermal treatment at 70 °C, cells appeared to be more elongated in the PLCL 8020 Sn sample isothermally crystallized at 50 °C (nuclei area was 490.3 ± 9.5 μm^2 for the PLCL8020 Bi and 466.3 ± 12.2 μm^2 for the PLCL 8020 Sn; aspect ratio was 1.81 ± 0.03 for the PLCL 8020 Bi and 1.82 ± 0.02 for the PLCL 8020 Sn). These results suggest that, not only the roughness of the surface, but also the crystal morphology of the sample may influence the cell fate.

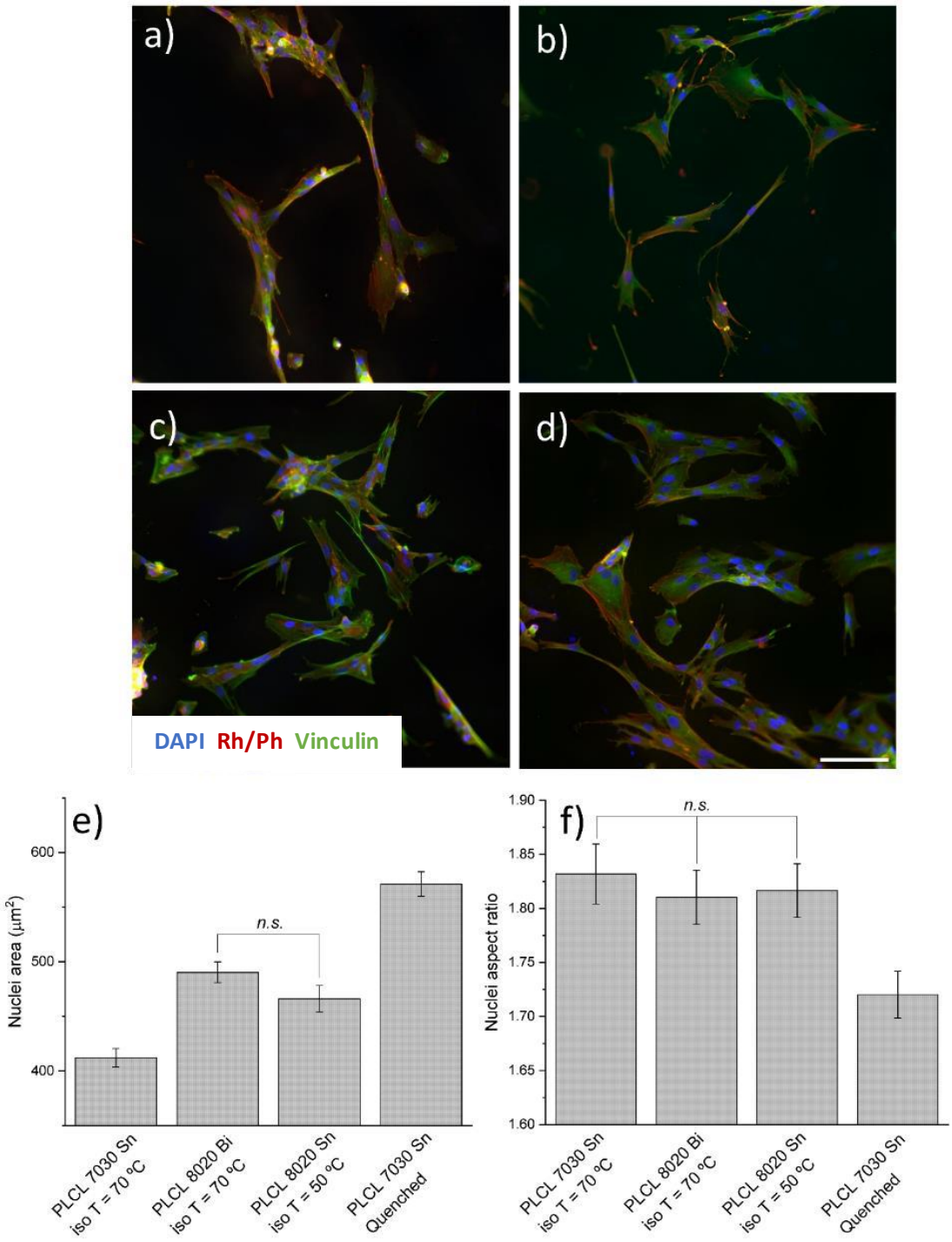

Figure 3.11. Micrographs of MRC-5 cells seeded on **a)** PLCL 7030 Sn subjected to an isothermal treatment at 70 °C, **b)** PLCL 8020 Bi subjected to an isothermal treatment at 70 °C, **c)** PLCL 8020 Sn subjected to an isothermal treatment at 50 °C and **d)** PLCL 7030 Sn subjected to a rapid quenching from the melt. Blue: DAPI (Nuclei); Red: Rhodamine-Phalloidin (Actin filaments); Green: Vinculin (Focal adhesions). Quantification of nuclei area **e)** and aspect ratio **f)** (N = 250). Error bars represent the standard error of the mean. n.s. indicates that no significant differences exist between the highlighted samples ($p < 0.05$).

The surface topography influences several important aspects of cells, including adhesion, proliferation and differentiation and strongly depends on the studied cell type. The strategy described in the present study, that relies on adjusting the chain microstructure and thermal treatments to tune the surface topography of the samples, would allow us to adjust the surface biophysical properties of the materials to fit within the requirements of the intended use. For example, osteoblasts show a better proliferation in samples with increasing surface roughness, while fibroblast prefer smoother surfaces [39]. Controlling the surface topography also allows preserving the characteristic phenotype of primary cultures (e.g., chondrocytes), which is vital for regenerative strategies that rely on tissue engineering techniques [4,40]. More recently, the impact of surface topography on the foreign body response, which will eventually determine the success of the implanted material for its intended use, has attracted increasing attention [8,41]. Thus, considering the importance of surface topography on several aspects of the biomaterials, we expect to further study the impact of these biophysical parameters on neuroinflammatory processes in the future, by using our thermoplastic elastomers with controllable surface topography and texture.

3.4. Conclusions

In the present study, a plethora of polymeric films displaying a variety of surface topographies were developed by precisely controlling the chain microstructure of lactide and caprolactone-based copolymers. The composition of the copolymers defined the mechanical properties of the resulting samples, which showed a plastic-like behaviour for those copolymers having 80 wt.% of L-lactide and an elastomeric behaviour for those copolymers having 70 wt.% of L-lactide. The selected catalyst ($SnOct_2$ vs. Ph_3Bi) determined the chain microstructure, resulting in a more random distribution of repetitive units when Ph_3Bi was used as a catalyst. This fact clearly determines the crystallization behaviour of the copolymers from the melt, which allowed us to obtain a wide variety of surface textures, ranging from smooth surfaces in the case of amorphous copolymers to rough surfaces in the case of copolymers having spherulitic or axialitic crystalline domains. In our preliminary in vitro study using human fibroblasts as model cells, we observed that cells interact differently depending on the surface biophysical properties of the films. This encourages us to further study the influence of surface topography and roughness derived from various crystallinity degrees and crystal morphologies on different cell processes, including inflammatory processes and foreign body responses.

3.5. References

[1] F.J. O'Brien, Biomaterials & scaffolds for tissue engineering, Materials Today. 14 (2011) 88–95. https://doi.org/10.1016/S1369-7021(11)70058-X.

[2] B.P. Chan, K.W. Leong, Scaffolding in tissue engineering: general approaches and tissue-specific considerations, Eur Spine J. 17 (2008) 467–479. https://doi.org/10.1007/s00586-008-0745-3.

[3] H. Ye, K. Zhang, D. Kai, Z. Li, X.J. Loh, Polyester elastomers for soft tissue engineering, Chem. Soc. Rev. 47 (2018) 4545–4580. https://doi.org/10.1039/C8CS00161H.

[4] E.C. Martínez, J.C.R. Hernández, M. Machado, J.F. Mano, J.L.G. Ribelles, M.M. Pradas, M.S. Sánchez, Human Chondrocyte Morphology, Its Dedifferentiation, and Fibronectin Conformation on Different PLLA Microtopographies, Tissue Engineering Part A. 14 (2008) 1751–1762. https://doi.org/10.1089/ten.tea.2007.0270.

[5] M.J. Dalby, S.J. Yarwood, M.O. Riehle, H.J.H. Johnstone, S. Affrossman, A.S.G. Curtis, Increasing fibroblast response to materials using nanotopography: morphological and genetic measurements of cell response to 13-nm-high polymer demixed islands, Exp Cell Res. 276 (2002) 1–9. https://doi.org/10.1006/excr.2002.5498.

[6] Y. Polo, J. Luzuriaga, J. Iturri, I. Irastorza, J.L. Toca-Herrera, G. Ibarretxe, F. Unda, J.R. Sarasua, J.R. Pineda, A. Larrañaga, Nanostructured scaffolds based on bioresorbable polymers and graphene oxide induce the aligned migration and accelerate the neuronal differentiation of neural stem cells, Nanomedicine. 31 (2021) 102314. https://doi.org/10.1016/j.nano.2020.102314.

[7] J. Luo, M. Walker, Y. Xiao, H. Donnelly, M.J. Dalby, M. Salmeron-Sanchez, The influence of nanotopography on cell behaviour through interactions with the extracellular matrix–a review, Bioactive Materials. (2021). https://doi.org/10.1016/j.bioactmat.2021.11.024.

[8] J.C. Doloff, O. Veiseh, R. de Mezerville, M. Sforza, T.A. Perry, J. Haupt, M. Jamiel, C. Chambers, A. Nash, S. Aghlara-Fotovat, J.L. Stelzel, S.J. Bauer, S.Y. Neshat, J. Hancock, N.A. Romero, Y.E. Hidalgo, I.M. Leiva, A.M. Munhoz, A. Bayat, B.M. Kinney, H.C. Hodges, R.N. Miranda, M.W. Clemens, R. Langer, The surface topography of silicone breast implants mediates the foreign body response in mice, rabbits and humans, Nat Biomed Eng. 5 (2021) 1115–1130. https://doi.org/10.1038/s41551-021-00739-4.

[9] E.S. Ereifej, C.S. Smith, S.M. Meade, K. Chen, H. Feng, J.R. Capadona, The Neuroinflammatory Response to Nanopatterning Parallel Grooves into the Surface Structure of Intracortical Microelectrodes, Adv. Funct. Mater. 28 (2018) 1704420. https://doi.org/10.1002/adfm.201704420.

[10] C. Bello-Álvarez, A. Etxeberria, Y. Polo, J.R. Sarasua, E. Zuza, A. Larrañaga, Lactide and Ethylene Brassylate-Based Thermoplastic Elastomers and Their Nanocomposites with Carbon Nanotubes: Synthesis, Mechanical Properties and Interaction with Astrocytes, Polymers. 14 (2022) 4656. https://doi.org/10.3390/polym14214656.

[11] J. Fernández, M. Montero, A. Etxeberria, J.R. Sarasua, Ethylene brassylate: Searching for new comonomers that enhance the ductility and biodegradability of polylactides, Polymer Degradation and Stability. 137 (2017) 23–34. https://doi.org/10.1016/j.polymdegradstab.2017.01.001.

[12] M. Malin, M. Hiljanen-Vainio, T. Karjalainen, J. Seppälä, Biodegradable lactone copolymers. II. Hydrolytic study of ε-caprolactone and lactide copolymers, Journal of Applied Polymer Science. 59 (1996) 1289–1298. https://doi.org/10.1002/(SICI)1097-4628(19960222)59:8<1289::AID-APP12>3.0.CO;2-1.

[13] J. Fernández, E. Meaurio, A. Chaos, A. Etxeberria, A. Alonso-Varona, J.R. Sarasua, Synthesis and characterization of poly (l-lactide/ε-caprolactone) statistical copolymers with well resolved chain microstructures, Polymer. 54 (2013) 2621–2631. https://doi.org/10.1016/j.polymer.2013.03.009.

[14] Y. Wang, M. Xia, X. Kong, S. John Severtson, W.-J. Wang, Tailoring chain structures of l -lactide and ε-caprolactone copolyester macromonomers using rac -binaphthyl-diyl hydrogen phosphate-catalyzed ring-opening copolymerization with monomer addition strategy, RSC Advances. 7 (2017) 28661–28669. https://doi.org/10.1039/C7RA05531E.

[15] Z.Y. Wei, L. Liu, J. Gao, P. Wang, M. Qi, The copolymerization of l-lactide and ε-caprolactone using magnesium octoate as a catalyst, Chinese Chemical Letters. 19 (2008) 363–366. https://doi.org/10.1016/j.cclet.2008.01.004.

[16] R. Verónica Castillo, A.J. Müller, J.M. Raquez, P. Dubois, Crystallization Kinetics and Morphology of Biodegradable Double Crystalline PLLA-b-PCL Diblock Copolymers | Macromolecules, (n.d.). https://doi.org/10.1021/ma100201g.

[17] R.-M. Ho, P.-Y. Hsieh, W.-H. Tseng, C.-C. Lin, B.-H. Huang, B. Lotz, Crystallization-Induced Orientation for Microstructures of Poly(l-lactide)-b-poly(ε-caprolactone) Diblock Copolymers, Macromolecules. 36 (2003) 9085–9092. https://doi.org/10.1021/ma0347868.

[18] H. Tsuji, Y. Tezuka, S.K. Saha, M. Suzuki, S. Itsuno, Spherulite growth of l-lactide copolymers: Effects of tacticity and comonomers, Polymer. 46 (2005) 4917–4927. https://doi.org/10.1016/j.polymer.2005.03.069.

[19] A. Pascual, H. Sardon, A. Veloso, F. Ruipérez, D. Mecerreyes, Organocatalyzed Synthesis of Aliphatic Polyesters from Ethylene Brassylate: A Cheap and Renewable Macrolactone, ACS Macro Lett. 3 (2014) 849–853. https://doi.org/10.1021/mz500401u.

[20] A. Sangroniz, L. Sangroniz, S. Hamzehlou, J. del Río, A. Santamaria, J.R. Sarasua, M. Iriarte, J.R. Leiza, A. Etxeberria, Lactide-caprolactone copolymers with tuneable barrier properties for packaging applications, Polymer. 202 (2020) 122681. https://doi.org/10.1016/j.polymer.2020.122681.

[21] D.W. Grijpma, G.J. Zondervan, A.J. Pennings, High molecular weight copolymers of l-lactide and ε-caprolactone as biodegradable elastomeric implant materials, Polymer Bulletin. 25 (1991) 327–333. https://doi.org/10.1007/BF00316902.

[22] Y. Shen, K.J. Zhu, Z. Shen, K.-M. Yao, Synthesis and characterization of highly random copolymer of ε-caprolactone and D,L-lactide using rare earth catalyst, J. Polym. Sci. A Polym. Chem. 34 (1996) 1799–1805. https://doi.org/10.1002/(SICI)1099-0518(19960715)34:9<1799::AID-POLA18>3.0.CO;2-1.

[23] I. Nifant'ev, P. Komarov, V. Ovchinnikova, A. Kiselev, M. Minyaev, P. Ivchenko, Comparative Experimental and Theoretical Study of Mg, Al and Zn Aryloxy Complexes in Copolymerization of Cyclic Esters: The Role of the Metal Coordination in Formation of Random Copolymers, Polymers. 12 (2020) 2273. https://doi.org/10.3390/polym12102273.

[24] F. Li, S. Rastogi, D. Romano, Easy access to ultra-high molecular weight polylactones using a bismuth catalyst, Journal of Catalysis. 415 (2022) 123–133. https://doi.org/10.1016/j.jcat.2022.09.015.

[25] H.R. Kricheldorf, G. Behnken, G. Schwarz, P. Simon, M. Brinkmann, High Molar Mass Poly(trimethylene carbonate) by Ph2BiOEt and Ph2BiBr-Initiated Ring-Opening Polymerizations, Journal of Macromolecular Science, Part A. 46 (2009) 353–359. https://doi.org/10.1080/10601320902724800.

[26] Z. Wei, C. Jin, Q. Xu, X. Leng, Y. Wang, Y. Li, Synthesis, microstructure and mechanical properties of partially biobased biodegradable poly(ethylene brassylate-co-ε-caprolactone) copolyesters, Journal of the Mechanical Behavior of Biomedical Materials. 91 (2019) 255–265. https://doi.org/10.1016/j.jmbbm.2018.12.019.

[27] J. Fernández, A. Larrañaga, A. Etxeberria, J.R. Sarasua, Tensile behavior and dynamic mechanical analysis of novel poly(lactide/δ-valerolactone) statistical copolymers, Journal of the Mechanical Behavior of Biomedical Materials. 35 (2014) 39–50. https://doi.org/10.1016/j.jmbbm.2014.03.013.

[28] J. Fernández, A. Etxeberria, J.R. Sarasua, Synthesis, structure and properties of poly(L-lactide-co--caprolactone) statistical copolymers, Journal of the Mechanical Behavior of Biomedical Materials. 9 (2012) 100–112. https://doi.org/10.1016/j.jmbbm.2012.01.003.

[29] Pretsch, E.; Seibl, J.; Simon, W. Tables of Spectral Data for Structure Determination Organic Compounds; 2015; Vol. 3; 626 ISBN 9783540124061., in: n.d.

[30] J.R. Sarasua, R.E. Prud'homme, M. Wisniewski, A. Le Borgne, N. Spassky, Crystallization and Melting Behavior of Polylactides, Macromolecules. 31 (1998) 3895–3905. https://doi.org/10.1021/ma971545p.

[31] J. Fernández, H. Amestoy, H. Sardon, M. Aguirre, A.L. Varga, J.-R. Sarasua, Effect of molecular weight on the physical properties of poly(ethylene brassylate) homopolymers, Journal of the Mechanical Behavior of Biomedical Materials. 64 (2016) 209–219. https://doi.org/10.1016/j.jmbbm.2016.07.031.

[32] K. Burg, Chapter 6 - Poly(α-ester)s, in: S.G. Kumbar, C.T. Laurencin, M. Deng (Eds.), Natural and Synthetic Biomedical Polymers, Elsevier, Oxford, 2014: pp. 115–121. https://doi.org/10.1016/B978-0-12-396983-5.00006-5.

[33] J. Kasperczyk, M. Bero, Coordination polymerization of lactides, 4. The role of transesterification in the copolymerization of L,L-lactide and ε-caprolactone, Die Makromolekulare Chemie. 194 (1993) 913–925. https://doi.org/10.1002/macp.1993.021940315.

[34] E. Lizundia, S. Petisco, J.R. Sarasua, Phase-structure and mechanical properties of isothermally melt-and cold-crystallized poly (L-lactide), J Mech Behav Biomed Mater. 17 (2013) 242–251. https://doi.org/10.1016/j.jmbbm.2012.09.006.

[35] E. Zuza, J.M. Ugartemendia, A. Lopez, E. Meaurio, A. Lejardi, J.-R. Sarasua, Glass transition behavior and dynamic fragility in polylactides containing mobile and rigid amorphous fractions, Polymer. 49 (2008) 4427–4432. https://doi.org/10.1016/j.polymer.2008.08.012.

[36] J. Fernández, A. Etxeberria, J.M. Ugartemendia, S. Petisco, J.-R. Sarasua, Effects of chain microstructures on mechanical behavior and aging of a poly(L-lactide-co-ε-caprolactone) biomedical thermoplastic-elastomer, Journal of the Mechanical Behavior of Biomedical Materials. 12 (2012) 29–38. https://doi.org/10.1016/j.jmbbm.2012.03.008.

[37] Y. Yuryev, P. Wood-Adams, M.-C. Heuzey, C. Dubois, J. Brisson, Crystallization of polylactide films: An atomic force microscopy study of the effects of temperature and blending, Polymer. 49 (2008) 2306–2320. https://doi.org/10.1016/j.polymer.2008.02.023.

[38] E. Costa Martínez, J.L. Escobar Ivirico, I. Muñoz Criado, J.L. Gómez Ribelles, M. Monleón Pradas, M. Salmerón Sánchez, Effect of poly(L-lactide) surface topography on the morphology of in vitro cultured human articular chondrocytes, J Mater Sci Mater Med. 18 (2007) 1627–1632. https://doi.org/10.1007/s10856-007-3038-1.

[39] T.P. Kunzler, T. Drobek, M. Schuler, N.D. Spencer, Systematic study of osteoblast and fibroblast response to roughness by means of surface-morphology gradients, Biomaterials. 28 (2007) 2175–2182. https://doi.org/10.1016/j.biomaterials.2007.01.019.

[40] E. Costa, C. González-García, J.L. Gómez Ribelles, M. Salmerón-Sánchez, Maintenance of chondrocyte phenotype during expansion on PLLA microtopographies, J Tissue Eng. 9 (2018). https://doi.org/10.1177/2041731418789829.

[41] C. Vallejo-Giraldo, K. Krukiewicz, I. Calaresu, J. Zhu, M. Palma, M. Fernandez-Yague, B. McDowell, N. Peixoto, N. Farid, G. O'Connor, L. Ballerini, A. Pandit, M.J.P. Biggs, Attenuated Glial Reactivity on Topographically Functionalized Poly(3,4-Ethylenedioxythiophene):P-Toluene Sulfonate (PEDOT:PTS) Neuroelectrodes Fabricated by Microimprint Lithography, Small. 14 (2018) e1800863. https://doi.org/10.1002/smll.201800863.

CHAPTER 4

Lactide and ethylene brassylate-based thermoplastic elastomers and their nanocomposites with carbon nanotubes: synthesis, mechanical properties and interaction with astrocytes

CHAPTER 4. Lactide and ethylene brassylate-based thermoplastic elastomers and their nanocomposites with carbon nanotubes: synthesis, mechanical properties and interaction with astrocytes

Abstract

Polylactide (PLA) is among the most commonly used polymers for biomedical applications thanks to its biodegradability and cytocompatibility. However, its inherent stiffness and brittleness are clearly inappropriate for the regeneration of soft tissues (e.g., neural tissue), which demands biomaterials with soft and elastomeric behaviour capable of resembling the mechanical properties of the native tissue. In this work, both L- and D,L-lactide were copolymerized with ethylene brassylate, a macrolactone that represents a promising alternative to previously studied comonomers (e.g., caprolactone) due to its natural origin. The resulting copolymers showed an elastomeric behaviour characterized by relatively low Young's modulus, high elongation at break and high strain recovery capacity. The thermoplastic nature of the resulting copolymers allows the incorporation of nanofillers (i.e., carbon nanotubes) that further enable the modulation of their mechanical properties. Additionally, nanostructured scaffolds were easily fabricated through a thermo-pressing process with the aid of a commercially available silicon stamp, providing geometrical cues for the adhesion and elongation of cells representative of the nervous system (i.e., astrocytes). Accordingly, the lactide and ethylene brassylate-based copolymers synthesized herein represent an interesting formulation for the development of polymeric scaffolds intended to be used in the regeneration of soft tissues, thanks to their adjustable mechanical properties, thermoplastic nature and observed cytocompatibility.

4.1. Introduction

Polylactides (PLA) are well-known biocompatible and bioresorbable polyesters used in several biomedical applications as drug delivery systems, implants and cellular scaffolds for tissue engineering applications [1]. However, due to its inherent stiffness (Young's modulus (E) of 1 - 3.5 GPa for poly(D,L-lactide)(PDLLA) and 2.7 - 4.1 GPa for poly(L-lactide)(PLLA)) and brittleness (elongation at break (ε) of 10% for PDLLA and PLLA) [2], the use of PLA for the regeneration of many tissues in the human body is restricted, because of the elastomeric and soft behaviour that these tissues generally present. Thus, several strategies such as increasing the molecular mass, cross-linking, incorporating nanoparticles/nanofibers [3] or copolymerization [4] are regularly considered to modulate the mechanical properties of PLA [5]. Among them, the copolymerization of lactide with (macro)lactones (e.g., caprolactone [6] or ethylene brassylate (EB) [4]) has been widely explored as a strategy to provide enhanced flexibility to the polymeric chain and the resulting polymeric devices [5]. EB is a macrolactone extracted from castor oil that represents a more economical approach to alternative counterparts (e.g., ε-caprolactone). In addition, its natural origin allows us to avoid dependence on fossil feedstock [7].

In the present chapter, EB was used for the synthesis of LA-based copolymers with adjustable mechanical properties that can match those of the nervous system, which shows Young´s modulus between 0.5 and 16 MPa and an ultimate strain of 61 - 81% [8–10]. Accordingly, lactide-ethylene brassylate (LA-EB) copolymers could represent an interesting alternative to the more widely explored poly(lactide-co-ε-caprolactone) (PLCL) copolymers [11,12], explored in the previous chapter. The LA-EB copolymers synthesized in the present chapter show thermoplastic behaviour, allowing its processing by both traditional (e.g., injection moulding, extrusion) or more advanced (e.g., electrospinning, 3D printing, lithography) fabrication techniques. Consequently, complex nanostructures mimicking the extracellular matrix where cells reside can be developed, improving in this way the interaction between cells and the copolymer in terms of proliferation, adhesion and cell fate [13]. Another advantage of thermoplastic (co)polyesters is the possibility of adding (nano)particles (e.g., carbon nanotubes (CNT)) into the polymeric matrix. CNTs are one carbon atom layers rolled as a cylinder that can improve mechanical properties, provide nanoroughness [14] to the polymer surface and provide electrical conductivity to the polymeric device [15]. In the biomedical field, CNTs have shown to be an ideal substrate due to their good compatibility and the ability to promote the adhesion and proliferation of various cell lines [16], particularly for the regeneration of the nervous system [17]. In the present study, poly(D,L-lactide-co-ethylene brassylate) (PDLEB) and poly(L-lactide-co-ethylene brassylate) (PLEB) copolymers were synthesized by ring-opening polymerization

using triphenyl bismuth as catalyst-initiator. To modulate their properties, CNTs were incorporated into the polymeric matrix at different concentrations.

Finally, with the aim of studying the interaction of our materials with cells representative of the nervous system, the metabolic activity and adhesion of mouse astrocytes (C8-D1A) were assessed in both flat and nanopatterned surfaces. Astrocytes are the most abundant glial cells in the nervous system and provide support and nutrients to neurons. When an injury occurs in the nervous system, a gap can be created between the nerves. In the regeneration process to rejoin the nerve cells, astrocytes can become reactive, contributing to the formation of a glial scar, a physical and chemical barrier that prevents the correct axonal regeneration [18]. Previous studies show that polymeric materials with specific topographies can influence the astrocytes' inflammatory response, which is translated into the bio-integration of the implanted material [19]. It has also been shown that CNTs can induce morphological changes in astrocytes, provoking even functional changes [20]. Considering the relevance of astrocytes for regenerative purposes, in the present chapter, their interaction with a fully implantable polymeric device is preliminarily studied after a thorough characterization of the synthesized copolymers in terms of mechanical, thermal, morphological and surface properties.

4.2. Materials and methods

4.2.1. Materials

Ethylene brassylate (EB) monomer was supplied by Sigma Aldrich (Spain), while D,L-lactide and L-lactide monomers were provided by Corbion (The Netherlands). The triphenyl bismuth (Ph_3Bi) catalyst was obtained from Gelest (USA). Dichloromethane and n-Hexane were supplied by Labbox (Spain). Multi-Walled Carbon Nanotubes (MWCNT), having an average diameter of 10-15 nm with 5-15 walls and 1-10 µm in length, were supplied by Arkema (France). Dulbecco's Modified Eagle Medium (DMEM), Hanks' Balanced Salt Solution (HBSS), Penicillin Streptomycin (P/S), Fetal Bovine Serum (FBS), AlamarBlue cell viability reagent and rhodamine-phalloidin were supplied by Fisher Scientific (Spain). Laminin, PBS (Phosphate-buffered saline), Diiodomethane, Fluoroshield with DAPI, Triton X-100 and Tween 20 were supplied by Sigma Aldrich (Spain), and 16% Formaldehyde solution was supplied by Thermo Fisher Scientific (USA). Chloroform was supplied by PanReac (Spain).

4.2.2. Synthesis

For the synthesis of the copolymers, we followed our previously described protocol [4]. Briefly, copolymers from D,L-LA or L-LA and EB were synthesized in bulk by one pot-one step ring-opening polymerization (ROP) with a feed molar composition of 70% LA and 30% EB. Polymerizations were carried out in a round bottom flask immersed in a controlled temperature oil bath at 140 °C. When the monomers were melted, a nitrogen stream was initiated under the surface of the melt to purge the flask for 15 min. Subsequently, the catalyst (Ph_3Bi) was added at 100:1 comonomers/catalyst molar ratio under stirring. After 72 h of reaction, the product was dissolved in dichloromethane and precipitated in excess of n-hexane (previously cooled at 4 °C) to remove the catalyst impurities and those monomers that had not reacted. Finally, the product was dried at room temperature and then subjected to a heat treatment at 100 °C for 1 h to ensure the complete elimination of any remaining solvent.

4.2.3. Incorporation of MWCNT in the polymeric matrix and composite preparation

First, the copolymer was dissolved in dichloromethane. Different amounts of MWCNT (0.1, 0.5 and 1 wt.%) were added while the polymeric solution was under stirring. This range of carbon nanotubes was selected based on our previous work [15], where the resulting polymeric matrix showed appropriate electrical conductivity and a slight stiffening with respect to the pristine polymer at these MWCNT ratios. The mixture was sonicated with a UP400St ultrasonic processor (Hielscher Ultrasonics, Germany) (with a 14 mm diameter sonotrode) for 20 min, with a 100% amplitude, in pulses of 1 s. The mixture was then transferred into a beaker under stirring until most of the solvent had been eliminated. The resultant product was vacuum-dried for 5 days to eliminate the remaining solvent. The system without MWCNT underwent the same process. Subsequently, films of 250 μm thickness were obtained by compression moulding using a Collin P 200 hydraulic press (Collin, Germany). First, a predetermined amount of copolymer was melted at 140 °C for poly(D,L-lactide-co-ethylene brassylate) (PDLEB) and 160 °C for poly(L-lactide-co-ethylene brassylate) (PLEB) for 5 min. Then, 250 bars were applied for 45 s. To eliminate any remaining solvent, the film was placed under vacuum and 60 °C for PDLEB and 85 °C for PLEB for 30 min. Then, the film was cut into pieces and then processed again by compression moulding to obtain the final film. The films were stored at -20 °C until their mechanical characterization to avoid any possible aging during their storage. To create a nanopattern on the surface of the films, lithography was carried out, as previously reported by us [11]. Briefly, a commercially available

silicon stamp with a 300 nm period nanopattern was replicated on the surface of the film by applying pressure and increasing the temperature to 200 °C [21].

4.2.4. Differential Scanning Calorimetry (DSC)

The thermal properties of the synthesized copolymers and final films were analysed by Differential Scanning Calorimetry (DSC) on a Q200 model (TA Instruments, USA). Samples weighing between 5 and 10 mg were encapsulated in hermetic aluminium pans to study the glass transition temperatures (T_g), melting temperature (T_m) and melting enthalpy (ΔH_m). Two scans were performed. Both scans were carried out from -80 to 180 °C in the case of PDLEB and from -80 to 200 °C in the case of PLEB, at 20 °C·min^{-1}.

4.2.5. Gel Permeation Chromatography (GPC)

The molecular weight (M_w) and dispersity index of the synthesized copolymers and final films were determined in a Waters 1515 GPC device equipped with two Styragel columns (10^2-10^4 Å) (Waters, Milford, MA, USA). Samples were prepared at a concentration of 10 mg·mL^{-1} in chloroform and filtered with a 0.2 µm pore size filter.

4.2.6. Nuclear Magnetic Resonance (NMR)

Proton and carbon nuclear magnetic resonance (^{1}H NMR and ^{13}C NMR) spectra were acquired in a Bruker Avance DPX 300 (Bruker, USA) at 300.16 MHz and 75.5 MHz of resonance frequency, respectively, using 5 mm O.D. sample tubes. From solutions of 0.7 mL of deuterated chloroform, all spectra were obtained at room temperature. Experimental conditions are the same as reported in the bibliography [4]. For ^{1}H NMR: 10 mg of sample; 3 s acquisition time; 1 s delay time; 8.5 µs pulse; spectral width 5000 Hz and 32 scans. For ^{13}C NMR: 40 mg, inverse gated decoupled sequence; 3 s acquisition time; 4 s delay time; 5.5 µs pulse; spectral width 18,800 Hz and more than 10,000 scans. Using the tables of structural determination from Prestch et al. [22], the different signals were assigned. By averaging the values of molar contents and the LA-EB dyad relative molar fractions that were obtained by means of ^{1}H and ^{13}C NMR spectroscopy, the copolymer composition data, average sequence lengths, and randomness character were calculated. The number average sequence lengths (l_i), the Bernoullian random number average

sequence lengths (l_i)random and the randomness character (R) were obtained using equations (Equations (1)-(4)):

$$l_{\mathrm{LA}} = \frac{(\mathrm{LA}-\mathrm{LA}) + \frac{1}{2}(\mathrm{LA}-\mathrm{EB})}{\frac{1}{2}(\mathrm{LA}-\mathrm{EB})} = \frac{2(\mathrm{LA})}{(\mathrm{LA}-\mathrm{EB})} \qquad (1)$$

$$l_{\mathrm{EB}} = \frac{(\mathrm{EB}-\mathrm{EB}) + \frac{1}{2}(\mathrm{LA}-\mathrm{EB})}{\frac{1}{2}(\mathrm{LA}-\mathrm{EB})} = \frac{2(\mathrm{EB})}{(\mathrm{LA}-\mathrm{EB})} \qquad (2)$$

$$(l_{\mathrm{LA}})_{\mathrm{random}} = \frac{1}{(\mathrm{EB})}; (l_{\mathrm{EB}})_{\mathrm{random}} = \frac{1}{(\mathrm{LA})} \qquad (3)$$

$$R = \frac{(l_{\mathrm{LA}})_{\mathrm{random}}}{l_{\mathrm{LA}}} = \frac{(l_{\mathrm{EB}})_{\mathrm{random}}}{l_{\mathrm{EB}}} \qquad (4)$$

where (LA) and (EB) are the lactide and ethylene brassylate molar fractions, and (LA-EB), (LA-LA) and (EB-EB) are the LA-EB, LA-LA and EB-EB average dyad relative molar fractions, respectively.

4.2.7. Electron microscopy analysis

Scanning electron microscopy (SEM) (HITACHI S-4800) was used to analyse the surface morphology of the scaffolds. Samples were coated with a 150 Å layer of gold in a JEL Ion Sputter JFC-1100 at 1200 V and 5 mA before being analysed. The successful dispersion of CNTs on polymeric matrix was studied by Transmission electron microscopy (TEM) (JEOL 1400 Plus) (JEOL, Tokyo, Japan).

4.2.8. Tensile test

The mechanical properties of the resulting films were determined by tensile test with an Instron 5565 testing machine at a crosshead displacement rate of 10 mm·min^{-1} at room temperature (21 ± 2 °C) and human body temperature (37 ± 2 °C). Samples of 100 mm in length and 10 mm wide were cut from films of 250 µm average thickness. All properties were determined as the mean value of at least four determinations.

4.2.9. Contact angle

Static contact angle measurements were carried out at room temperature by sessile drop method in order to evaluate the surface energy of copolymeric films. To calculate it, the Fowkes' method was applied by equation (5), where $\gamma_l = \gamma_l^d + \gamma_l^p$ are the total, γ_l^d are the dispersive and γ_l^p are the polar components of the liquid surface energy. Water (γ_l^d= 21.8 mJ·m^{-2} and γ_l^p= 51 mJ·m^{-2}) and diiodomethane (γ_l^d= 50.8 mJ·m^{-2} and γ_l^p= 0 mJ·m^{-2}) were used as the test liquids [23]. Briefly, at least 4 drops of 10 µL were placed on the surface of the films. Then, average values of contact angles were obtained using a Krüss Drop Shape Analyzer DSA100.

$$\gamma_l(1+\cos\theta) = 2\left(\sqrt{\gamma_l^d\gamma_s^d} + \sqrt{\gamma_l^p\gamma_s^p}\right) \qquad (5)$$

where, γ_s^d and γ_s^p are de dispersive and polar components of the surface energy for solid surface respectively.

4.2.10. Cell Viability assay

C8-D1A cells (ATCC, USA) were cultured in Dulbecco's Modified Eagle Medium (DMEM) supplemented with 10% FBS and 1% P/S. Cultures were maintained in a humidified atmosphere (5% CO_2, 95% relative humidity) at 37 °C. Three circular samples of 10 mm diameter were punched out from each system and placed in a 24 well plate. The circular samples were extensively washed with ethanol and subsequently washed with PBS before being air dried inside the biosafety cabinet. Finally, they were placed under ultraviolet light for 15 min. To enhance cell attachment, laminin (1:200) was used to cover the films and wells. Samples were incubated for 2 h at 37 °C, and subsequently washed with PBS to remove the excess of laminin, before astrocytes were seeded. To assess the cell viability, 10,000 cells were seeded per well. After either 24 h or 48 h, the cell medium was replaced by cell medium containing 10% of AlamarBlue reagent. Cells were incubated for 4 h sheltered from light. Finally, the metabolic activity was determined by measuring the fluorescence (λ_{ex} = 480 nm/λ_{em} = 595 nm) of the media on a BioTek Synergy H1 plate reader.

4.2.11. Immunostaining

C8-D1A cells were seeded on the films in the same way as explained for the cell viability assay. After 48 h, cells were fixed with 4% PFA for 10 min at room temperature. Then, PFA was aspirated and the samples were washed with sterile HBSS twice. A solution of 0.5% Triton X-100 in PBS was added to permeabilize the membrane of the cells and kept under slight agitation for 10 min. The solution was removed and the samples were washed with PBS under slight agitation for 5 min, twice. Then, 300 µL per well of rhodamine-phalloidin (Rd/Ph) solution was added, and the plate was incubated under slight agitation for 15 min. Rd/Ph solution was removed and the samples were washed twice with 0.1% Tween 20 in PBS for 5 min under slight agitation. Finally, samples were washed with PBS for 5 min under slight agitation, and were kept in fresh PBS before observing them under fluorescence microscope. Nuclei staining with DAPI was carried out directly on the samples by adding a drop of mounting medium before observing them under the microscope (Nikon Eclipse Ts2).

4.2.12. Statistical Analysis

At least 4 measurements for AlamarBlue were assayed. Results were presented as the mean average ± SD or SEM. One-way ANOVA, non-parametric Holm-Sidak or Kruskal-Wallis tests were used to compare data from several groups, and they were followed by a Dunn's post hoc analysis. We considered statistical significance to be *p<0.05.

4.3. Results and Discussion

4.3.1. Synthesis and initial characterization of the copolymers

Table 4.1. summarizes the initial characterization of the synthesized copolymers. The reaction was carried out at 140 °C for 3 days. In the case of poly(D,L-lactide-co-ethylene brassylate) (PDLEB), the resulting copolymer presented a M_w of 242,850 g·mol^{-1} and a T_g of 33.5 ± 2.0 °C, which are higher than the ones referenced in bibliography for copolymers with similar composition [4]. In the case of poly(L-lactide-co-ethylene brassylate) (PLEB), the copolymer had a M_w of 325,790 g·mol^{-1} and a T_g of 41.0 ± 4.5 °C. Additionally, the PLEB copolymer presented a melting point with a T_m of 158.0 ± 1.5 °C and a crystallinity degree (χ) of 29.1% (Figure 4.1.).

Table 4.1. Characterization of the synthesized copolymers.

	PDLEB	PLEB
M_w (g·mol^{-1})	242,850	325,790
T_g (°C) (2nd scan)	33.5 ± 2.0	41.0 ± 4.5
T_m (°C) (1st scan)	-	158.0 ± 1.5
ΔH_m-ΔH_{cc} (J g^{-1}) (1st scan)	-	26.4
χ (%)	-	29.1
l_{LA}	16.00	11.36
l_{EB}	1.30	1.45
R	0.83	0.78
% (weight) LA	86.8	80.6
% (weight) EB	13.2	19.4
% (molar) LA	92.5	88.7
% (molar) EB	7.5	11.3

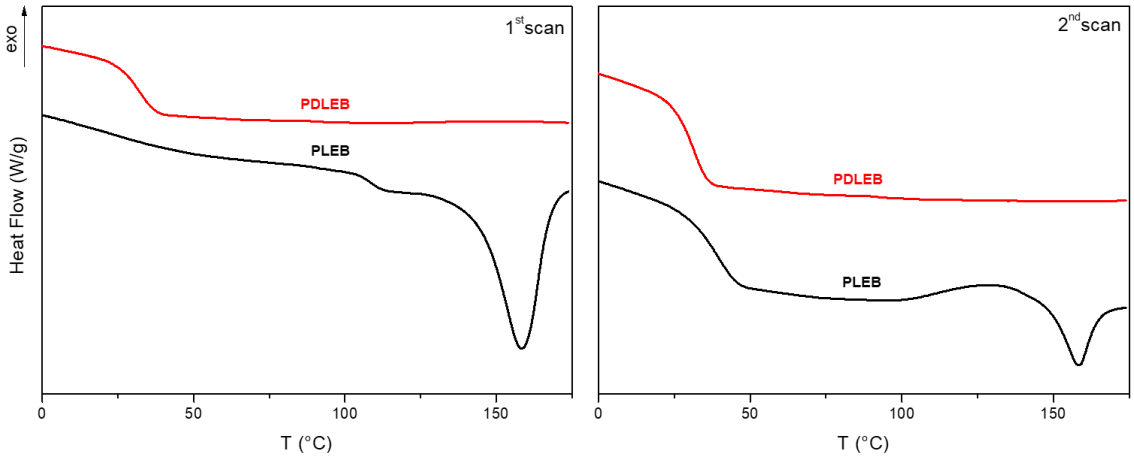

Figure 4.1. DSC thermograms of the synthesized copolymers.

As reported in bibliography, the conversion of LA is significantly higher than EB [4]. After the synthesis, only 13.2 % and 19.4 % (in weight) of EB became part of PDLEB and PLEB copolymers, respectively. As a result of this slower reaction rate, LA was consumed more quickly than EB. Along with this, the randomness character (R) value was 0.83 for PDLEB and 0.78 for PLEB, which led to random distribution of sequences ($R \rightarrow 1$). The incorporation of EB promotes the decrease in the average sequence lengths of LA (l_{LA}) as it has been reported in bibliography [4]. For

example, a PDLEB (co)polymer with 97% in D,L-LA presents a l_{LA} of 30.81, in contrast to our PDLEB that showed a l_{LA} of 16.00 and of 11.36 for the PLEB counterpart. In that same study, the reported EB-unit average sequence length presents a l_{EB} of 0.93, which is lower than the one observed in our PDLEB (l_{EB} of 1.30) and PLEB (l_{EB} of 1.45) copolymers. As a result, the chain microstructure of our (co)polymers is more randomly distributed. The molar compositions depicted in Table 4.1. were calculated by averaging the results obtained from ^{1}H and ^{13}C NMR spectroscopy (Figure 4.2.).

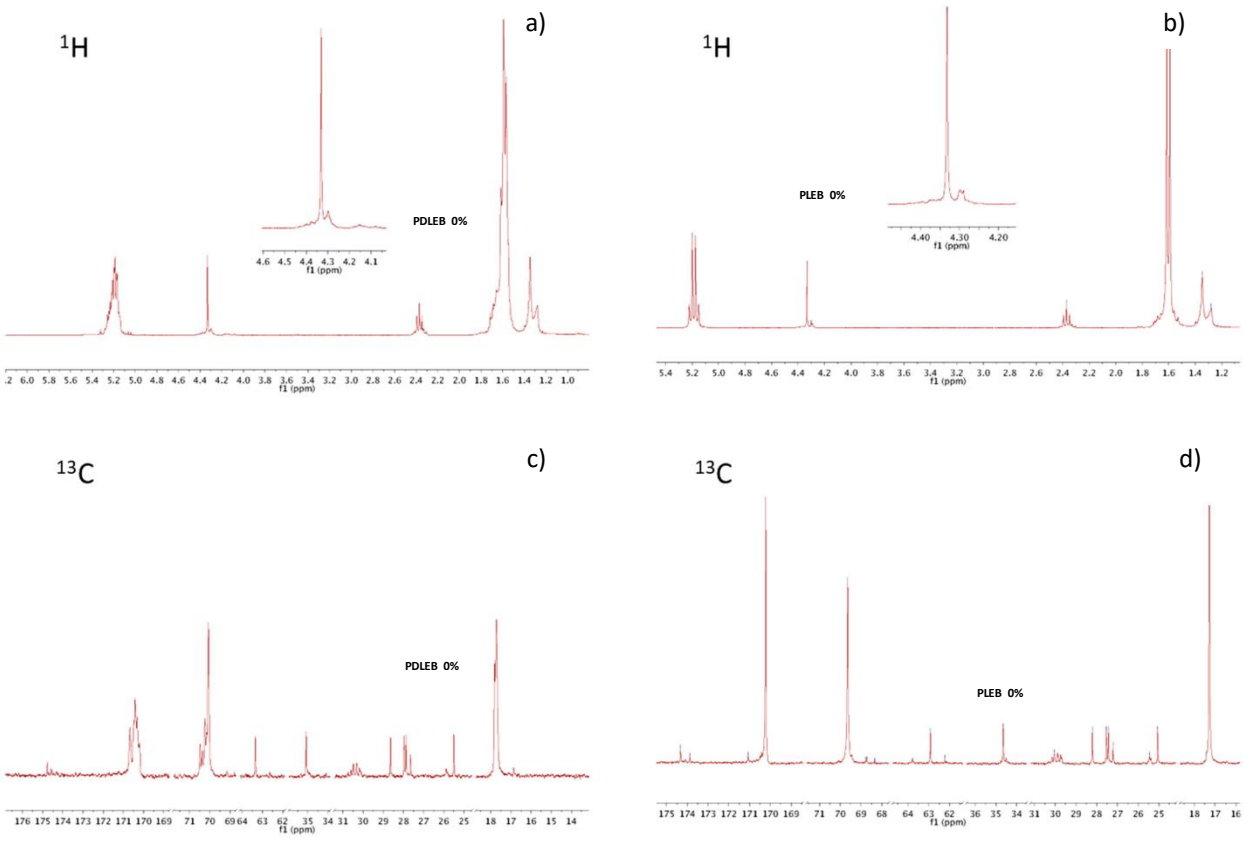

Figure 4.2. a) ^{1}H NMR spectrum of PDLEB 0% CNT. **b)** ^{1}H NMR spectrum of PLEB 0%CNT. **c)** ^{13}C NMR spectrum of PDLEB 0% CNT. **d)** ^{13}C NMR spectrum of PLEB 0% CNT.

4.3.2. Incorporation of MWCNTs in the polymeric matrix and preparation of composites

The processing conditions followed to incorporate the CNTs in the polymer matrix induced a decrease in the M_w. Table 4.2. shows that PDLEB films had a final M_w between 190,150 g·mol^{-1} and 215,390 g·mol^{-1}, which represents a lost in M_w between 11.3% - 21.7% with respect to the

initial molecular weight of the synthesized copolymer. In the case of PLEB films, with final M_w ranging from 210,170 g·mol^{-1} to 256,410 g·mol^{-1}, they experimented a decrease between 21.3% - 33.6%. In both cases, the addition of CNTs did not seem to play a major role in the observed molecular weight decrease.

Table 4.2. Molecular weights of the resulting films after their processing and incorporation of CNTs.

M_w (g·mol^{-1})	**PDLEB**				**PLEB**			
%CNTs	0%	0.1%	0.5%	1%	0%	0.1%	0.5%	1%
Synthesized	242,850				325,790			
Final film	207,540	190,150	194,120	215,390	250,050	210,170	256,410	216,270
ΔM_w (%)	14.5	21.7	20.1	11.3	23.2	35.5	21.3	33.6

Table 4.3. shows the thermal properties of the resulting films, which are also represented in Figure 4.3. For PDLEB, the T_g decreased from 33.5 ± 2.0 °C to values between 25.0 ± 1.5 °C and 28.0 ± 2.0 °C in the 1st scan. For PLEB, the T_g decreased from 41.0 ± 4.5 °C to values between 30.0 ± 1.0 °C and 37.4 ± 4.2 °C. The incorporation of CNTs seemed to slightly increase the observed T_g in the case of PLEB. This might be ascribed to the capacity of CNTs to reduce the mobility of the polymeric chains in the amorphous phase [24].

Table 4.3. Thermal properties of the resulting films after their processing and incorporation of CNTs.

Film	**PDLEB**			
%CNTs	**0%**	**0.1%**	**0.5%**	**1%**
T_g (°C) (1st scan)	28.0 ± 2.0	25.0 ± 1.5	27.0 ± 0.5	27.0 ± 2.0
T_g (°C) (2nd scan)	28.0 ± 3.0	27.0 ± 3.0	29.0 ± 1.0	27.0 ± 2.0
	PLEB			
%CNTs	**0%**	**0.1%**	**0.5%**	**1%**
T_g (°C) (1st scan)	30.0 ± 1.0	34.0 ± 1.0	33.5 ± 1.0	37.4 ± 4.2
T_m (°C) (1st scan)	156.0 ± 0.0	159.0 ± 0.0	158.0 ± 1.0	159.3 ± 0.7
ΔH_m-ΔH_{cc} (J·g^{-1}) (1st scan)	12.0 ± 1.0	11.0 ± 0.5	8.6 ± 2.7	10.1 ± 1.6
T_g (°C) (2nd scan)	30.0 ± 0.0	36.0 ± 2.0	33.5 ± 2.0	34.7 ± 2.4

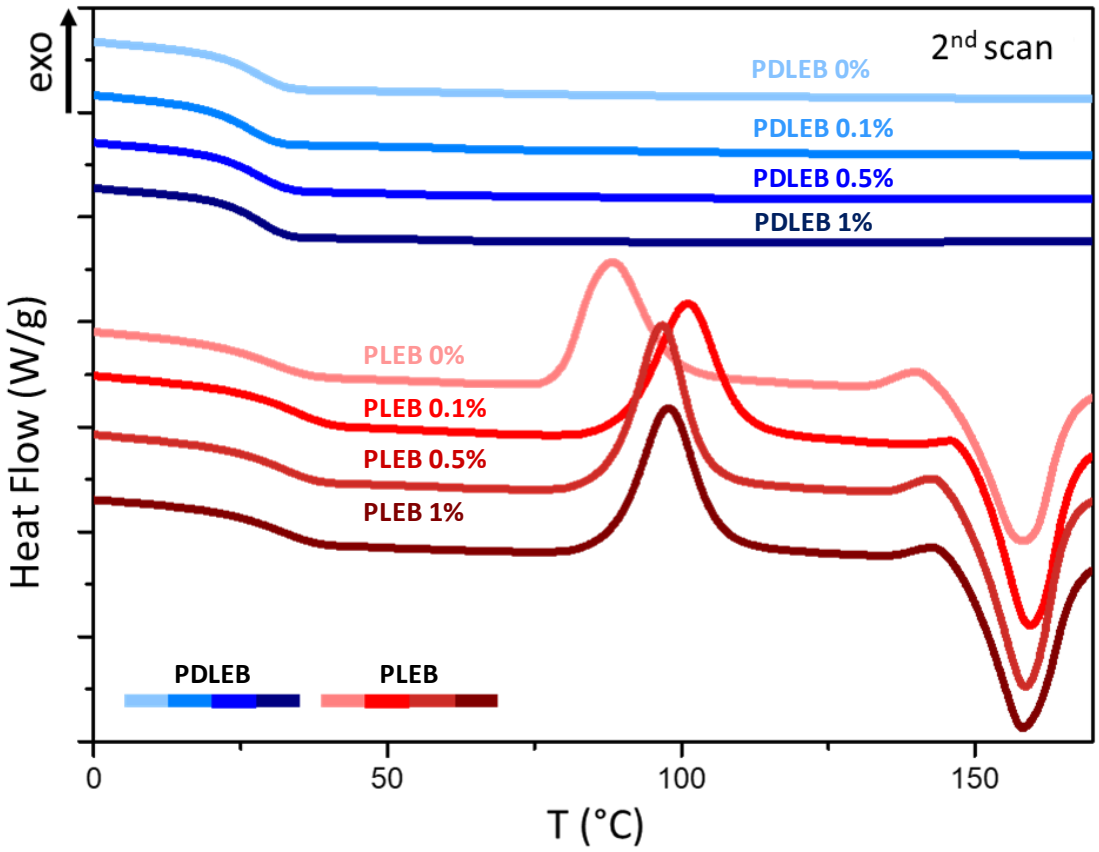

Figure 4.3. DSC thermogram (2nd scan) of final films.

The successful incorporation of MWCNTs and their dispersion in the polymeric matrix were assessed by transmission electron microscopy (TEM). Figure 4.4. shows the TEM micrographs of PDLEB films with either 0.5% (Figure 4.4.a) or 1% (Figure 4.4.c) CNTs, while Figure 4.4.b and Figure 4.4.d shows PLEB with 0.5% and 1% CNT, respectively. The incorporation of 1% CNTs resulted in the observation of many bundles of CNTs. In contrast, when 0.5% CNTs were incorporated, a relatively good dispersion with fewer bundles was observed.

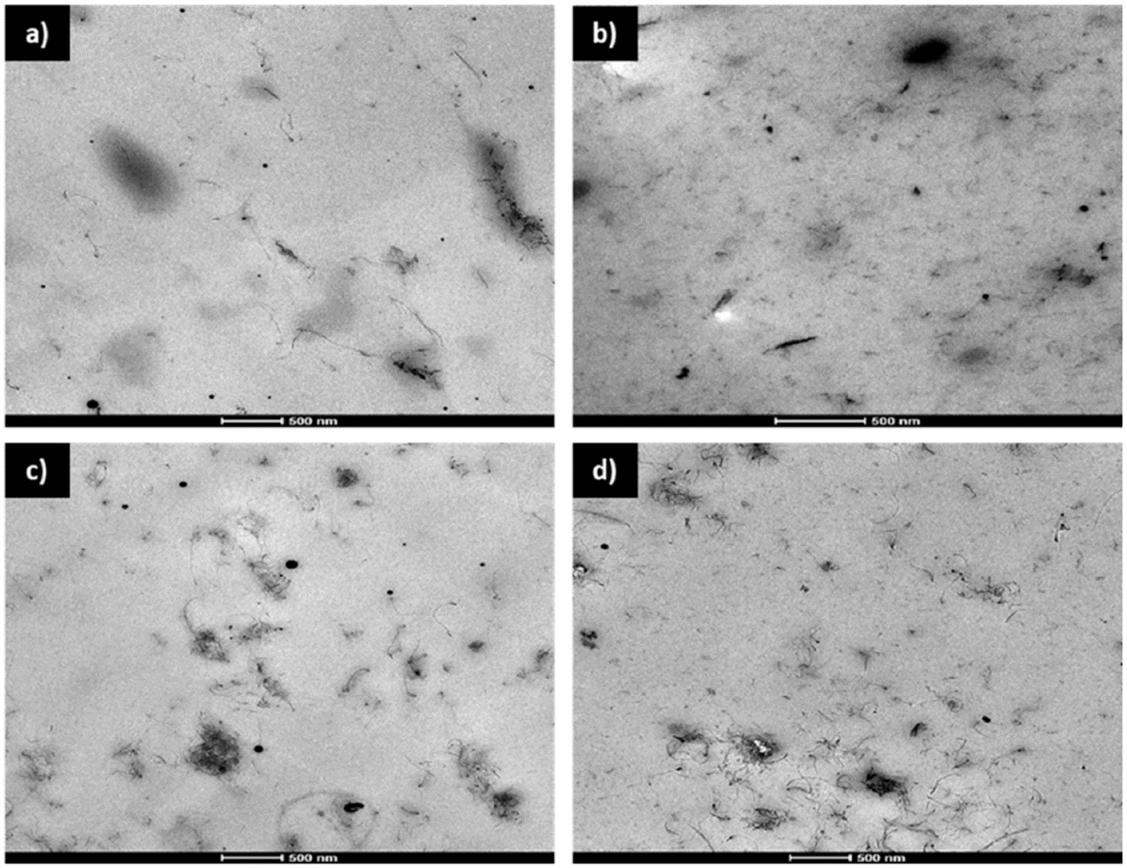

Figure 4.4. Transmission Electron Micrographs (TEM) from PDLEB samples of 0.5% CNT **a)** and 1% CNTs **c)**; and PLEB samples of 0.5% CNTs **b)** and 1% CNTs **d)**.

4.3.3. Mechanical properties

Stress-strain curves of the synthesized copolymers at room temperature are presented in Figure 4.5. The PDLEB samples showed a typical elastomeric behaviour with relatively low Young´s modulus and high elongation at break. In contrast, the PLEB samples showed a plastic behaviour, characterized by a well-defined yield point and lower elongation at break and strain recovery after break.

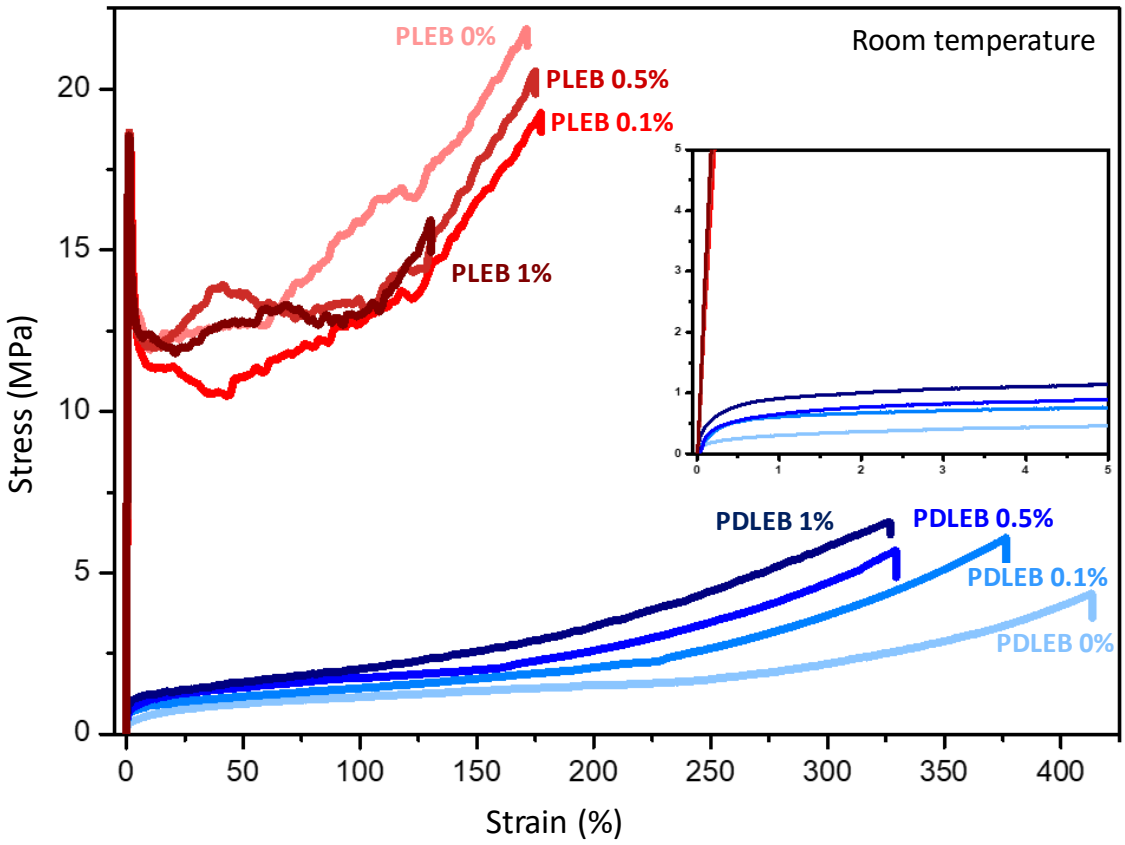

Figure 4.5. Mechanical properties of PDLEB and PLEB copolymers with different % of CNTs at room temperature.

Figure 4.6. shows the elastomeric behaviour of both (co)polymers PDLEB and PLEB at body temperature (37 °C). PLEB samples showed the strain-hardening phenomena at high deformations, whereas PDLEB samples displayed a more linear behaviour, keeping a constant stress value with the deformation.

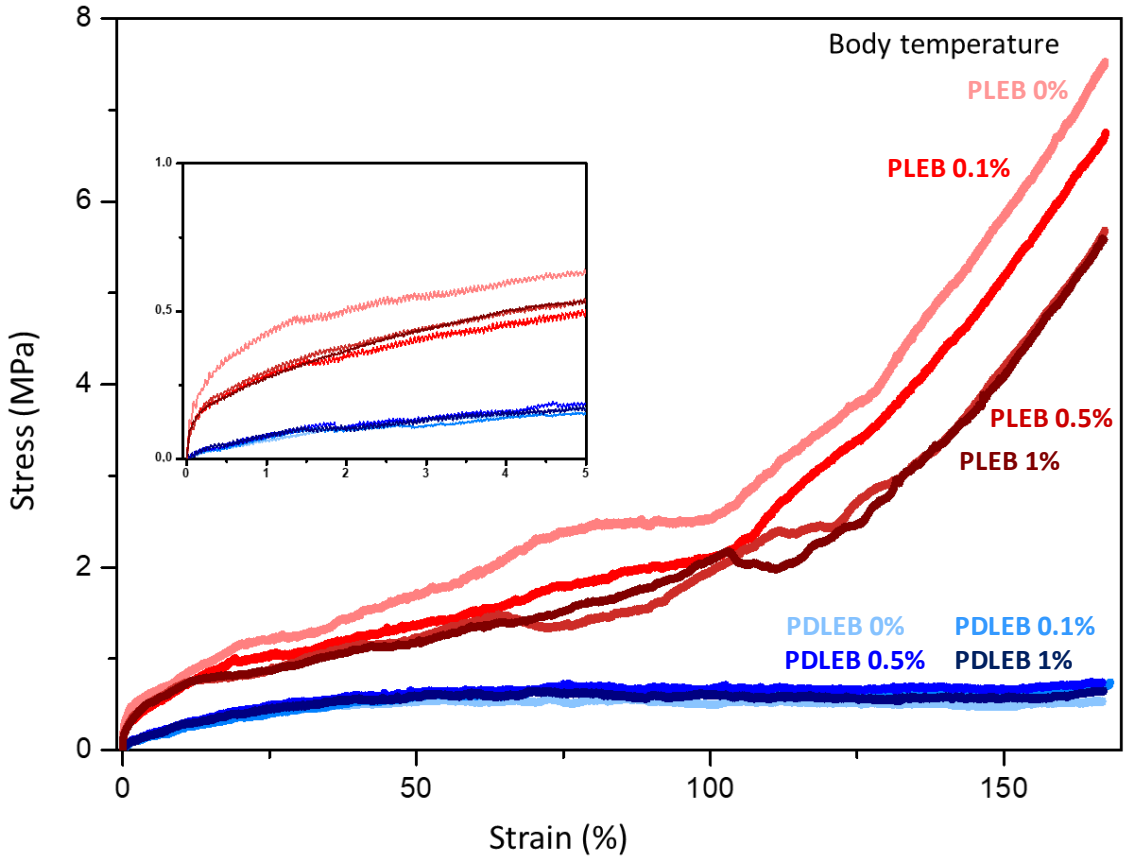

Figure 4.6. Mechanical properties of PDLEB and PLEB copolymers with different % of CNTs at body temperature.

The mechanical properties for PDLEB and PLEB copolymers are also summarized in Table 4.4. The incorporation of D,L- or L-lactide in the copolymer had a strong impact on the strength-related mechanical properties. In this sense, those copolymers synthesized with L-lactide showed much higher values for Young´s modulus and strength, but lower values of elongation at break and strain recovery after break. As an illustration, the films with no CNTs had a Young´s modulus and yield strength at room temperature of 2076.6 ± 171.0 and 14.1 ± 2.5 MPa respectively for PLEB films, whereas these values were much lower for the PDLEB counterpart (Young´s modulus: 390.3 ± 28.8 MPa/Yield strength: 0.7 ± 0.1 MPa). However, the elongation at break and strain recovery after break were respectively 177.2 ± 7.6 and 27.5 ± 1.1% for PLEB films, but increased to 397.2 ± 21.1 and 91.5 ± 2.0% for the PDLEB counterpart. The lower glass transition temperature of PDLEB copolymers, together with the lack of crystalline domains in their structure, could be associated to the "softer" behaviour of the PDLEB films in comparison to PLEB films. This same behaviour was also observed at body temperature (i.e., 37 °C) but with lower strength-related values, due to the proximity of the glass transition temperature and the corresponding glassy-to-rubbery transition.

Table 4.4. Mechanical properties of the resulting films at ambient temperature (Ta) and body temperature (T37).

	PDLEB	Young´s modulus (MPa)	Secant Modulus at 2% (MPa)	Ultimate tensile Strength (MPa)	Elongation at break (%)	Yield strength or Offset Yield strength at 10% (MPa)	Strain recovery (%)
Ta	0%	390.3 ± 28.	19.4 ± 1.7	3.8 ± 0.4	397.2 ± 21.1	0.7 ± 0.1*	91.5 ± 2.0
T37			6.6 ± 0.6	0.7 ± 0.1	> 167	0.3 ± 0.1*	72.7 ± 2.2
Ta	0.1%	763.9 ± 61.8	26.7 ± 5.6	5.9 ± 0.2	382.0 ± 25.5	1.6 ± 0.2*	95.6 ± 1.0
T37			4.5 ± 0.2	0.7 ± 0.1	> 167	0.3 ± 0.1*	83.2 ± 3.1
Ta	0.5%	1337.5 ± 102.6	146.4 ± 9.9	9.4 ± 0.5	322.0 ± 17.8	2.5 ± 0.3*	93.4 ± 0.8
T37			5.7 ± 0.6	0.9 ± 0.1	> 167	0.4 ± 0.1*	74.1 ± 3.8
Ta	1%	1181.4 ± 41.9	77.5 ± 13.1	5.4 ± 0.4	307.4 ± 19.1	1.2 ± 0.2*	96.6 ± 0.3
T37			6.3 ± 0.5	0.8 ± 0.1	> 167	0.4 ± 0.0*	71.5 ± 4.8
	PLEB						
Ta	0%	2076.6 ± 171.0	638.8 ± 81.2	21.6 ± 0.4	177.2 ± 7.6	14.1 ± 2.5	27.1 ± 1.1
T37			23.5 ± 1.1	6.9 ± 0.6	> 167	0.9 ± 0.1*	66.3 ± 3.4
Ta	0.1%	2318.0 ± 187.1	729.8 ± 119.1	19.1 ± 2.4	171.6 ± 13.6	16.3 ± 2.3	28.5 ± 0.6
T37			30.6 ± 0.8	6.4 ± 0.5	> 167	0.8 ± 0.3*	65.0 ± 2.5
Ta	0.5%	2395.6 ± 158.6	689.3 ± 105.8	19.1 ± 3.2	165.4 ± 15.8	17.2 ± 3.4	19.2 ± 1.8
T37			24.1 ± 2.3	6.0 ± 0.6	> 167	0.8 ± 0.2*	61.5 ± 2.9
Ta	1%	2449.5 ± 299.2	679.7 ± 78.5	18.3 ± 1.2	123.2 ± 10.3	18.3 ± 1.2	21.2 ± 0.6
T37			16.5 ± 1.5	5.8 ± 0.6	> 167	0.8 ± 0.2*	62.4 ± 3.6

*Offset Yield strength was calculated at a 10% of strain using the secant modulus at 2% as elastic modulus (E).

Regarding the effect of CNTs, the addition of CNTs significantly increased the Young´s modulus in PDLEB films from 390.3 ± 28.8 MPa for 0% CNTs to 763.9 ± 61.8 for 0.1% CNTs and 1337.5 ± 102.6 MPa for 0.5% CNTs. However, the PDLEB sample containing 1% CNTs showed a decreased Young´s modulus of 1181.4 ± 41.9 MPa, which can be ascribed to the poor dispersion of CNTs in the polymer matrix as observed in TEM images [15]. For PLEB, the Young's modulus did not experience a significant increase with respect to the amount of CNTs, but there was a small

difference between the samples with CNTs (2318.0 ± 187.1 MPa for 0.1% CNTs, 2395.6 ± 158.6 MPa for 0.5% CNTs and 2449.5 ± 299.2 MPa for 1% CNTs) and those without (2076.6 ± 171.0 MPa for 0% CNTs). Regarding the yield strength for PDLEB, which was calculated as offset yield strength at 10%, it suffered an increase from 0.7 ± 0.1 MPa for 0% CNTs to 1.6 ± 0.2 MPa for 0.1% CNTs and 2.5 ± 0.3 MPa for 0.5% CNTs. Contrarily, the 1% CNTs PDLEB sample showed a decrease to 1.2 ± 0.2 MPa, in line with the decrease showed in Young's modulus. On the other hand, for PLEB the yield point increased slightly from 14.1 ± 2.5 MPa for 0% to 16.3 ± 2.3 MPa for 0.1%, 17.2 ± 3.4 MPa for 0.5% and 18.3 ± 1.2 MPa for 1%, also in line with the trend observed for the Young's modulus. The elongation at break was also affected by the incorporation of CNTs. In the case of PDLEB, this value decreased with the addition of carbon nanotubes (397.2 ± 21.1% for 0%, 382.0 ± 25.5% for 0.1% CNTs, 322.0 ± 17.8% for 0.5% CNTs and 307.4 ± 19.1% for 1% CNTs). Similarly, for PLEB, the elongation at break decreased slightly with the addition of carbon nanotubes (177.2 ± 7.6% for 0%, 171.6 ± 13.6% for 0.1% CNTs, 165.4 ± 15.8% for 0.5% CNTs and 123.2 ± 10.3% for 1% CNTs). For strain recovery, in both cases, the observed value was not influenced by the amount of CNTs. In this regard, the strain recovery for PDLEB samples was between 91.5 ± 2.0% and 96.6 ± 0.3% , while for PLEB these values were between 19.2 ± 1.8% and 28.5 ± 0.6%. Regarding the mechanical properties at body temperature (37 °C), the effect of CNTs on the mechanical properties of the PDLEB and PLEB films was negligible. The softer behaviour of the copolymers at body temperature may result in the deformation of the matrix around the nanofillers, with little to no stress transfer between the two phases.

4.3.4. Contact angle

Regarding the contact angle measurements (Table 4.5.), it seems that the incorporation of CNTs did not affect the calculated surface energy of the films. However, a slight difference was observed between the PDLEB and PLEB films. For PDLEB films, the total surface energy (γ_{total}) was between 78.0 and 79.1 $mJ \cdot m^{-2}$ while for PLEB films, the γ_{total} was between 71.5 and 74.2 $mJ \cdot m^{-2}$. The lower surface energy of the PLEB samples in comparison to PDLEB samples suggest a slightly more hydrophobic nature of the L-lactide containing copolymers. This can be ascribed to the semicrystalline nature of this copolymer, which results in a poorer interaction with water due to the more compact polymeric chains in the crystalline phase.

Table 4.5. Contact angle measurements with water and diiodomethane as liquid test.

%CNTs	Θ_{water} (°)	$\Theta_{diiodomethane}$ (°)	γ_s^d (mJ·m^{-2})	γ_s^p (mJ·m^{-2})	γ_{total} (mJ·m^{-2})
PDLEB					
0%	69.5 ± 5.4	25.8 ± 0.4	45.9	32.8	78.7
0.1%	71.0 ± 1.2	23.5 ± 1.0	46.7	31.3	78.0
0.5%	70.9 ± 0.7	19.9 ± 1.5	47.8	31.3	79.1
1%	71.0 ± 1.7	20.5 ± 0.6	47.6	31.3	78.9
PLEB					
0%	73.8 ± 2.1	29.9 ± 0.8	44.3	29.0	73.3
0.1%	75.3 ± 1.4	28.6 ± 0.7	44.8	27.5	72.3
0.5%	76.1 ± 2.6	29.0 ± 2.5	44.6	26.8	71.5
1%	73.1 ± 0.5	28.9 ± 0.7	44.7	29.5	74.2

4.3.5. Cell viability assay and immunostaining

The interaction between the synthetized non-nanostructured samples and the neural cells was studied by seeding astrocytes (C8-D1A) on the surface of the materials. After damage to the neural system, astrocytes migrate towards the injured site and are activated due to the proinflammatory and prooxidant environment, generating the well-known glial scar and creating a physical barrier that hinders regeneration [18,25]. In this scenario, the cytocompatibility of the polymeric samples with astrocytes may directly affect the regeneration of the injured site after implantation [17]. Firstly, the metabolic activity of cells was tested by means of the AlamarBlue assay to study the possible impact of the sample composition and presence of CNTs (Figure 4.7).

Our results showed that, after 24 h of incubation, the astrocytes seeded over our polymeric scaffolds containing increasing amounts of CNT presented a higher metabolic activity compared to the cells seeded directly on the tissue culture plastic. For PLEB, the metabolic activity was incremented as the amount of CNTs increased (PLEB 0% CNT 113.8 ± 8.3%, PLEB 0.1% CNT 146.2 ± 13.2%, PLEB 0.5% CNT 151.2 ± 9.0%, PLEB 1% CNT 158.3 ± 12.5%) (*$p<0.05$, Dunn´s method One-way ANOVA Analysis of Variance on Ranks). These results suggested that the incorporation of CNTs on PLEB scaffolds was beneficial for astrocyte culture at short periods. Actually, the CNTs content has been reported to have a positive impact on the viability of astrocytes in vitro compared to polymeric substrates alone [11,15,16,26]. Nevertheless, after 48 h of incubation, the PLEB scaffolds showed a decrease in metabolic activity in comparison with samples at 24 h (PLEB 0% CNT 94.5 ± 9.2%, PLEB 0.1% CNT 78.5 ± 7.2%, PLEB 0.5% CNT 121.5 ± 15.7%, PLEB 1%

CNT 93.4 ± 5.6%). This result can be ascribed to the crystallization (Table 4.6.) of samples after incubation at 37 °C for 48 h.

Table 4.6. Crystallinity of PLEB films after 48 h at 37 °C submerged in culture media.

	PLEB			
% CNTs	0%	0.1%	0.5%	1%
***X* (%) 0 h**	14.4	11.7	13.5	11.7
***X* (%) 48 h at 37 °C**	30.4	31.1	31.3	31.7

Indeed, PLEB samples appeared to be more fragile and bend after incubation for 48 h with the culture media, which may have resulted in a substrate that compromises the cell viability.

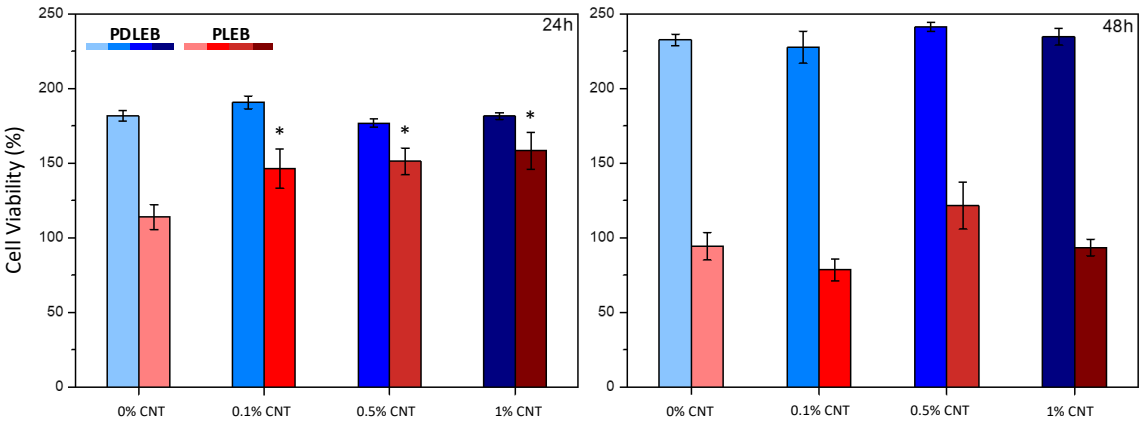

Figure 4.7. Metabolic activity of C8-D1A cells seeded on the studied samples after 24 h and 48 h. (* $p < 0.05$ compared to the sample not containing CNTs. Dunn´s method One-way ANOVA Analysis of Variance on Ranks); 100% metabolic activity was ascribed to C8-D1A cells seeded on the tissue culture plastic in the absence of our samples, and relative values were calculated for the rest of the samples.

For PDLEB, the metabolic activity was augmented in a similar manner with respect to the cells seeded on the tissue culture plastic in all of our polymeric scaffolds irrespective of the amount of CNTs. The metabolic activity of C8-D1A cells was higher than the one observed on the tissue culture plastic after 24 h (PDLEB 0% CNT 181.5 ± 3.5%, PDLEB 0.1% CNT 190.7 ± 4.3%, PDLEB 0.5% CNT 176.8 ± 2.9%, PDLEB 1% CNT 181.6 ± 2.2%); and also 48 h (PDLEB 0% CNT 232.5 ± 3.8 %, PDLEB 0.1% CNT 227.6 ± 10.7 %, PDLEB 0.5% CNT 241.2 ± 3.1 %, PDLEB 1% CNT 234.6 ± 5.7 %). Our results suggested a better cell proliferation on PDLEB scaffolds independently on the CNT content with no statistical difference between the polymeric samples. Nevertheless, it needs to be considered that the activation of reactive astrogliosis also supposes a raise in metabolic

activity [27], together with a morphological change from thinner to stellate conformation with bigger body size, cellular hypertrophy and thickened processes [28]. Hence, an immunostaining assay against rhodamine-phalloidin (Rd/Ph) was performed to better assess the influence of the material properties on astrocyte activation. Our results showed no activated astrocyte morphology when seeded on PLEB, but cells appeared to have a squeezed appearance which could be ascribed to the increased metabolic activity after 24 h and the decrease after 48 h, due to a possible cell death. Astrocytes seeded on the PDLEB samples maintained a similar thin morphology independent of the CNT content with no appearance of activated morphology (Figure 4.8.). Thus, although future experiments should include GFAP staining and inflammatory molecular experiments to discard this possibility of astrocytic activation, the differences on cell viability assays might be ascribed to a better proliferation of the astrocytes on PDLEB substrates rather than to the possible proinflammatory activation. We can conclude that all the PDLEB scaffolds tested were cyto-compatible and supported the growth of astrocytes. Our results clearly encourage the use of soft amorphous copolymers rather than non-amorphous in combination with CNTs for the culture of astrocytes and possibly other neural cells.

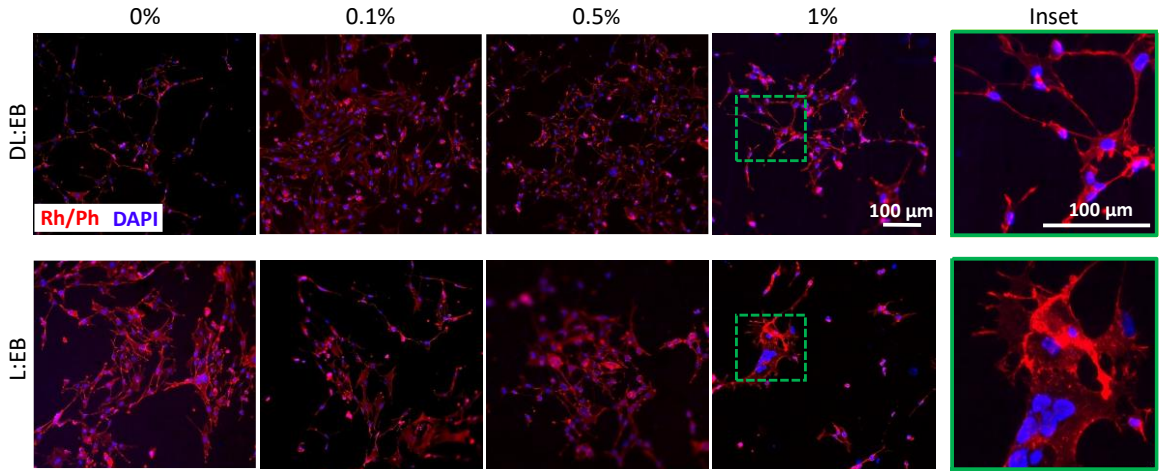

Figure 4.8. Immunostaining against rhodamine/phalloidin (Rh/Ph) and DAPI showing the morphology of the astrocytes cultured over PLEB and PDLEB containing increasing amounts of CNT after 48 h. Scale bar 100 µm in the micrographs and the insets.

Finally, as aligned guided regeneration is a must for a correct reinnervation after injury to the nervous system [18], we also studied the effect of the nanostructure on the astrocyte alignment. Astrocytes seeded on nanostructured scaffolds were able to align, following the nanograting axis (Figure 4.9.). An aligned nanotopography has even been ascribed to modulate the reactive response of astrocytes [28], which could be beneficial for future experiments on neural culture and tissue regeneration.

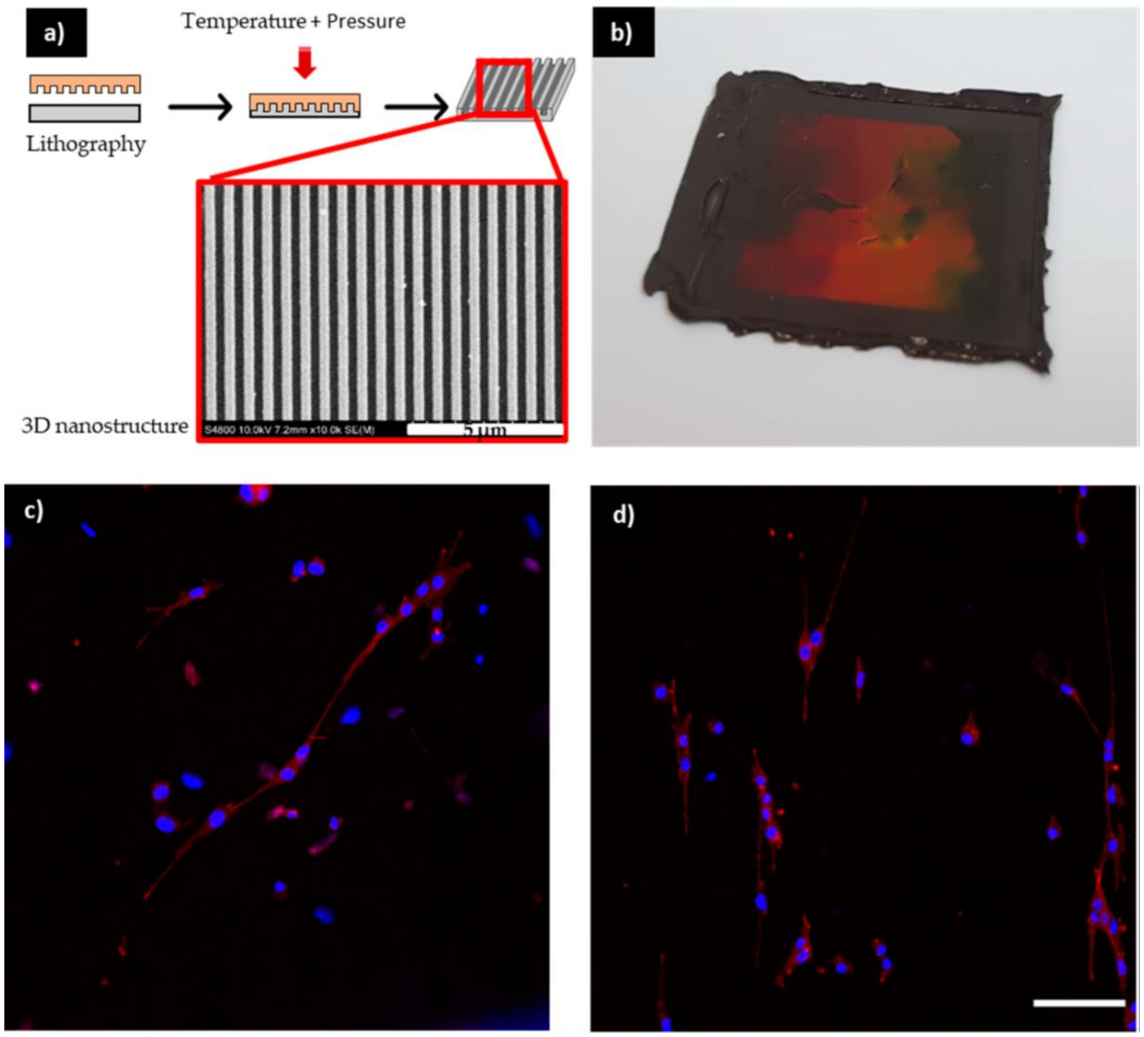

Figure 4.9. a) Schematic representation of the fabrication of the nanostructured film and SEM micrograph of the nanostructured film, **b)** photograph of the nanostructured film, **c)** C8-D1A seeded on nanostructured PLEB 0.5% CNTs film and **d)** C8-D1A seeded on nanostructured PDLEB 0.5% CNTs film. Scale bar 100 µm.

4.4. Conclusions

The present chapter describes the synthesis of lactide and ethylene brassylate copolymers and their nanocomposites with carbon nanotubes. The mechanical properties of the resulting copolymers can be adjusted by the composition (L-lactide vs. D,L-lactide), as well as by the incorporation of carbon nanotubes. The resulting copolymers displayed a soft and elastomeric behaviour at body temperature, making them interesting as scaffolds for the regeneration of soft tissues, including the neural tissue. Regarding their cytocompatibility with cells from the nervous system (i.e., astrocytes), the softer mechanical behaviour and the absence of crystalline domains in the formulation containing D,L-lactide seems to be more appropriate for the interaction of C8-D1A cells in terms of metabolic activity and cell morphology. Finally, the thermoplastic nature of these copolymers was exploited for the fabrication of nanostructured films, capable of supporting the aligned growth of cells on their surface. Overall, the copolymers presented in this work represent a promising alternative to the more widely studied poly(lactide-co-caprolactone) copolymers for the fabrication of polymeric devices resembling the mechanical properties of soft tissues.

4.5. References

[1] Biomedical applications of biodegradable polymers - Ulery - 2011 - Journal of Polymer Science Part B: Polymer Physics - Wiley Online Library, (n.d.). https://onlinelibrary.wiley.com/doi/full/10.1002/polb.22259 (accessed December 5, 2022).

[2] K. Van De Velde, P. Kiekens, Ein Jahrhundert Bahnelektroindustrie, Eb-Elektr. Bahnen. 99 (2001) 483.

[3] Yu. Voznyak, J. Morawiec, A. Galeski, Ductility of polylactide composites reinforced with poly(butylene succinate) nanofibers, Composites Part A: Applied Science and Manufacturing. 90 (2016) 218–224. https://doi.org/10.1016/j.compositesa.2016.07.011.

[4] J. Fernández, M. Montero, A. Etxeberria, J.R. Sarasua, Ethylene brassylate: Searching for new comonomers that enhance the ductility and biodegradability of polylactides, Polymer Degradation and Stability. 137 (2017) 23–34. https://doi.org/10.1016/j.polymdegradstab.2017.01.001.

[5] A. Larrañaga, E. Lizundia, A review on the thermomechanical properties and biodegradation behaviour of polyesters, European Polymer Journal. 121 (2019) 109296. https://doi.org/10.1016/j.eurpolymj.2019.109296.

[6] A. Sangroniz, L. Sangroniz, S. Hamzehlou, J. del Río, A. Santamaria, J.R. Sarasua, M. Iriarte, J.R. Leiza, A. Etxeberria, Lactide-caprolactone copolymers with tuneable barrier properties for packaging applications, Polymer. 202 (2020) 122681. https://doi.org/10.1016/j.polymer.2020.122681.

[7] A. Pascual, H. Sardon, A. Veloso, F. Ruipérez, D. Mecerreyes, Organocatalyzed Synthesis of Aliphatic Polyesters from Ethylene Brassylate: A Cheap and Renewable Macrolactone, ACS Macro Lett. 3 (2014) 849–853. https://doi.org/10.1021/mz500401u.

[8] G.H. Borschel, K.F. Kia, W.M. Kuzon, R.G. Dennis, Mechanical properties of acellular peripheral nerve, J Surg Res. 114 (2003) 133–139. https://doi.org/10.1016/s0022-4804(03)00255-5.

[9] A.J. Ryan, W.A. Lackington, A.J. Hibbitts, A. Matheson, T. Alekseeva, A. Stejskalova, P. Roche, F.J. O'Brien, A Physicochemically Optimized and Neuroconductive Biphasic Nerve Guidance Conduit for Peripheral Nerve Repair, Adv Healthc Mater. 6 (2017). https://doi.org/10.1002/adhm.201700954.

[10] C.E. Dumont, W. Born, Stimulation of neurite outgrowth in a human nerve scaffold designed for peripheral nerve reconstruction, J Biomed Mater Res B Appl Biomater. 73 (2005) 194–202. https://doi.org/10.1002/jbm.b.30202.

[11] Y. Polo, J. Luzuriaga, J. Iturri, I. Irastorza, J.L. Toca-Herrera, G. Ibarretxe, F. Unda, J.R. Sarasua, J.R. Pineda, A. Larrañaga, Nanostructured scaffolds based on bioresorbable polymers and graphene oxide induce the aligned migration and accelerate the neuronal differentiation of neural stem cells, Nanomedicine. 31 (2021) 102314. https://doi.org/10.1016/j.nano.2020.102314.

[12] J. Song, B. Sun, S. Liu, W. Chen, Y. Zhang, C. Wang, X. Mo, J. Che, Y. Ouyang, W. Yuan, C. Fan, Polymerizing Pyrrole Coated Poly (l-lactic acid-co-ε-caprolactone) (PLCL) Conductive Nanofibrous Conduit Combined with Electric Stimulation for Long-Range Peripheral Nerve Regeneration, Frontiers in Molecular Neuroscience. 9 (2016). https://www.frontiersin.org/articles/10.3389/fnmol.2016.00117 (accessed October 7, 2022).

[13] H. Peng, X. Liu, R. Wang, F. Jia, L. Dong, Q. Wang, Emerging nanostructured materials for musculoskeletal tissue engineering, J. Mater. Chem. B. 2 (2014) 6435–6461. https://doi.org/10.1039/C4TB00344F.

[14] A. Fraczek-Szczypta, Carbon nanomaterials for nerve tissue stimulation and regeneration, Materials Science and Engineering: C. 34 (2014) 35–49. https://doi.org/10.1016/j.msec.2013.09.038.

[15] C. Vallejo-Giraldo, E. Pugliese, A. Larrañaga, M.A. Fernandez-Yague, J.J. Britton, A. Trotier, G. Tadayyon, A. Kelly, I. Rago, J.-R. Sarasua, E. Dowd, L.R. Quinlan, A. Pandit, M.J. Biggs, Polyhydroxyalkanoate/carbon nanotube nanocomposites: flexible electrically conducting elastomers for neural applications, Nanomedicine (Lond). 11 (2016) 2547–2563. https://doi.org/10.2217/nnm-2016-0075.

[16] B.S. Harrison, A. Atala, Carbon nanotube applications for tissue engineering, Biomaterials. 28 (2007) 344–353. https://doi.org/10.1016/j.biomaterials.2006.07.044.

[17] G.-Z. Jin, M. Kim, U.S. Shin, H.-W. Kim, Effect of carbon nanotube coating of aligned nanofibrous polymer scaffolds on the neurite outgrowth of PC-12 cells, Cell Biology International. 35 (2011) 741–745.

[18] S.K. Seidlits, J.Y. Lee, C.E. Schmidt, Nanostructured scaffolds for neural applications, Nanomedicine. 3 (2008) 183–199. https://doi.org/10.2217/17435889.3.2.183.

[19] C. Vallejo-Giraldo, K. Krukiewicz, I. Calaresu, J. Zhu, M. Palma, M. Fernandez-Yague, B. McDowell, N. Peixoto, N. Farid, G. O'Connor, L. Ballerini, A. Pandit, M.J.P. Biggs, Attenuated Glial Reactivity on Topographically Functionalized Poly(3,4-Ethylenedioxythiophene):P-Toluene Sulfonate (PEDOT:PTS) Neuroelectrodes Fabricated by Microimprint Lithography, Small. 14 (2018) e1800863. https://doi.org/10.1002/smll.201800863.

[20] M.K. Gottipati, I. Kalinina, E. Bekyarova, R.C. Haddon, V. Parpura, Chemically Functionalized Water-Soluble Single-Walled Carbon Nanotubes Modulate Morpho-Functional Characteristics of Astrocytes, Nano Lett. 12 (2012) 4742–4747. https://doi.org/10.1021/nl302178s.

[21] J.R. Pineda, Y. Polo, B. Pardo-Rodríguez, J. Luzuriaga, V. Uribe-Etxebarria, P. García-Gallastegui, J.R. Sarasua, A. Larrañaga, G. Ibarretxe, In vitro preparation of human Dental Pulp Stem Cell grafts with biodegradable polymer scaffolds for nerve tissue engineering, Methods Cell Biol. 170 (2022) 147–167. https://doi.org/10.1016/bs.mcb.2022.02.012.

[22] Pretsch, E.; Seibl, J.; Simon, W. Tables of Spectral Data for Structure Determination Organic Compounds; 2015; Vol. 3; 626 ISBN 9783540124061., in: n.d.

[23] H. Zhou, F. Wang, Y. Wang, C. Li, C. Shi, Y. Liu, Z. Ling, Study on contact angles and surface energy of MXene films, RSC Adv. 11 (2021) 5512–5520. https://doi.org/10.1039/D0RA09125A.

[24] S. Barrau, C. Vanmansart, M. Moreau, A. Addad, G. Stoclet, J.-M. Lefebvre, R. Seguela, Crystallization Behavior of Carbon Nanotube−Polylactide Nanocomposites, Macromolecules. 44 (2011) 6496–6502. https://doi.org/10.1021/ma200842n.

[25] J.M. Cregg, M.A. DePaul, A.R. Filous, B.T. Lang, A. Tran, J. Silver, Functional regeneration beyond the glial scar, Experimental Neurology. 253 (2014) 197–207. https://doi.org/10.1016/j.expneurol.2013.12.024.

[26] X.-Y. Xiong, Y. Tang, Q.-W. Yang, Metabolic changes favor the activity and heterogeneity of reactive astrocytes, Trends in Endocrinology & Metabolism. 33 (2022) 390–400. https://doi.org/10.1016/j.tem.2022.03.001.

[27] K.H. Lee, M. Cha, B.H. Lee, Crosstalk between Neuron and Glial Cells in Oxidative Injury and Neuroprotection, International Journal of Molecular Sciences. 22 (2021) 13315. https://doi.org/10.3390/ijms222413315.

[28] D. Dai, L. He, Y. Chen, C. Zhang, Astrocyte responses to nanomaterials: Functional changes, pathological changes and potential applications, Acta Biomater. 122 (2021) 66–81. https://doi.org/10.1016/j.actbio.2020.12.013.

CHAPTER 5

Lactide and ethylene brassylate-based thermoplastic elastomers and their nanocomposites with carbon nanotubes: nanopatterned surface as a strategy to alleviate neuroinflammation

CHAPTER 5. Lactide and ethylene brassylate-based thermoplastic elastomers and their nanocomposites with carbon nanotubes: nanopatterned surface as strategy to alleviate neuroinflammation after biomaterial implantation

Abstract

The poly(D,L-Lactide-co-Ethylene Brassylate) (PDLEB) and poly(L-Lactide-co-Ethylene Brassylate) (PLEB) composites with carbon nanotubes synthesized and characterized in the previous chapter, were here utilized to fabricate nanopatterned scaffolds to modulate the inflammatory response of microglia. Due to the soft and elastomeric behaviour at body temperature capable of resembling the mechanical properties of the neural tissue and the absence of crystalline domains, PDLEB seems to be more appropriate for the development of biomaterials intended to be used in the regeneration of the nervous system. Accordingly, PDLEB scaffolds were studied in this chapter as a support for microglia, paying particular attention to the inflammatory response by cells, which was evaluated in terms of nitrites and TNF-α release. The developed scaffolds did not induce an inflammatory response by microglia. Moreover, when microglia were stimulated with the pro-inflammatory LPS, the polymer was able to mitigate the inflammatory response. Accordingly, PDLEB represents an interesting material for the development of polymeric scaffolds that need to interface with the neural tissue, thanks to its appropriate mechanical properties and the absence of an inflammatory response by cells associated with the neuroimmune response.

5.1 Introduction

Traditionally, biomaterials have been designed to minimize their interaction with the surrounding cells, tissues and organs, thus being considered as bioinert materials. Nowadays, however, biomaterials are designed to actively and smartly interact with the human body with the aim of accelerating or improving their regenerative capacity, i.e., bioactive. Accordingly, there is an increasing awareness among researchers regarding the effects of the biomaterials on the cell fate and interactions of the biomaterials with components of living systems [1].

Biomaterials have been successfully used for several applications in the nervous system such as regenerative (e.g., scaffolds to promote peripheral or central nerve regeneration [2,3]), therapeutic (e.g., intracranial electrodes to treat Parkinson´s and Alzheimer´s disease [4]) or monitorization (e.g., intracortical microelectrodes to record action potentials of neurons to understand and treat neurological diseases/disorders [5]) devices. For these applications, the biomaterial and their properties (e.g., mechanical, physico-chemical or surface properties) should be selected carefully to guarantee the success of the implanted device [6], since their interaction with the host tissue could initiate a cascade of neuroinflammatory responses that could lead to a chronic foreign body response and the encapsulation of the biomaterial by the glial scar [5]. Considering the surface of the device being the first contact with the biological environment, surface properties such as roughness and topography will be of great relevance for its correct behaviour with the surrounding tissue. Whit this in mind, recent studies are focusing in developing biomaterials with nano- and micro- topographies with the aim of modulating the cell fate (e.g., adhesion, proliferation and differentiation of stem cells) [7] or attenuating the immune response towards the implanted device (being able to even suppress it along with the associated fibrosis, thus minimizing compatibility complications (e.g., breast implants)) [8]. Different studies highlight the role of the surface properties on the inflammatory response. For example, a decrease on the astrocytic coverage was observed on nanoporous gold surfaces in comparison to the smooth gold surface (from 23% to 10%), while neuronal surface was not affected [9]. In another study, platinum electrodes coated with an electrically conductive polymer (PEDOT:PSS) and with the surface modified by microimprint lithography [10] were able to reduce the adhesion of reactive astrocytes in comparison to the non-modified surfaces. These strategies were also tested in vivo, where nanopatterned microelectrodes were compared to smooth control implants in a murine model [5], showing that molecular inflammatory and oxidative stress markers (i.e., IL-1β, TNF-α, NOS2) were attenuated when the nanopatterned microelectrode was implanted with respect to the smooth control. Nevertheless, most of these studies use biomaterials that are much stiffer than the nervous tissue such as gold [9], silicon [5]

or platinum [11] with elastic moduli in the range of few hundreds of GPa, whereas the elastic moduli of the brain is in the order of few KPa. This represents an additional limitation for the integration of the implanted biomaterial within the nervous tissue due to the well-known mechanical mismatch mediated by local micromotions that eventually lead to glial scar formation [12]. Bioresorbable polyesters, as poly(lactide) (PLA), poly(caprolactone) (PCL) and their copolymers show great potential for their use as biomaterials thanks to their biodegradability [13] and cytocompatibility (i.e., they are FDA-approved (co)polymers Generally Recognized as Safe (GRAS)). In the present chapter, poly(D,L-lactide-co-ethylene brassylate) (PDLEB) and poly(L-Lactide-co-Ethylene Brassylate) (PLEB) copolymers, synthesized and characterized in Chapter 4, were used to study their interaction with murine microglia (i.e., BV2 cells). Their elastomeric behaviour compatible with nervous tissue and their thermoplastic nature, allowed us to formulate various films with flat and nanopatterned topography. Considering that BV2 cells owns immunological functions and are determinant in the neuroinflammatory response to an implantable device, the interaction between our materials and BV2 cells has been studied in terms of cell viability and the expression of different typical inflammatory markers (i.e., nitrites and TNF-α release, ROS production and Iba-1 expression). In the present chapter, surface topography and the suitable mechanical properties have been considered to develop a fully implantable polymeric device capable of attenuating the onset of a proinflammatory response by the host tissue in vitro, thus reducing glial scar formation and accordingly improving the integration and performance of the implanted material.

5.2. Materials and methods

5.2.1. Materials

Poly(D,L-Lactide-co-Ethylene Brassylate) (PDLEB) and Poly(L-Lactide-co-Ethylene Brassylate) (PLEB) were previously synthesized in Chapter 4. Silicon stamp was purchased from NIL Technology (Denmark) (with the following specifications: period: 700 nm; linewidth: 365 nm; depth: 350 nm). Dulbecco's Modified Eagle Medium (DMEM), Hanks' Balanced Salt Solution (HBSS), Penicillin Streptomycin (P/S), Fetal Bovine Serum (FBS), AlamarBlue cell viability reagent and rhodamine-phalloidin were supplied by Fisher Scientific (Spain). Fluoroshield with DAPI, Triton X-100, Tween 20, DCFH-DA and Lipopolysaccharides (LPS) from Escherichia coli O111:B4 were purchased from Sigma Aldrich (Spain). Invitrogen Griess Reagent Kit, for nitrite quantitation was provided by Thermo Fisher. DuoSet ELISA Ancillary Reagent Kit 2 was obtained from Bio-

Techne (USA). 16% Formaldehyde solution was supplied by Thermo Fisher Scientific (USA). Recombinant Anti-Iba1 antibody [EPR16588] (ab178846) was purchased from Abcam (UK).

5.2.2. Nanotopography fabrication

In order to replicate the nanotopography of a silicon stamp on the surface of the polymeric films synthesized in Chapter 4, a nanolithography process was carried out. For this purpose, a commercially available silicon stamp was used by placing it on polymeric films of PDLEB or PLEB with 150 µm of thickness. Then, by applying heat (200 °C) and a compressive force of 20 N for 15 min, the nanopattern was replicated on the polymeric surface.

5.2.3. Scanning electron microscopy (SEM)

SEM was used to assess the surface morphology of the scaffolds. Firstly, samples were coated with a 150 Å layer of gold in a JEL Ion Sputter JFC-1100 at 1200 V and 5 mA and then analysed in a HITACHI S-4800.

5.2.4. Cell Viability assay

BV2 cells (AcceGen) were cultured in Dulbecco's Modified Eagle Medium (DMEM) supplemented with 10% FBS and 1% P/S. Cultures were maintained in a humidified atmosphere (5% CO_2, 95% relative humidity) at 37 °C. Three circular samples of 10 mm diameter were punched out from each system of PDLEB and PLEB with increasing concentration of carbon nanotubes (0%, 0.1%, 0.5% and 1%) and placed in a 48-well plate. The samples were extensively washed with ethanol and subsequently washed with PBS before being air dried inside the biosafety cabinet. Finally, they were placed under ultraviolet light for 15 min. To assess the cell viability, 50,000 cells were seeded per well. Control cells were seeded directly on wells. After either 24 h or 48 h, the cell medium was replaced by cell medium containing 10% of AlamarBlue reagent. Cells were incubated for 4 h sheltered from light. Finally, the metabolic activity was determined by measuring the fluorescence (λ_{ex} = 480 nm/λ_{em} = 595 nm) of the media on a BioTek Synergy H1 plate reader. Also, cell viability was measured in cells stimulated with different concentrations of LPS (0, 5, 10 and 20 ng·mL^{-1}). Firstly, 50,000 cells were seeded per well directly on wells in a 48-well plate. After 24 h of incubation with increasing concentrations of LPS, the cell medium was replaced by cell medium containing 10% of AlamarBlue reagent and incubated for 4 h protecting

it from light. Finally, metabolic activity was measured as previously described. In order to study the cell viability of cells in contact with nanostructured samples, BV2 cells were seeded on PDLEB samples with 0% and 0.5% CNT (with and without nanostructure) and stimulated with 20 ng·mL^{-1} LPS for 24 h. Following the protocol described above, the metabolic activity was determined.

5.2.5. Griess assay

Nitrite concentration in cell media was measured by Griess Reagent Kit. Cells were stimulated with different concentration of LPS (0, 5, 10 and 20 ng·mL^{-1}) in different ways. On the one hand, BV2 cells were only stimulated for 48 h before the measurement. On the other hand, cells were insulted in two steps: firstly a stimulation with medium containing LPS for 24 h; afterwards, medium was measured and replaced with fresh medium containing the same concentrations of LPS, incubated and measured after another 24 h. Other experiments were carried out using the Griess Reagent Kit, where BV2 cells were seeded on samples of PDLEB with different concentrations of CNT (0, 0.1, 0.5 and 1% CNT) and with or without a nanostructured topography. In these situations, half of the cells were stimulated with a concentration of 20 ng·mL^{-1}of LPS for 24 h, while the other half were not. Measurements of medium from each time-point were carried out as described by the supplier using a BioTek Synergy H1 plate reader (λ = 548 nm).

5.2.6. ELISA assay

TNF-α concentration secreted by cells was measured using Mouse TNF-α ELISA kit (R&D Systems). Cells were stimulated with different concentration of LPS (0, 5, 10 and 20 ng·mL^{-1}) in different ways. On the one hand, BV2 cells were only stimulated for 48 h before the measurement. On the other hand, cells were insulted in two steps: firstly, a stimulation with medium containing LPS for 24 h; afterwards, medium was stored at -80 °C and replaced with fresh medium containing the same concentrations of LPS. Cells were incubated for another 24 h and then the medium was aspirated and also stored at -80 °C. Other experiments were carried out using the Mouse TNF-α ELISA kit, where BV2 cells were seeded on samples of PDLEB with different concentrations of CNT (0, 0.1, 0.5 and 1% CNT) and with or without a nanostructured topography. In these situations, half of the cells were stimulated with a concentration of 20 ng·mL^{-1} of LPS for 24 h, while the other half were not. Measurements of medium from each time-

point were carried out as described by the supplier using a BioTek Synergy H1 plate reader (λ = 450 nm).

5.2.7. Flow cytometry for reactive oxygen species

Flow cytometry for reactive oxygen species assay was performed in a Beckman Coulter Gallios cytometer analyser. Firstly, 50,000 cells were seeded per well in a 48-well plate and were stimulated with LPS in different concentrations (0, 5, 10 and 20 $ng \cdot mL^{-1}$) for 24 h. Then cells were incubated with DCFH-DA for 1 h, which is used as indicator of reactive oxygen species (ROS). Finally, cells were washed, trypsinized, centrifuged and resuspended in order to perform the measurements.

5.2.8. Immunostaining

In order to detect the expression of Iba-1, BV2 cells were seeded at a density of 50,000 cells per well in 48-well plate having glass coverslip on the bottom of the plate. Subsequently, a stimulation with LPS (20 $ng \cdot mL^{-1}$) was carried out in half of the samples for 24 h. Then, cells were fixed with 4% PFA for 10 min at room temperature. Afterward, PFA was aspirated and the samples were washed with sterile HBSS twice. A solution of 0.5% Triton X-100 in PBS was added to permeabilize the cell membrane and kept under slight agitation for 10 min. The solution was removed and the samples were washed with PBS under slight agitation for 5 min, twice. Then, the solution containing 0.1% primary antibody (Iba-1), 0.05% Triton X-100 and 1% BSA in PBS was added in a drop method and coverslips were placed in a humidity chamber overnight at 4 °C. After overnight incubation, the samples were washed 3 times with a solution of 0.05% Tween 20 in PBS under slight agitation for 5 min. Subsequently, the solution containing 0.5% secondary antibody (AlexaFluor 488 donkey anti-rabbit IgG), 0.1% Tween 20 and 1% BSA in PBS was added in the same way that the primary antibody solution, incubating it for 2.5 h at 4°C. Finally, the samples were washed once with 0.05% Tween 20 in PBS for 5 min under slight agitation and washed twice with PBS in the same way, to keep in fresh PBS before observing them under fluorescence microscope. Nuclei staining with DAPI was carried out directly on the samples by adding a drop of mounting medium before observing them under the microscope (Nikon Eclipse Ts2)

5.3. Results and Discussion

5.3.1. Preliminary characterization of the nanostructured samples

Due to the thermoplastic nature of PDLEB and PLEB copolymers synthesized in Chapter 4, it is possible to create a nanopattern on the surface of the film by means of lithography. In this way, by a thermo-pressing process at 200 °C and 20 N using a commercially available silicon stamp, films were nanostructured (Figure 5.1.a.and b).

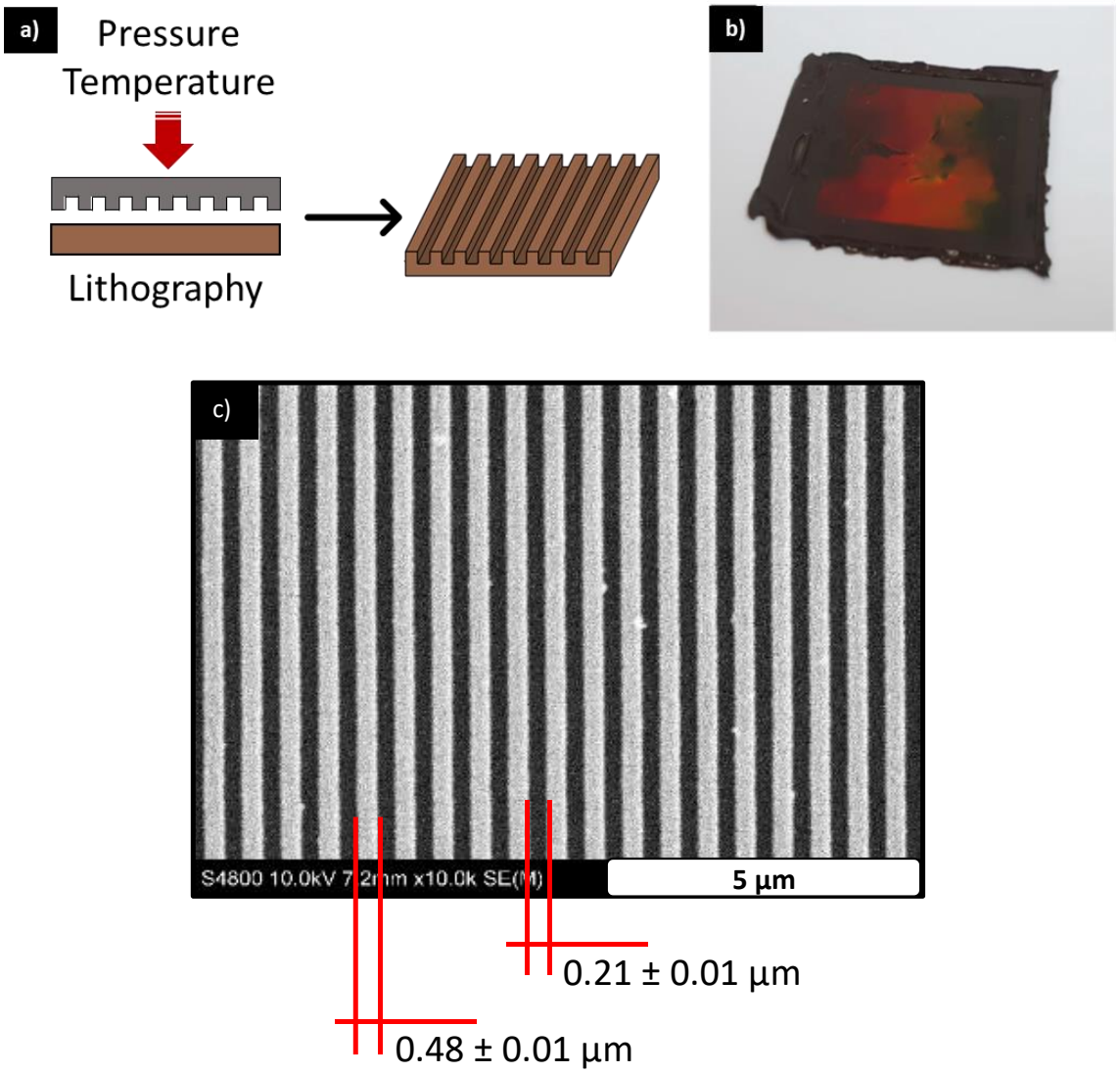

Figure 5.1. a) Schematic representation of the fabrication of the nanostructured film. **b)** Photograph of the resultant nanostructured film. **c)** SEM micrograph of the nanostructured film.

The resultant nanostructure was analysed by SEM and the faithful replication was confirmed by measuring the ridges (0.48 ± 0.01 µm) and grooves (0.21 ± 0.01 µm) (Figure 5.2.c). Finally, circular samples of 10 mm diameter were punched out for cell culture studies.

5.3.2. Cell Viability assay on non-nanostructured films

The interaction between the synthesized non-nanostructured films and microglia (BV2 cells) was studied by seeding BV2 cells on the surface of the circular samples of the PDLEB and PLEB films containing different amounts of CNT. After the implantation of any device in the nervous system, a neuroimmune response mediated by reactive astrocytes and microglia takes place. This phenomenon leads to a chronic response against a foreign body and the consequent encapsulation of the device by the glial scar, suppressing its function [5]. In this context, the cytocompatibility and the cellular survival are vital to guarantee the viability of the implanted device. Thus, the metabolic activity of BV2 cells was first tested by AlamarBlue assay to study the viability of cells in contact with the polymeric samples and the possible effect of CNT (Figure 5.2.).

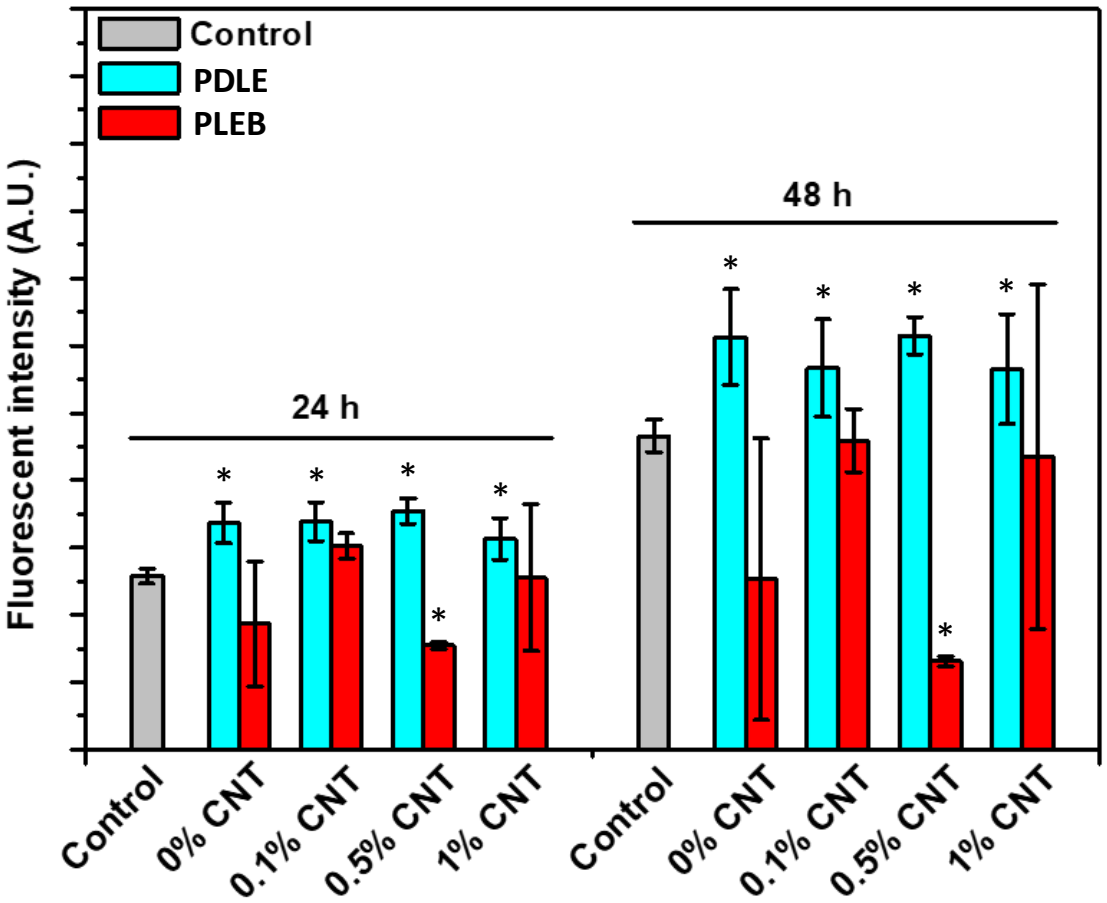

Figure 5.2. Metabolic activity of cells seeded on PDLEB and PLEB with different CNT concentrations. (* $p < 0.05$ compared to the control sample. Dunn´s method One-way ANOVA Analysis of Variance on Ranks).

Our results showed that, after 24 h of incubation, the microglia seeded over the PDLEB scaffolds present a higher metabolic activity compared to the cells seeded directly on the tissue culture

plastic (i.e., control). In addition, it seems that the incorporation of CNTs did not cause significant differences in the metabolic activity of BV2 cells. On the other hand, PLEB samples showed irregular values of the metabolic activity irrespective of the amount of CNTs. After 48 h of incubation, a similar trend was observed: the metabolic activity of cells seeded on PDLEB samples increased in comparison with the control cells. Cells seeded over PLEB still presented an irregular behaviour, showing metabolic activities below control levels. This behaviour observed in the microglia seeded over PLEB samples was similar to the one reported for astrocytes in Chapter 4. Likewise, the circular samples showed morphological changes after the incubation at 37 °C and a crystallization process occurred, that may have affected the cell viability [14]. The higher fluorescent intensity observed both in the control and in the PDLEB samples, suggested that BV2 cells are able to grow/proliferate when seeded in our developed materials.

5.3.3. Establishment of the inflammatory model

In order to study the interaction and the inflammatory response of BV2 cells towards our synthesized copolymers, an inflammatory model needs to be first established. Lipopolysaccharide (LPS) is the major component of the outer membrane of Gram-negative bacteria [15], and has been accordingly widely used to induce inflammation in models of neurodegeneration [16]. In our particular case, we used LPS to stimulate microglia and create an inflammatory milieu. For this purpose, BV2 cells were firstly seeded on a cell culture plate and insulted with different concentrations of a LPS solution (0, 5, 10 and 20 $ng \cdot mL^{-1}$). After 24 h of incubation, the AlamarBlue assay was carried out and the results were analysed. Figure 5.3. shows an increment on the metabolic activity after 24 h of incubation as the LPS concentration increased in comparison to the control cells (5 $ng \cdot mL^{-1}$ 111.7 ± 3.7%, 10 $ng \cdot mL^{-1}$ 114.5 ± 3.0% and 20 $ng \cdot mL^{-1}$ 115.6 ± 8.1%). As previously reported, this increased metabolic activity could be associated with an inflammatory state of the cells [17,18].

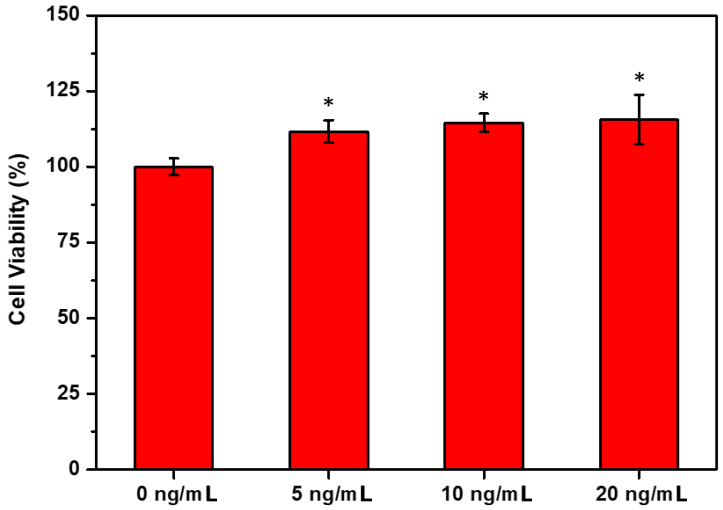

Figure 5.3. Metabolic activity of cells seeded on wells and stimulated with LPS (0, 5, 10 and 20 ng·mL^{-1}) (* $p < 0.05$ compared to the sample containing 0 ng·mL^{-1} of LPS. Dunn´s method One-way ANOVA Analysis of Variance on Ranks).

Considering that an inflammatory condition of cells is related with the detection of nitrogen compounds (i.e., neuronal nitric oxide synthase (nNOS), inducible nitric oxide synthase (iNOS) and endothelial nitric oxide synthase (eNOS)) [19,20], the release of these markers by cells stimulated with increasing concentrations of LPS was studied. To that end, the release of nitrites was quantified using the Griess Reagent kit. Firstly, BV2 cells were seeded and stimulated with LPS solutions (0, 5, 10 and 20 ng·mL^{-1}) in different ways with the aim of establishing the most suitable protocol to induce an inflammatory state. Figure 5.4. shows the results obtained after LPS treatments; it can be observed how nitrite concentration in the supernatant of the cells increased as the LPS concentration increased. In addition, a higher nitrite concentration was monitored at 48 h when the insult of 20 ng·mL^{-1} was supplied in two doses (48 h 32.8 ± 2.6 µM) that in one (24 h 12.3 ± 0.8 µM, 48 h (single-dose) 13.8 ± 1.6 µM).

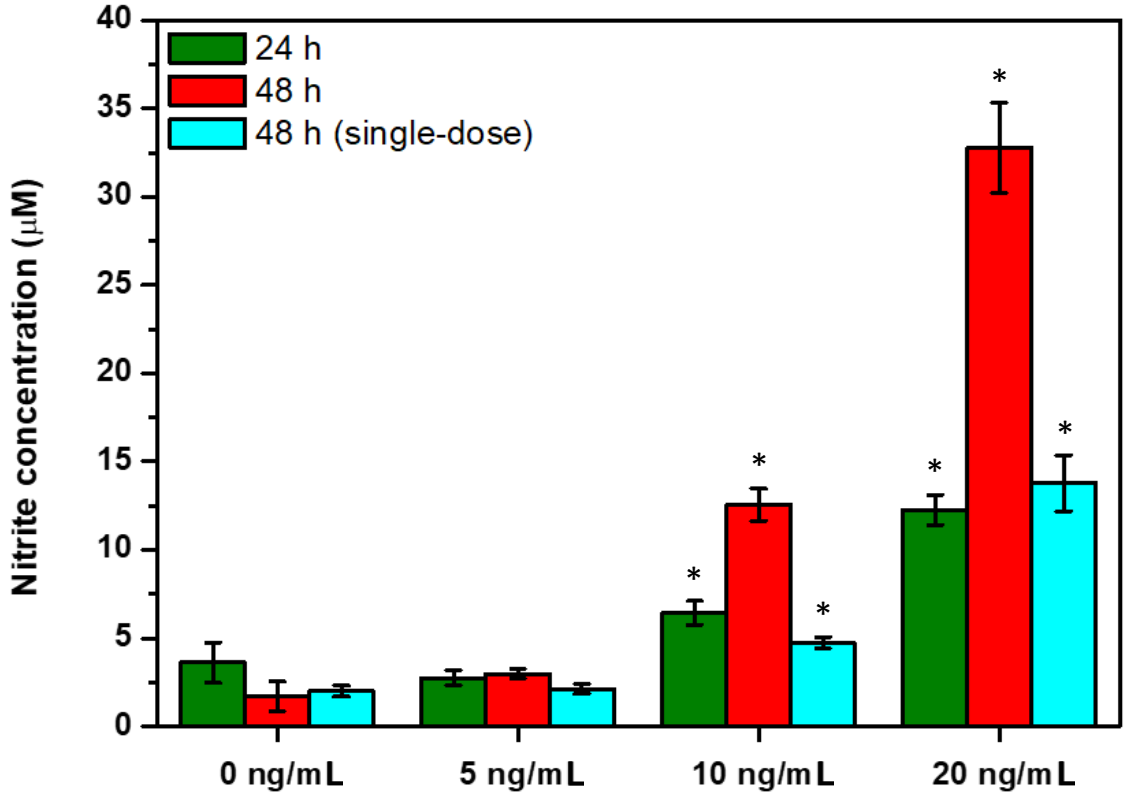

Figure 5.4. Nitrite concentration in cells stimulated with LPS at different time points. (* $p < 0.05$ compared to the sample containing 0 ng·mL^{-1} of LPS. Dunn´s method One-way ANOVA Analysis of Variance on Ranks).

Other characteristic marker of an inflammatory state of the cells is the secretion of proinflammatory cytokines, such as TNF-α [21,22]. By performing an ELISA assay, TNF-α was detected and quantified in the supernatant of microglia under the same conditions described above for the detection of nitrites. In this case, the TNF-α concentration (Figure 5.5.) was higher when the cells were insulted in one single dose, being higher at 24 h (1927.8 ± 50.0 pg·mL^{-1}) than 48 h (1579.1 ± 176.5 pg·mL^{-1}).

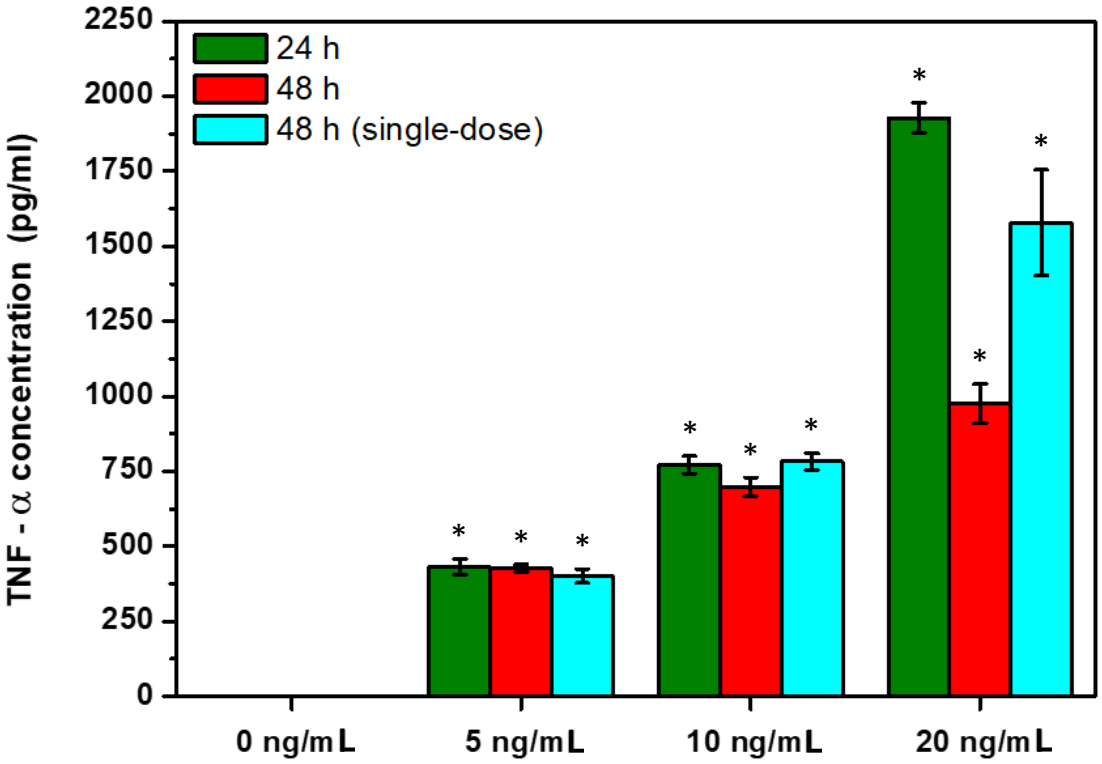

Figure 5.5. TNF-α concentration in cells stimulated with LPS at different time points. (* $p < 0.05$ compared to the sample containing 0 ng·mL^{-1} of LPS. Dunn´s method One-way ANOVA Analysis of Variance on Ranks).

Also, in order to complete the inflammatory model, reactive oxygen species (ROS) were measured by flow cytometry. ROS are also another indicator of an inflammatory state of cells [23]. Once the cells were stimulated with different concentrations of LPS (0, 5, 10 and 20 ng·mL^{-1}) for 24 h, BV2 cells were incubated with DCFH-DA, which is used as an indicator of the presence of ROS intracellularly. Figure 5.6., shows the results where a shift of the curves to the right should be seen as LPS concentration increased. Unfortunately, a correlation between the increase of LPS and the detection of ROS was not observed.

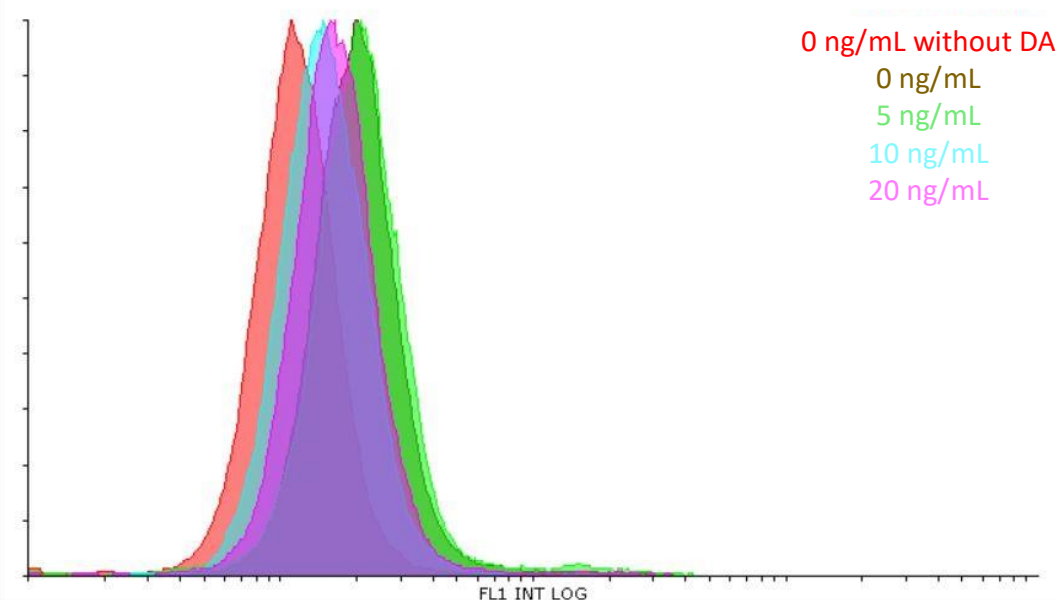

Figure 5.6. ROS in BV2 cells stimulated with LPS at different concentrations.

Iba-1 is one of the most widely used protein markers [24] to confirm microglia activation. This intracellular protein is related to the reorganization of microglia cytoskeleton and support the phagocytosis process [25]. Accordingly, it has been reported that the expression of Iba-1 is increased in activated microglia, suggesting that the increased expression of Iba-1 can be used as a marker for microglial activation [26]. In the human brain, this protein is a sensitive marker for microglial activation correlated to the intensity of tissue damage both in inflammation and cerebral hypoxia [27]. In particular, Iba-1 is a diagnostic marker used for routine immunohistochemistry on either microglial cell lines or nerve pathologies like spinal cord injury [28] and brain tumours [29]. Hence, an immunostaining assay against Iba-1 was performed to better assess the influence of LPS on microglia activation. Our results showed that after 24 h of LPS stimulation at a concentration of 20 $ng \cdot mL^{-1}$ (Figure 5.7.b), BV2 cells showed an increased expression of Iba-1, while untreated cells barely showed any expression of this protein.

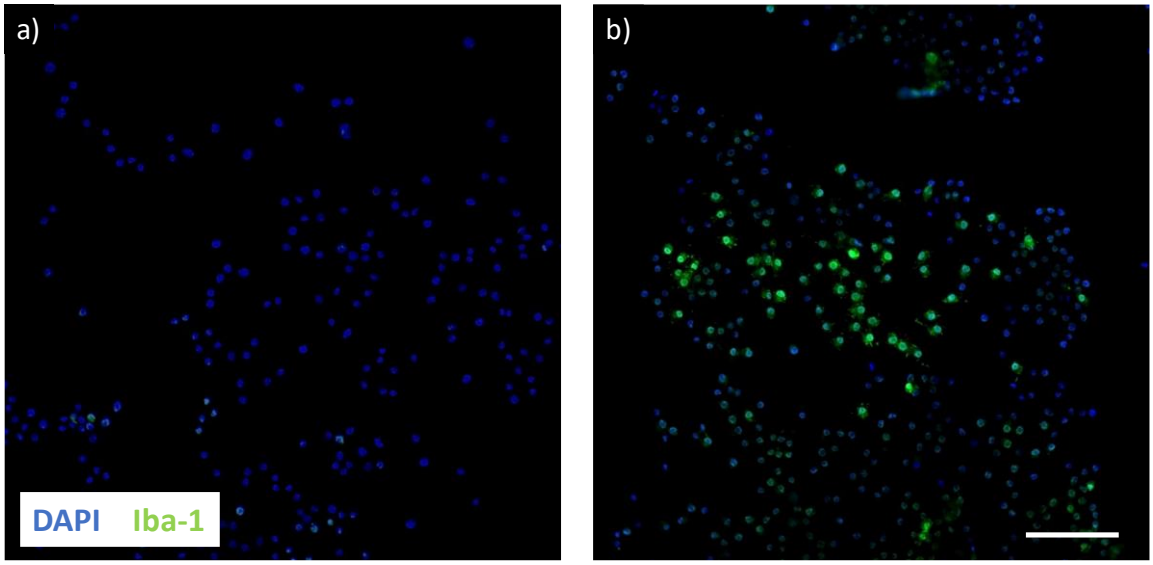

Figure 5.7. Iba-1 expression in BV2 cells. **a)** BV2 without LPS stimulus, **b)** BV2 stimulated with LPS (20 ng·mL^{-1}) for 24 h. Scale bar 100 µm.

5.3.4. BV2 interaction with PDLEB. Nitrite and TNF- α secretion by BV2 cells

Inflammatory response after a device implantation will determine its viability since chronic inflammation can cause detrimental consequences to the surrounding cells and tissues around the implant. Hence, the thorough analysis of those events occurring after device implantation is a must to guarantee safety and functionality aspects of the biomaterial. For this reason, in this chapter, the interaction between BV2 cells and PDLEB samples was explored to study how our material could modify this response. Firstly, to know if the addition of carbon nanotubes (CNT) could have any effect on the behaviour of BV2 cells, microglia were seeded on samples of PDLEB with increasing concentrations of CNT (0, 0.1, 0.5 and 1%). Half of the samples were insulted with a LPS solution (20 ng·mL^{-1}) to induce an inflammatory response and test if our samples would mitigate or reduce this response. Figure 5.8.above shows how the nitrite levels of cells seeded on materials and without the LPS insult were at same levels as the negative control (i.e., BV2 cells seeded on tissue culture plastic without LPS stimulus).

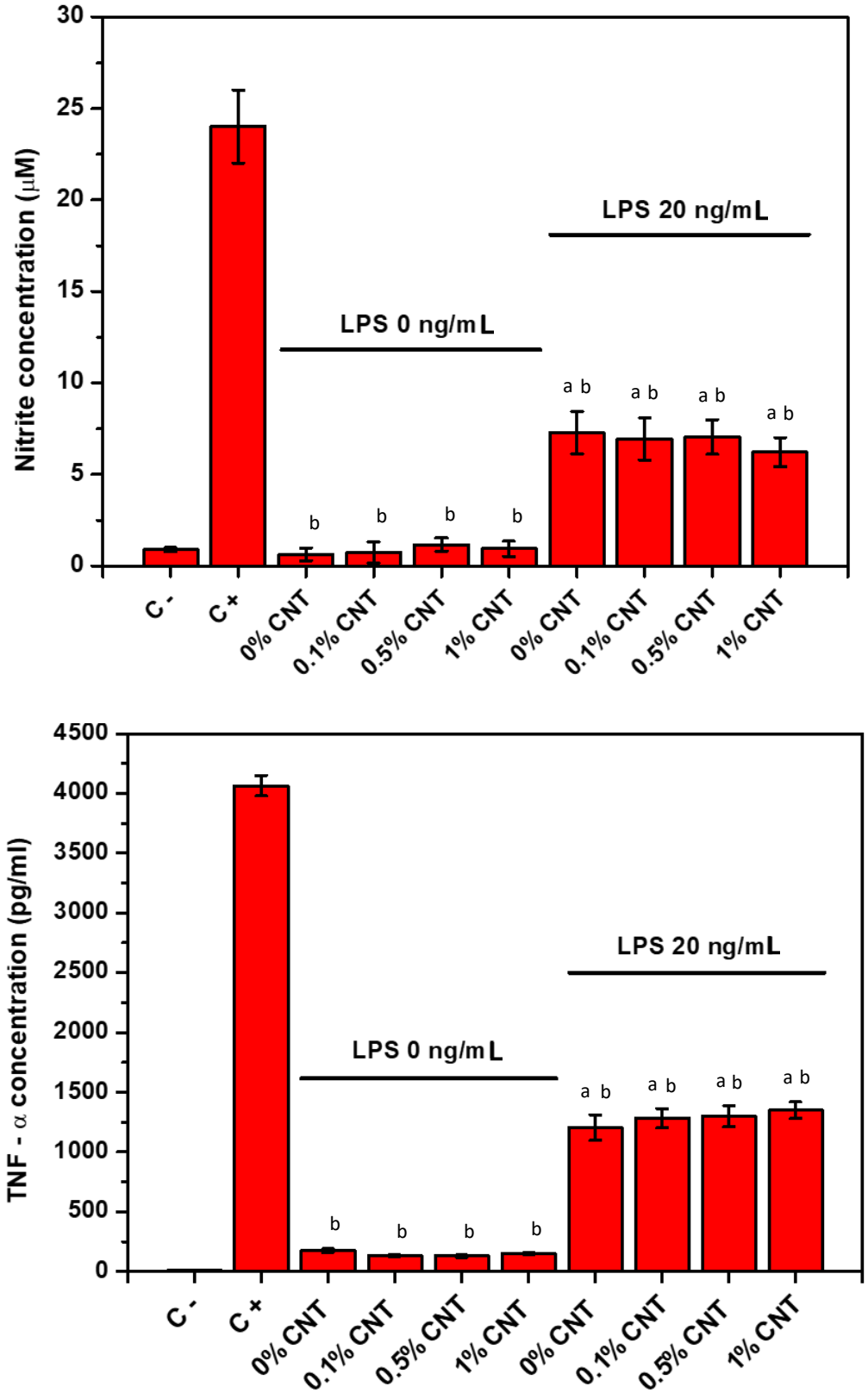

Figure 5.8. (above) Nitrite concentration in cells seeded on different materials and stimulated with LPS. (below) TNF-α concentration in cells seeded on different materials and stimulated with LPS. ("a" $p < 0.05$ compared to the negative control. "b" $p < 0.05$ compared to the positive control. Dunn´s method One-way ANOVA Analysis of Variance on Ranks).

On the other hand, although cells insulted with LPS showed a higher nitrite concentration than the negative control, this level is far below the positive control (i.e., BV2 cells seeded on tissue culture plastic with LPS stimulus). This result suggests that our materials do not produce a secretion of nitrites by their own and, in addition, they were able to attenuate the nitrite secretion. On the same way, secretion of TNF-α by BV2 cells seeded on PDLEB with 0, 0.1, 0.5 and 1% of CNTs was also measured (Figure 5.8.below). In Figure 5.8.below it can be seen how the TNF-α follow the same tendency that nitrite release, showing that TNF-α concentration in the cell supernatant was very close (but slightly higher) to the negative control on cells seeded on PDLEB samples without LPS stimulus. On the other hand, BV2 cells seeded on materials with the LPS stimulus showed, again, a higher concentration of TNF-α but far below the positive control. In both assays, a correlation between the release of nitrites and TNF-α with the concentration of CNTs was not clearly observed. Subsequently, and knowing the potential role of the topography on cell behaviour, BV2 cells were seeded on PDLEB samples with 0% and 0.5% CNTs and with two different topographical surfaces (flat vs. nanopatterned). Following the same protocol, nitrite and TNF-α concentration were quantified. Figure 5.9.above shows the nitrite concentration released in cell medium after the incubation of cells on different substrates.

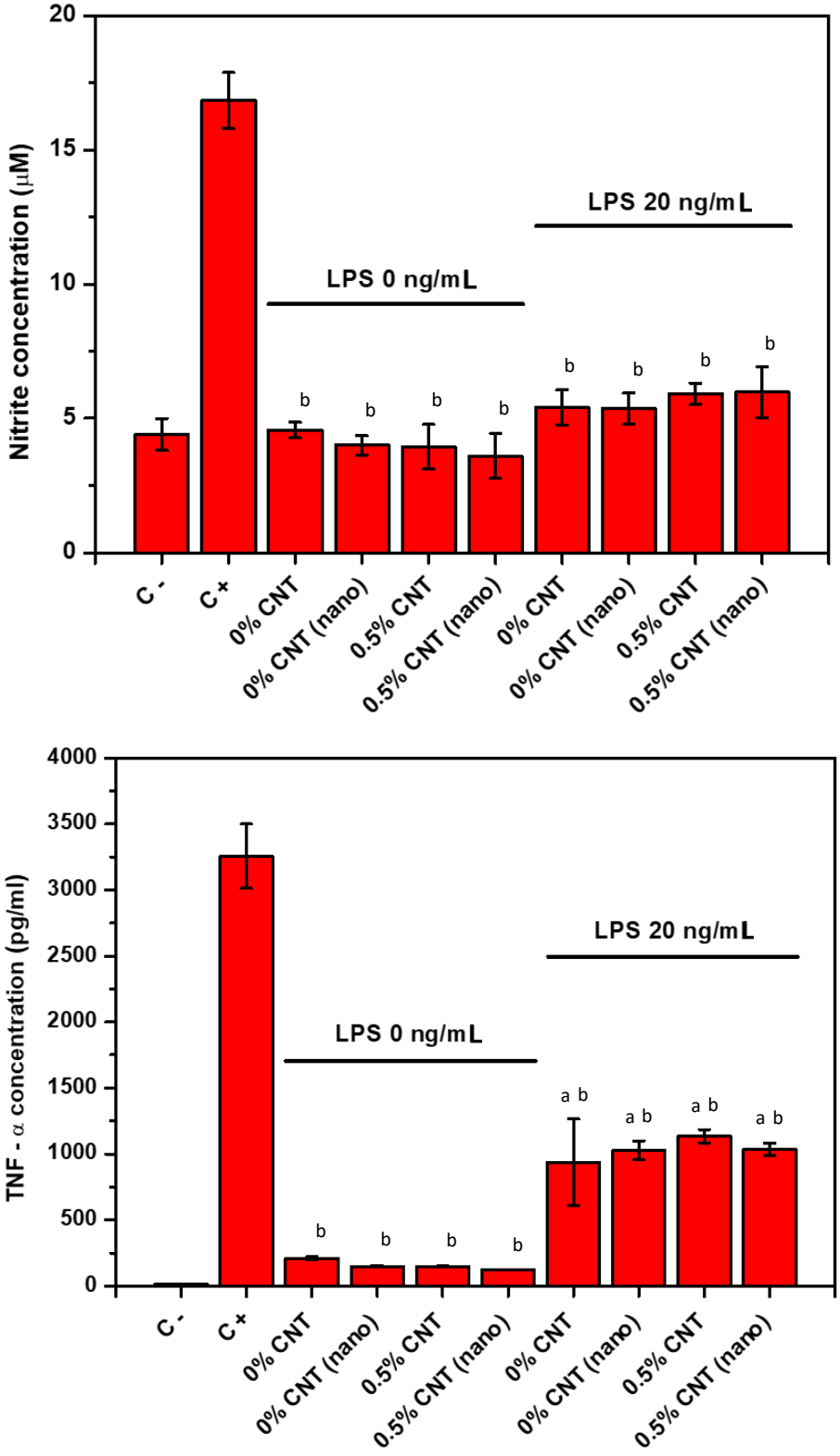

Figure 5.9. (above) Nitrite concentration in cells seeded on different materials and surfaces and stimulated with LPS. (below) TNF-α concentration in cells seeded on different materials and surfaces and stimulated with LPS. ("a" $p < 0.05$ compared to the negative control. "b" $p < 0.05$ compared to the positive control. Dunn´s method One-way ANOVA Analysis of Variance on Ranks).

In the absence of LPS stimulus, similar levels to the negative control were observed. In the presence of LPS, nitrite concentration was smaller than in the positive control. Regarding the results achieved from the TNF-α release (Figure 5.9.below), a similar trend was observed: samples without the LPS stimulation showed values near to the negative control, whereas cells with LPS stimulation showed results far below of the positive control. In the same way that CNTs, the surface topography seems to have no effects on the cell behaviour in comparison with non-nanostructured samples.

To confirm that these observations cannot be associated to potential cell death induced by the surface topography, a viability assay was performed where cells were seeded over PDLEB samples with 0 and 0.5% CNTs and with and without a nanostructured topography. Again, half of cells were stimulated with a solution of 20 $ng \cdot mL^{-1}$ of LPS, while the other half not. Then the metabolic activity was measured by AlamarBlue assay. As shown in Figure 5.10., no significant differences were observed in the metabolic activity of BV2 cells seeded on the different samples. Once again, the observed metabolic activity was slightly higher when cells were stimulated with LPS.

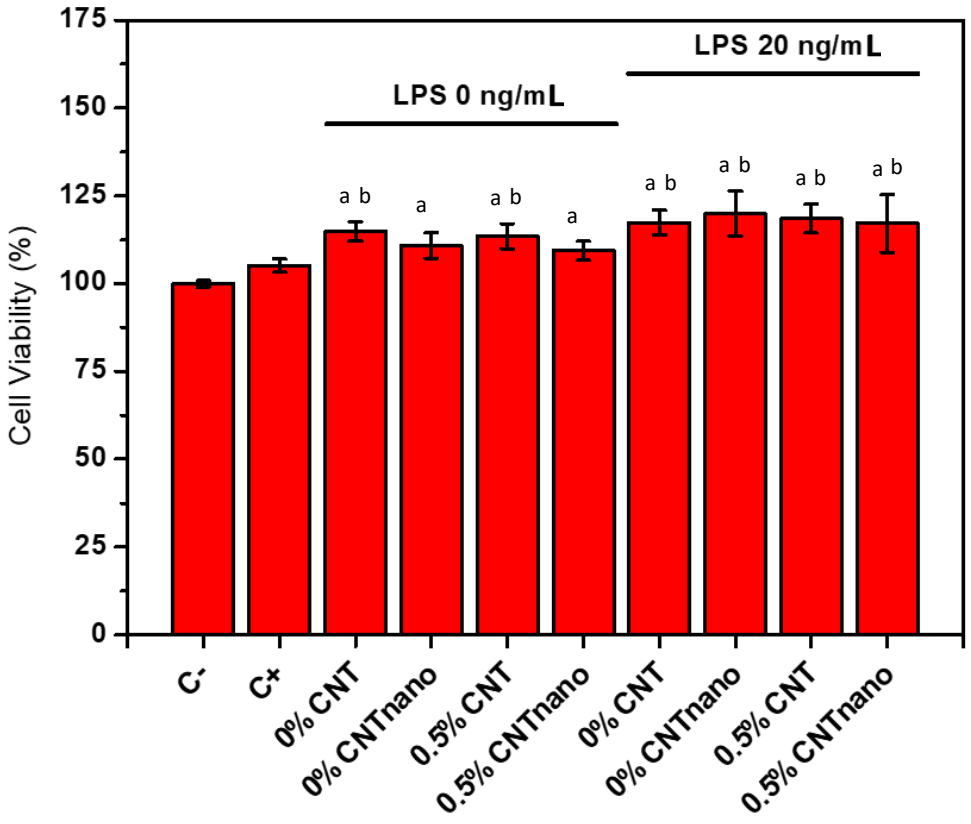

Figure 5.10. Metabolic activity of cells seeded on different materials and surfaces and stimulated with LPS. ("a" $p < 0.05$ compared to the negative control. "b" $p < 0.05$ compared to the positive control. Dunn´s method One-way ANOVA Analysis of Variance on Ranks).

5.4 Conclusions

The present chapter describes the fabrication of scaffolds, based on nanocomposites of lactide and ethylene brassylate with carbon nanotubes, to control the proinflammatory state of microglia in vitro. Due to the thermoplastic nature of the material, it is possible to recreate a pattern on their surface by nanolithography to create nanopatterned scaffolds. In line with the results observed in Chapter 4 regarding the cytocompatibility with cells from the nervous system (astrocytes and microglia), the softer mechanical behaviour and the absence of crystalline domains in poly(D,L-Lactide-co-Ethylene Brassylate) (PDLEB) seems to be more appropriate for the interaction of microglia (BV2 cells) in terms of metabolic activity. Subsequently, a model of inflammation where cells were characterized by the release of nitrites and TNF-α, the production of reactive oxygen species and the expression of Iba-1 was established to analyse the interaction between our scaffolds and BV2 cells. Finally, BV2 cells were seeded on PDLEB scaffolds and analysed in term of nitrites and TNF-α release, showing that our scaffolds do not cause an inflammatory response on cells and when an inflammation condition is induced, the materials can partially attenuate it. Overall, the scaffolds presented herein represent the first steps for the fabrication of polymeric devices for their interaction with soft tissues avoiding an inflammatory response in the implantation area.

5.5. References

[1] D.F. Williams, On the nature of biomaterials, Biomaterials. 30 (2009) 5897–5909. https://doi.org/10.1016/j.biomaterials.2009.07.027.

[2] J. Wang, Y. Cheng, L. Chen, T. Zhu, K. Ye, C. Jia, H. Wang, M. Zhu, C. Fan, X. Mo, In vitro and in vivo studies of electroactive reduced graphene oxide-modified nanofiber scaffolds for peripheral nerve regeneration, Acta Biomaterialia. 84 (2019) 98–113. https://doi.org/10.1016/j.actbio.2018.11.032.

[3] S. Ma, J. Zhou, T. Huang, Z. Zhang, Q. Xing, X. Zhou, K. Zhang, M. Yao, T. Cheng, X. Wang, X. Wen, F. Guan, Sodium alginate/collagen/stromal cell-derived factor-1 neural scaffold loaded with BMSCs promotes neurological function recovery after traumatic brain injury, Acta Biomaterialia. 131 (2021) 185–197. https://doi.org/10.1016/j.actbio.2021.06.038.

[4] J.K. Krauss, N. Lipsman, T. Aziz, A. Boutet, P. Brown, J.W. Chang, B. Davidson, W.M. Grill, M.I. Hariz, A. Horn, M. Schulder, A. Mammis, P.A. Tass, J. Volkmann, A.M. Lozano, Technology of deep brain stimulation: current status and future directions, Nat Rev Neurol. 17 (2021) 75–87. https://doi.org/10.1038/s41582-020-00426-z.

[5] E.S. Ereifej, C.S. Smith, S.M. Meade, K. Chen, H. Feng, J.R. Capadona, The Neuroinflammatory Response to Nanopatterning Parallel Grooves into the Surface Structure of Intracortical Microelectrodes, Adv. Funct. Mater. 28 (2018) 1704420. https://doi.org/10.1002/adfm.201704420.

[6] Y. Li, Y. Xiao, C. Liu, The Horizon of Materiobiology: A Perspective on Material-Guided Cell Behaviors and Tissue Engineering, Chem. Rev. 117 (2017) 4376–4421. https://doi.org/10.1021/acs.chemrev.6b00654.

[7] X. Zhang, X. Cui, D. Wang, S. Wang, Z. Liu, G. Zhao, Y. Zhang, Z. Li, Z.L. Wang, L. Li, Piezoelectric Nanotopography Induced Neuron-Like Differentiation of Stem Cells, Advanced Functional Materials. 29 (2019) 1900372. https://doi.org/10.1002/adfm.201900372.

[8] J.C. Doloff, O. Veiseh, R. de Mezerville, M. Sforza, T.A. Perry, J. Haupt, M. Jamiel, C. Chambers, A. Nash, S. Aghlara-Fotovat, J.L. Stelzel, S.J. Bauer, S.Y. Neshat, J. Hancock, N.A. Romero, Y.E. Hidalgo, I.M. Leiva, A.M. Munhoz, A. Bayat, B.M. Kinney, H.C. Hodges, R.N. Miranda, M.W. Clemens, R. Langer, The surface topography of silicone breast implants mediates the foreign body response in mice, rabbits and humans, Nat Biomed Eng. 5 (2021) 1115–1130. https://doi.org/10.1038/s41551-021-00739-4.

[9] C.A.R. Chapman, H. Chen, M. Stamou, J. Biener, M.M. Biener, P.J. Lein, E. Seker, Nanoporous Gold as a Neural Interface Coating: Effects of Topography, Surface Chemistry, and Feature Size, ACS Appl. Mater. Interfaces. 7 (2015) 7093–7100. https://doi.org/10.1021/acsami.5b00410.

[10] C. Vallejo-Giraldo, K. Krukiewicz, I. Calaresu, J. Zhu, M. Palma, M. Fernandez-Yague, B. McDowell, N. Peixoto, N. Farid, G. O'Connor, L. Ballerini, A. Pandit, M.J.P. Biggs, Attenuated Glial Reactivity on Topographically Functionalized Poly(3,4-Ethylenedioxythiophene):P-Toluene Sulfonate (PEDOT:PTS) Neuroelectrodes Fabricated by Microimprint Lithography, Small. 14 (2018) e1800863. https://doi.org/10.1002/smll.201800863.

[11] A. Kelly, N. Farid, K. Krukiewicz, N. Belisle, J. Groarke, E.M. Waters, A. Trotier, F. Laffir, M. Kilcoyne, G.M. O'Connor, M.J. Biggs, Laser-Induced Periodic Surface Structure Enhances Neuroelectrode Charge Transfer Capabilities and Modulates Astrocyte Function, ACS Biomater. Sci. Eng. 6 (2020) 1449–1461. https://doi.org/10.1021/acsbiomaterials.9b01321.

[12] K.C. Spencer, J.C. Sy, K.B. Ramadi, A.M. Graybiel, R. Langer, M.J. Cima, Characterization of Mechanically Matched Hydrogel Coatings to Improve the Biocompatibility of Neural Implants, Sci Rep. 7 (2017) 1952. https://doi.org/10.1038/s41598-017-02107-2.

[13] A. Larrañaga, E. Lizundia, A review on the thermomechanical properties and biodegradation behaviour of polyesters, European Polymer Journal. 121 (2019) 109296. https://doi.org/10.1016/j.eurpolymj.2019.109296.

[14] C. Bello-Álvarez, A. Etxeberria, Y. Polo, J.R. Sarasua, E. Zuza, A. Larrañaga, Lactide and Ethylene Brassylate-Based Thermoplastic Elastomers and Their Nanocomposites with Carbon Nanotubes: Synthesis, Mechanical Properties and Interaction with Astrocytes, Polymers. 14 (2022) 4656. https://doi.org/10.3390/polym14214656.

[15] A. Varki, R.D. Cummings, J.D. Esko, H.H. Freeze, P. Stanley, C.R. Bertozzi, G.W. Hart, M.E. Etzler, Essentials of Glycobiology, Cold Spring Harbor Laboratory Press, 2009. https://www.ncbi.nlm.nih.gov/books/NBK1908/ (accessed September 24, 2023).

[16] C.R.A. Batista, G.F. Gomes, E. Candelario-Jalil, B.L. Fiebich, A.C.P. De Oliveira, Lipopolysaccharide-Induced Neuroinflammation as a Bridge to Understand Neurodegeneration, IJMS. 20 (2019) 2293. https://doi.org/10.3390/ijms20092293.

[17] S. Nair, K.S. Sobotka, P. Joshi, P. Gressens, B. Fleiss, C. Thornton, C. Mallard, H. Hagberg, Lipopolysaccharide-induced alteration of mitochondrial morphology induces a metabolic shift in

microglia modulating the inflammatory response in vitro and in vivo, Glia. 67 (2019) 1047–1061. https://doi.org/10.1002/glia.23587.

[18] C. Lauro, C. Limatola, Metabolic Reprograming of Microglia in the Regulation of the Innate Inflammatory Response, Front. Immunol. 11 (2020) 493. https://doi.org/10.3389/fimmu.2020.00493.

[19] N.I. Vargas-Maya, F. Padilla-Vaca, O.E. Romero-González, E.A.S. Rosales-Castillo, Á. Rangel-Serrano, S. Arias-Negrete, B. Franco, Refinement of the Griess method for measuring nitrite in biological samples, Journal of Microbiological Methods. 187 (2021) 106260. https://doi.org/10.1016/j.mimet.2021.106260.

[20] R.S. Kumar, P. Antonisamy, A.I. Almansour, N. Arumugam, D.M. Al-thamili, R.R. Kumar, H.-R. Kim, K.-B. Kwon, Discovery of novel cage-like heterocyclic hybrids as anti-inflammatory agents through the inhibition of nitrite, PGE2 and TNF-α, Bioorganic Chemistry. 91 (2019) 103180. https://doi.org/10.1016/j.bioorg.2019.103180.

[21] B.M. Facchin, G.O. dos Reis, G.N. Vieira, E.T.B. Mohr, J.S. da Rosa, I.F. Kretzer, I.G. Demarchi, E.M. Dalmarco, Inflammatory biomarkers on an LPS-induced RAW 264.7 cell model: a systematic review and meta-analysis, Inflamm. Res. 71 (2022) 741–758. https://doi.org/10.1007/s00011-022-01584-0.

[22] J. Zou, P. Guo, N. Lv, D. Huang, Lipopolysaccharide-induced tumor necrosis factor-α factor enhances inflammation and is associated with cancer (Review), Molecular Medicine Reports. 12 (2015) 6399–6404. https://doi.org/10.3892/mmr.2015.4243.

[23] S.J. Forrester, D.S. Kikuchi, M.S. Hernandes, Q. Xu, K.K. Griendling, Reactive Oxygen Species in Metabolic and Inflammatory Signaling, Circulation Research. 122 (2018) 877–902. https://doi.org/10.1161/CIRCRESAHA.117.311401.

[24] S.P. Yun, T.-I. Kam, N. Panicker, S. Kim, Y. Oh, J.-S. Park, S.-H. Kwon, Y.J. Park, S.S. Karuppagounder, H. Park, S. Kim, N. Oh, N.A. Kim, S. Lee, S. Brahmachari, X. Mao, J.H. Lee, M. Kumar, D. An, S.-U. Kang, Y. Lee, K.C. Lee, D.H. Na, D. Kim, S.H. Lee, V.V. Roschke, S.A. Liddelow, Z. Mari, B.A. Barres, V.L. Dawson, S. Lee, T.M. Dawson, H.S. Ko, Block of A1 astrocyte conversion by microglia is neuroprotective in models of Parkinson's disease, Nat Med. 24 (2018) 931–938. https://doi.org/10.1038/s41591-018-0051-5.

[25] A.M. Jurga, M. Paleczna, K.Z. Kuter, Overview of General and Discriminating Markers of Differential Microglia Phenotypes, Front. Cell. Neurosci. 14 (2020) 198. https://doi.org/10.3389/fncel.2020.00198.

[26] H.X. Fan-Jun Shi, H.X. Fan-Jun Shi, Is Iba-1 protein expression a sensitive marker for microglia activation in experimental diabetic retinopathy?, Qwer. 14 (2020) 200–208. https://doi.org/10.18240/ijo.2021.02.04.

[27] F. Drago, P.-E. Sautière, F. Le Marrec-Croq, A. Accorsi, C. Van Camp, M. Salzet, C. Lefebvre, J. Vizioli, Microglia of medicinal leech (Hirudo medicinalis) express a specific activation marker homologous to vertebrate ionized calcium-binding adapter molecule 1 (Iba1/alias aif-1), Developmental Neurobiology. 74 (2014) 987–1001. https://doi.org/10.1002/dneu.22179.

[28] S. Dijkstra, E.E. Geisert JR., W.H. Gispen, P.R. Bär, E.A.J. Joosten, Up-regulation of CD81 (target of the antiproliferative antibody; TAPA) by reactive microglia and astrocytes after spinal cord injury in the rat, Journal of Comparative Neurology. 428 (2000) 266–277. https://doi.org/10.1002/1096-9861(20001211)428:2<266::AID-CNE6>3.0.CO;2-0.

[29] M.B. Graeber, B.W. Scheithauer, G.W. Kreutzberg, Microglia in brain tumors, Glia. 40 (2002) 252–259. https://doi.org/10.1002/glia.10147.

CHAPTER 6

General conclusions and future perspectives

Chapter 6. General conclusions and future perspectives

6.1. General conclusions

CHAPTER 3. Thermoplastic elastomers based on lactide and caprolactone: the influence of chain microstructure on surface topography and subsequent interaction with cells

1. **Obtaining copolymers with different polymeric microstructures and different crystallization behaviours.** The selected catalyst and the monomer feed ratio used in the copolymer synthesis determined the chain microstructure and the crystallinity degree. Copolymers synthetized with Ph_3Bi resulted in more random distribution of LA repetitive units than those with $SnOct_2$, which lead to a lower crystallinity degree.

2. **Creation of different topographies through thermal treatments.** Due to the different chain microstructures and the L-LA content, different crystallization behaviours from the melt were achieved, obtaining a variety of surface textures (both smooth and rough surfaces).

3. **Obtaining different mechanical properties resulting from the composition and microstructure of the copolymers.** Copolymers with 80 wt.% of L-lactide showed a plastic-like behaviour while copolymers with 70 wt.% of L-lactide showed an elastomeric behaviour.

4. **Differences in cellular behaviour depending on surface topography.** Cells seeded on PLCL 7030 Sn samples treated isothermally at 70 °C (R_a of 110 nm and spherulitic morphology of 14 µm) showed an elongated morphology, while cells seeded on PLCL 7030 Sn quenched samples (R_a of 1.7 nm and smooth surface) showed a more spread morphology.

Chapter 4. Lactide and ethylene brassylate-based thermoplastic elastomers and their nanocomposites with carbon nanotubes: synthesis, mechanical properties and interaction with astrocytes

1. **Obtaining copolymers with elastomeric behaviour at body temperature suitable for interaction with soft tissues, including neural tissue.** Different mechanical properties at room temperature were obtained by the addition of carbon nanotubes and the use of L-LA or D,L-LA. In addition, at body temperature, two different mechanical behaviours were achieved, where copolymers synthesized with D,L-LA showed a more elastomeric behaviour than those synthesized with L-LA.

2. **Cytocompatibility with cells of the nervous system.** The mechanical behaviour and the absence of crystalline regions in the copolymer with D,L-lactide is more appropriate for the interaction with C8-D1A cells. A higher metabolic activity and a better cell morphology was observed in those synthesized with D,L-LA,.

3. **The thermoplastic nature allows the manufacture of nanostructured films, capable of supporting the aligned growth of cells on their surface.** Using a nanopatterned silicon stamp, the nanostructure was successfully replicated on the film surface by a thermo-pressing process. Cells seeded on nanostructured materials were able to be aligned with the pattern.

4. **Study how topography can affect the inflammatory process.** These copolymeric substrates are a promising alternative to polylactide-co-caprolactone copolymers for the fabrication of polymeric devices for soft tissue applications (i.e., neural tissue). For this use, an inflammatory control is necessary to ensure the viability of the implanted device.

CHAPTER 5. Lactide and ethylene brassylate-based thermoplastic elastomers and their nanocomposites with carbon nanotubes: nanopatterned surface as strategy to alleviate neuroinflammation after biomaterial implantation

1. **Cytocompatibility with microglia of the nervous system.** The mechanical properties and the absence of crystalline regions in the copolymer with D,L-lactide is more appropriate for the interaction with BV2 cells. A higher metabolic activity and a better cell morphology was observed in those synthesized with D,L-LA.

2. **LPS stimulation to induce an inflammatory response.** To create an inflammatory model, cell activity, nitrites concentration, TNF-α, ROS and Iba-1 were measured in BV2 cells after the LPS stimulus, resulting that an insult of 20 $ng \cdot mL^{-1}$ of LPS for 24 h is adequate to induce an inflammatory response on microglia.

3. **Poly(D,L-Lactide-co-Ethylene Brassylate) (PDLEB) copolymer to mitigate the inflammatory response.** The results showed that PDLEB scaffolds did not cause an inflammatory response on cells. In addition, when an inflammatory condition is introduced, the materials can partially mitigate it.

6.2. Future perspectives

In this thesis project, a range of lactide-based copolymers showing mechanical properties compatible with the nerve tissue were synthesized and characterized. Besides, various processes (e.g., thermal treatments, CNTs addition and nanolithography) were explored with the aim of modifying the surface topography of the films to finally study their interaction with cells relevant of the nervous system (e.g., astrocytes, microglia). In Chapter 3, a variety of topographies were obtained by applying thermal treatments to PLCL films. The most representative topographies showing different roughness values were subsequently used as a support for MRC-5 cells to study the impact of the topography on cell behaviour. In Chapter 4, a new copolymer based on ethylene brassylate and D,L-LA (PDLEB) or L-LA (PLEB) was synthetized and subsequently reinforced with CNTs. As the target of this thesis is the nerve tissue, astrocytes were firstly used to study their interaction with our synthesized copolymers. Finally, in Chapter 5, the interaction of those copolymers synthesized in Chapter 4 with microglia was carried out. As an implantable device will usually lead to an inflammatory response, the interaction was studied in terms of cell viability, TNF-α release and nitrites production. The obtained results were promising, since PDLEB copolymers showed a good interaction with microglia cells, allowing them to attach and proliferate on the copolymer surface, and not inducing any inflammatory response by cells. Even when a proinflammatory environment was induced, microglia seeded on our materials showed a partial reduction of this state. With this in mind, and knowing that both astrocytes and microglia are determinant in the immune response after a device implantation, the interaction of astrocytes with the inflammatory model generated on this thesis should be further studied in the future. To achieve this, astrocytes could be stimulated with conditioned media from microglia previously stimulated with LPS. The coculture of both astrocytes and microglia seeded on our samples could also be an option to study their behaviour in contact with our materials. Other point that could be interesting to study is how the material could interfere with the substances released by cells. That is, whether the material could modify or even absorb some of them avoiding their detection by routine techniques. Another important point could be the study of the degradation by-products on the inflammatory response on microglia. Other point that could be explored is the electrical conductivity that CNTs could provide to the copolymer and that could be exploited for the electrical stimulation of cells. During this thesis, some preliminary studies of conductivity were carried out but clear results were not obtained. This point will be important, considering that conductive materials could help neurons to proliferate and induce a complete/better repair of the damaged tissue.